A STUDY OF PHASE RESETTING, MUTUAL ENTRAINMENT, AND MODIFIED VENTRICULAR PARASYSTOLE USING A MODEL OF COUPLED HEART CELLS

By

Toni Foster

B. Sc. (Mathematics/Computer Science) University of Victoria

A THESIS SUBMITTED IN PARTIAL FULFILLMENT OF

THE REQUIREMENTS FOR THE DEGREE OF

MASTER OF SCIENCE

in

THE FACULTY OF GRADUATE STUDIES

DEPARTMENT OF MATHEMATICS, INSTITUTE OF APPLIED MATHEMATICS

We accept this thesis as conforming

to the required standard

THE UNIVERSITY OF BRITISH COLUMBIA

March 1992

In presenting this thesis in partial fulfilment of the requirements for an advanced degree at the University of British Columbia, I agree that the Library shall make it freely available for reference and study. I further agree that permission for extensive copying of this thesis for scholarly purposes may be granted by the head of my department or by his or her representatives. It is understood that copying or publication of this thesis for financial gain shall not be allowed without my written permission.

Department of Mathematics, Institute of Applied Mathematics
The University of British Columbia
Vancouver, Canada
V6T 1Z2

Date: March 23, 1992

Abstract

Several aspects of cardiac electrophysiology including phase-resetting and entrainment are investigated through the dynamic interactions of coupled mathematical models of cardiac cells. Unlike previous studies of cell interaction which have used simplified models of a *general* cardiac cell or oscillators characterized only by their phase transition curves the present work incorporates the more physiologically realistic cell models of the Hodgkin-Huxley type. Furthermore, this caricature of the heart includes models representing cells from each of the major components of the heart's electrical conduction system, the SA node, AV node, Purkinje fibre network, and ventricular myocardium. Since there does not exist a model for an AV node cell, a new model is created by modifying the SA node cell equations.

Because spontaneously firing cardiac cells exhibit a wide range of oscillation frequencies, certain physiologically based parameters in the model equations were altered to produce a similar range of intrinsic frequencies in the model cells. These model cells are coupled by assuming that direction-dependent and purely resistive coupling currents flow between them. Furthermore, these coupling currents incorporate a time delay representing the intercell impulse propagation time which is significant between different regions of the heart. Each of the conduction components, the SA and AV nodes, Purkinje fibre network, and ventricular myocardium, can be modelled with either one or several of their model cells. These model *components* can then be coupled with appropriate conductances and propagation time delays to model the spread of waves of excitation from one region of the heart to another.

When cells interact, their intrinsic cycles may be perturbed. These alterations or

phase-shifts which determine the ultimate rhythm of coupled cells are studied for various combinations of the model cells and different strengths of interaction. In each case results are plotted in a phase response curve whose shape is found to depend on such things as coupling conductance and cell frequency. Phase-resetting is a prerequisite to the entrainment of cells in which there are m cycles of one cell for every n cycles of another. The phenomenon of entrainment is studied as part of the behavior of a healthy heart where it provides the mechanism by which cells synchronize to produce a single wave of excitation for each heartbeat. Mutual entrainment is also studied in a commonly occurring pathological situation, modulated ventricular parasystole. It is demonstrated that the particular pattern of m:n entrainment is dependent on the differences in the intrinsic frequencies of the cells and on the strength of the interaction. Results obtained using different types of model cells located in different regions of the heart are compared and contrasted to those of previous studies of adjacent cells which are identical.

Table of Contents

List of Tables

List of Figures

Acknowledgements

Thank God it's over! Thanks also to Dr. Robert Miura for his indispensible guidance in the preparation of this thesis and Drs. Leah Edelstein-Keshet and Brian Seymour for giving it the final OK. Thanks to Rob for being here to share this whole Master's thing with me and for being such an entirely excellent office-mate and friend. I would also like to acknowledge the much needed financial assistance of the Bank of Foster and NSERC. Finally, special thanks to Mark for his support and encouragement and for continually reminding me that life is too short not to have fun.

Chapter 1

Introduction

The heart's function is to provide the energy necessary to circulate blood through the cardiovascular system. Electrical excitations originating from specialized regions spread throughout the heart causing atrial, and then ventricular, muscle contractions. In humans, this process takes place continuously at an average rate of 60 to 100 times per minute for an entire lifetime. It is not surprising that, despite decades of research, many aspects of the physiology of such a sophisticated organ are still not understood. For example, the mechanism behind one of the most fundamental properties of cardiac cells, their ability to synchronize to a common frequency, enabling the heart to beat in a regular manner, is not known [30,39]. Fundamental aspects of cardiac *pathophysiology* also are poorly understood. Although, it is known that cardiac arrhythmias (irregular rhythms) are caused by abnormalities in either the *initiation* or the *conduction* of a wave of excitation, the causes of the abnormalities themselves are, in many cases, not known. Abnormal initiation refers to the formation of waves at either abnormal locations or at rates outside the usual range. Abnormal conduction of a wave of excitation refers to either a change in the conduction velocity or in the path taken over the cardiac tissue. The result of these malfunctions is sometimes an arrhythmia known as ventricular fibrillation in which the ventricles can contract at rates as high as 500 beats per minute. Clearly, a knowledge of the mechanisms which trigger the onset of such life-threatening arrhythmias is vital to their prevention and treatment. The lack of a complete understanding of the physiology of the heart, combined with its essential role in human health, has

provided the motivation for ongoing research. Much of this research has been directed at both the mechanical and electrical aspects of the heart's functioning.

The mechanical properties of the myocardium (heart muscle) have been studied by, amongst others, Horowitz [19] using a microstructural model based on the structural arrangement of cardiac muscle cells and properties of the complex connective tissue. Such studies have been aimed at obtaining a suitable mathematical description of the time-varying properties of active muscle tissue. With such a mathematical description, finite element models [16,20,23,33,36] have been employed to describe regional mechanics of the heart wall by continuous distributions of stress and strain. This approach was used by McCulloch [29] who also compared his results with experimental measurements.

The electrical properties of cardiac tissue, which are the focus of this thesis, have, for the most part, been studied independently of the mechanical properties. The heart's electrical activity is caused by the opening and closing of ionic channels in the cardiac cell membrane. The resulting flow of electric current between adjacent cells has been modelled theoretically using systems of nonlinear ordinary differential equations. Models based on these ideas will be employed in the present study. The resulting systems of equations can be very complex and usually cannot be solved analytically. As an alternative to this approach, low dimensional finite difference equations have been used to model the responses of cardiac tissue to various inputs such as periodic stimulation [9,11,12,14,18,21,26,37]. In addition, cellular automata (finite state) models of cardiac conduction have been applied to the study of the patterns of electrical activity in the heart ([10], chapter 18).

1.1 Cardiac Physiology

1.1.1 Action Potentials

All cells have an electrical potential (voltage) across their membranes. These *membrane potentials* exist because the ionic concentrations inside the cells are different from those in the interstitial fluid outside the cells. The resulting concentration gradients cause the flow of ions across the semipermeable membranes and generate electrical gradients.

Abrupt changes in the permeability of the membrane to specific ions, mainly sodium and potassium, and to a lesser extent calcium, cause an abrupt rise (depolarization) in membrane potential. The muscle contractions which cause the heart to pump blood are triggered by these sudden voltage changes called *action potentials* in cardiac muscle cells.

All cardiac muscle cells are excitable [6]. That is, they can respond to a given stimulus by the production of an action potential. Some cells of the myocardium, however, have the ability to spontaneously depolarize and, thereby, *initiate* action potentials. These cells, known as *pacemakers* or *spontaneous* cells, are located in various regions throughout the heart. For the remainder of the myocardial cells, which do not possess this inherent rhythmicity (*nonpacemaker* or *nonspontaneous* cells), an action potential is generated only by external stimulation.

Although the action potentials of different excitable cardiac cells are not identical, they share a common qualitative time sequence characterized by some or all of the following five separate phases (Figure 1.1). Phase 4 (as it is normally denoted), the resting phase, is the transmembrane potential recorded between impulses. For a nonspontaneous cell this potential will be constant; however, for a pacemaker cell this phase is characterized by a slow spontaneous depolarization. When either this depolarization or an external stimulus causes the membrane potential to reach a critical value, called

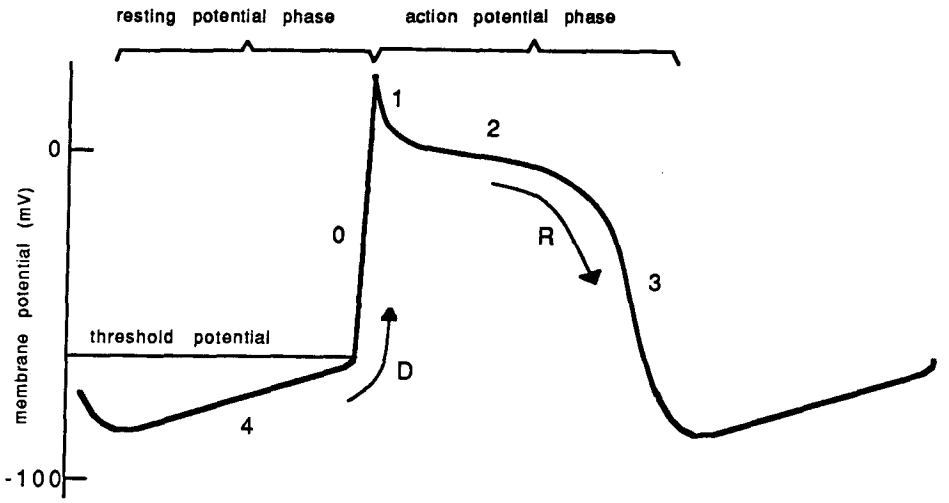

Figure 1.1: Diagrammatic representation of a cardiac cell transmembrane action potential. Numbers indicate phases. The letters, D and R, indicate regions of membrane depolarization and repolarization, respectively.

the *threshold* potential, rapid depolarization (phase 0) occurs. This sharp upstroke is followed by an early rapid *re*polarization or decrease in membrane potential (phase 1), a prolonged phase of slow repolarization (phase 2) constituting a plateau, and a final phase of rapid repolarization (phase 3) to the resting level.

1.1.2 The Conduction Path in a Healthy Heart

Action potentials propagate within the heart by crossing the membranes between adjacent cells. This cell-to-cell flow of electric current is the means by which a wave of excitation is conducted throughout the heart. In a healthy heart there is a specialized network of cardiac cells specifically adapted to generate and conduct the wave of excitation for each heartbeat. The major components of this network are: the sinoatrial (SA or sinus) node, the atrioventricular (AV) node, the Purkinje fibre system, and the ventricular myocardium (muscle cells). The different membrane electrical properties of

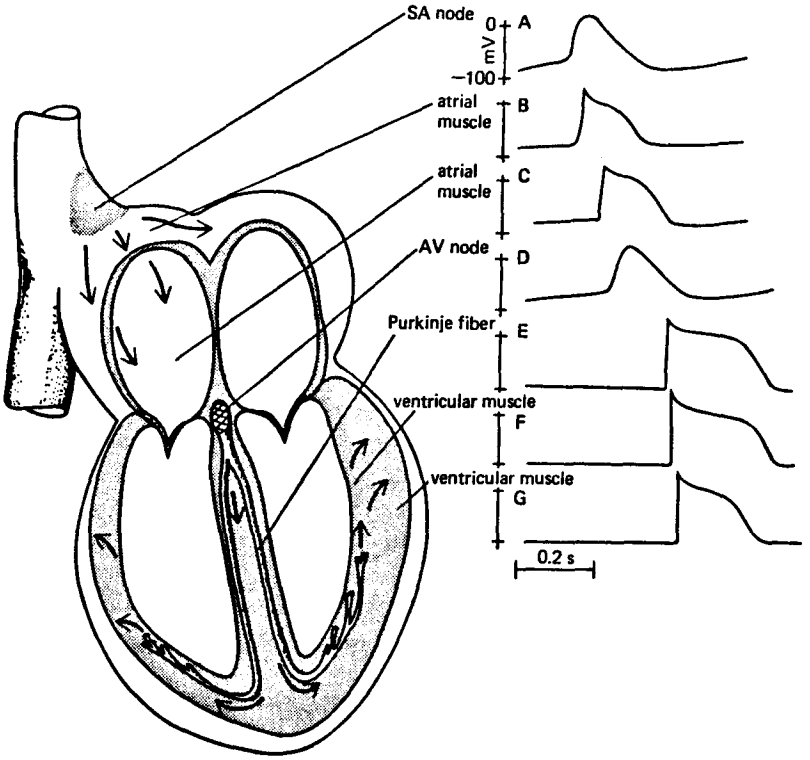

Figure 1.2: Cardiac cells and their action potentials (taken from [17], p.22).

the cells in each of these components are reflected in the variations amongst their action potentials (Figure 1.2).

The SA node, located in the wall of the upper right atrium (Figure 1.2), is a group of pacemaker cells which, among all cells in a healthy heart, exhibit the most rapid spontaneous depolarization during the resting phase [4,6,38]. Consequently, SA node cells reach their threshold and generate action potentials at a rate faster than other cardiac cells which then become entrained to the SA node rhythm. For this reason, the SA node is sometimes referred to as the heart's *primary* pacemaker.

The excitation initiated at the SA node spreads radially throughout the atria. At the base of the atrium the wave of excitation encounters a small mass of specialized cells called the AV node (Figure 1.2). The conduction velocity of the excitation is

slowed through the AV node, which provides the only contiguous bridge of cardiac tissue crossing the cartilaginous structure that separates the atria from the ventricles. There is a substantial delay before the wave of excitation emerges at the base of the AV node and enters the Purkinje fibre system. The Purkinje fibres are specialized large-diameter conducting fibres spreading throughout the ventricles in finer and finer branches which terminate on ordinary ventricular muscle (myocardial) cells. Conduction of the excitation through the Purkinje fibre network is extremely rapid causing the left and right ventricles to contract nearly in unison.

1.1.3 Conduction Time in a Healthy Heart

The temporal displacements of the action potentials in Figure 1.2 indicates the time required for a wave of excitation to propagate throughout the heart. Approximately 80-120 msec are required for atrial depolarization and a further 50 msec for passage through the AV node. Thus, from the generation of the first action potential at the SA node to the emergence of the wave of excitation at the lower portion of the AV node into the Purkinje fibre network requires an average of about 160 msec. The spread of the action potential over the ventricles requires an average of 60-100 msec and the total duration of the activation process of the entire heart has an average value of 250 msec [6]. Under pathological conditions these conduction times between different regions of the heart can vary considerably. For example, a wave of excitation may require more than 200 msec to pass through the AV node and, in some situations such as when there is damaged tissue, the excitation may not be conducted at all.

1.2 Modelling the Heart as a System of Coupled Nonlinear Oscillators

Pacemaker (spontaneous) cells from different regions of the heart may have widely varying intrinsic oscillation rates [4,6,17]. Even cells from a small localized region are unlikely to have identical intrinsic frequencies [30]. Experimentally, it is known that when cells with different frequencies are coupled their cycle lengths may be altered [9,30,39]. In certain cases, the cells may become entrained so that there are m cycles of one for every n cycles of another. Synchronization, a particular case of this m:n entrainment in which the coupled cells oscillate with a *common* frequency, may also occur. For example, the pacemaker cells of the SA node synchronize to produce a single wave of excitation for each heartbeat [30]. The mechanism by which coupled cells become entrained is not completely understood; however, it is thought that the electric currents caused by the flow of ions between adjacent cells may mediate the process [5,30,39].

Theoretical work on the entrainment of pacemaker cells was investigated as early as 1928 when van der Pol and van der Mark [35] simulated some typical phenomena (including synchronization) of the heartbeat using three coupled electronic relaxation oscillators. The analogy between the behavior of mathematical forced oscillators and the heartbeat led to the idea of considering the heart as a system of coupled nonlinear oscillators where the periodic stimuli are provided by one or more pacemaker cells. Since that time, many other studies [5,9,18,30,34,39] have also used coupled oscillators to model the entrainment of cardiac cells.

In 1962 Denis Noble modified Hodgkin and Huxley's equations describing the transmembrane potentials of squid giant axons to model the electrical activity of Purkinje fibre cells [31]. Since then, new models for the Purkinje fibre cell, as well as models for other cardiac cells, have been developed. These Hodgkin-Huxley-type models involve voltage- and time-dependent conductances in parallel with a capacitance and include

as many as nine ionic channels. These models cannot be solved analytically; therefore, their use in modelling entrainment phenomena requires extensive numerical computations. For this reason, many previous studies of the propagation of the cardiac impulse through systems of coupled cells have chosen not to use these models but rather to use finite difference equations and oscillators characterized only by their phase transition curves [9,11,12,14,18,21,26,37]. Others have used *simplified* Hodgkin-Huxley-type models of the cardiac action potential to model the behavior of a *general* heart cell [5,34,39]. Furthermore, many of those who *have* used the more physiologically realistic Hodgkin-Huxley-type models have chosen a specific type of cell (for example, an SA node cell [30]) and studied interactions among cells of only that particular type. In some of these studies, the propagation of action potentials from cell to cell is modelled by invoking a purely resistive coupling current between *adjacent* cells. Since even a small area of cardiac tissue is comprised of hundreds of cells, solving complex Hodgkin-Huxley-type oscillators numerically would be far too time consuming and costly; therefore, this type of adjacent-cell-coupling has meant that studies of the propagation of the cardiac action potential have been restricted to small localized regions of the heart.

1.3 The Present Work

In this thesis, a simple model of the *entire* heart is created and used to study phenomena observed in cardiac electrophysiology. This study is focussed on those aspects due to impulse *initiation* and *conduction*, since it is abnormalities in these areas which are the cause of cardiac arrhythmias. In order to limit the number of cells and yet retain a physiologically realistic model, only a small number of cells representing the major components of the heart's conduction system are included. The models for these cells of the SA node, AV node, Purkinje fibre system, and ventricular myocardium are of the

Hodgkin-Huxley type.

The intrinsic (free-running) oscillation frequency of a particular type of spontaneous cardiac cell varies widely under different physiological conditions. For example, in a healthy heart, cells of the AV node oscillate between 45 and 60 cycles/min, whereas in a particular pathological state called AV junctional tachycardia, they can fire at more than 250 beats/min [4,6]. In order to model a wide range of cardiac phenomena, a means of altering the intrinsic frequencies of the pacemaker cells of the model (this excludes the ventricular myocardial cell which is nonspontaneous [1,6]) was devised. The model, which is presented in detail in Chapter 2, allows the coupling of any number of each of the four types of cells where the intrinsic frequencies of the *pacemaker* cells can be specified in some range.

As in previous studies, coupling in the model is achieved through the addition of purely resistive coupling currents which flow between interacting cells with the strength of the interaction controlled by the choice of an appropriate value of the coupling conductance. The difference between this new model and those of previous studies is that here the interacting model cells are not necessarily physically adjacent and may, in fact, be from completely different regions of the heart. A real excitation travelling from one region of the heart to another will likely take a path over the tissue which is different from the path taken by an excitation travelling in the reverse direction. Consequently, the coupling currents flowing between the model cells also must be different in each direction. In addition, the propagation times of the excitation between various regions of the heart are significant (Section 1.1.3); therefore, an excitation generated at a cell from one region does not immediately affect the activity of a cell from another region. These latencies are incorporated into the model by means of appropriately chosen delays added to the coupling currents. In previous studies of *adjacent* cells these propagation time delays were not required since an action potential generated at one cell affects its

neighbouring cells almost immediately simply by crossing the intercell membranes.

When two cells of different intrinsic oscillation periods are coupled, the action potentials initiated at one may cause subthreshold responses in the other. These induced responses in a cell can either accelerate or delay its subsequent discharge compared to its unperturbed oscillation. This *phase shifting* causes changes in the basic rhythms of the cells and, in a real heart, is the cause of both the normal healthy periodic heartbeat as well as the abnormal rhythms (arrhythmias) observed in pathological situations. Chapter 3, through the use of phase response curves (PRCs), presents an investigation of the phase shifts which determine the ultimate rhythm of coupled cells. PRCs are obtained for various pairs of coupled cells of different intrinsic periods and for different strengths of interaction. The effects of the coupling conductance and the type of cells being coupled on the shape of PRCs are studied. The magnitude of the phase shifts induced in one cell by another determine whether or not the cells may be synchronized to a common frequency. Previous studies have indicated that a slower cell (one with a longer period of oscillation) may be entrained to a faster cell. This is also demonstrated with the present model. In addition, the PRCs obtained with the present model indicate that a fast cell may become synchronized to a slower cell.

In Chapter 4, cells are coupled to demonstrate that the present model can simulate two of the most basic functions of a healthy heart, namely the activation of a nonspontaneous muscle cell and the production of a heartbeat. Each cardiac impulse spreads throughout the ventricles by activating nonspontaneous muscle cells causing their contraction. Questions such as: (1) "What is the effect of the coupling conductance on the level of activation of the muscle cell?" and, (2) "How does the coupling affect the intrinsic period of the cell providing the stimulus?" are investigated. The second basic function of a healthy heart is the production of a heartbeat. The spread of waves of excitation from the SA node throughout the rest of the heart is modelled to determine

whether, as in a real heart, each model cell along the conduction path will be excited in turn and become entrained to the SA node rhythm.

Modulated ventricular parasystole, a particular pathological situation in which impulses are initiated at an abnormal (nonsinus) location is studied in Chapter 5 using a simple two-cell model. Computations are repeated for cells of different intrinsic frequencies and, in each case, ranges of the coupling conductances at which the cells beat synchronously are determined. Various patterns of m:n entrainment, in which there are m beats of one cell to every n of the other, are demonstrated. These patterns of entrainment are also readily observable in clinical electrocardiogram (ECG) recordings. Questions such as: (1) "How does the common period of two cells exhibiting 1:1 entrainment relate to their intrinsic periods?", (2) "How do the intrinsic periods affect the strength of interaction required to obtain the synchronization of the cells?" and, (3) "For equal values of the direction dependent coupling conductances, do different cells exert equal influences on each other?" are investigated.

Finally, a discussion of results and suggestions for further research are given in Chapter 6.

Chapter 2

The Model

2.1 Methods

The action potentials of the cells which comprise the major components of the heart's conduction system, the SA and AV nodes, Purkinje fibre network, and ventricular myocardium, were simulated using sets of differential equations of the Hodgkin-Huxley type. Existing models were available for all but the AV node cell, for which a new set of equations was developed. These individual cells were coupled by means of resistive coupling currents which model the flow of ionic currents across intercell membranes. The strength of the cell interaction is determined by a user-defined value of the membrane conductance. For cells which are separated by some distance, the propagation time for a wave of excitation travelling between them was incorporated into the model by a delay in the resistive coupling terms. Because two coupled cells may not exert equal influences on each other, the coupling conductances and delays are direction dependent. Each of the four components (SA node, AV node, Purkinje fibre network, and ventricular myocardium) can be modelled by one model cell, or a few model cells coupled with appropriate conductances and delays. These model *components* can, in turn, be coupled to model the propagation of waves of excitation from one region of the heart to another.

The mathematical models were programmed in FORTRAN and run on an IBM 3090/150S mainframe with Vector Facility using the routine LSODE in the ODEPACK package (Hindmarsh 1980) to perform the integration of the stiff systems. The solutions

of the sets of differential equations showed constant rhythms after approximately 3 seconds; therefore, the solutions at 3 seconds were used as initial values in all computations. The model allows the user to specify, not only the length of time coupled cells will interact, but also the exact time within a computation the interaction will begin and end. The values of all dynamic variables can be stored upon termination of a computation so that it can be resumed at a later time. Results of all computations were stored on disk and later plotted using the Tell-a-Graf graphics package.

2.2 Modelling Individual Cells

The electrical activities of individual cells have been modelled using Hodgkin-Huxley-type models. These models are based on the fact that the changes in membrane potential responsible for initiating muscle contraction are primarily caused by the flow of ionic currents through individual channels in the cell membrane. Experimentally, this flow of ions can be measured through a single channel in a small patch of membrane using what is known as the patch-clamp technique. This technique involves measuring the transmembrane potential of a cell and clamping the membrane potential at a fixed voltage by counteracting any ionic currents with an injected current of equal magnitude. Experiments have shown that there are many different types of channels in a cardiac cell membrane. These channels differ in their permeabilities to different ions and in their responses to changes in the transmembrane potential. The total ionic current flowing across the cell membrane at any particular time is the sum of the currents due to individual ions, such as Na^+ and K^+, flowing across all channels in the membrane.

In a patch-clamp experiment the transmembrane potential of a cell is clamped at a certain potential and once a steady state current is attained, the membrane potential is clamped to a new potential value. There are three types of behavior observed as a new

steady state is achieved. The current at the new potential will (1) instantaneously reach its new steady state value, (2) take some time to be activated as appropriate channels open, thus gradually reach its steady state value, or (3) take some time to be activated but then gradually, as channels close, become inactivated. In the first case, the current is time-independent and is often referred to as a *background* current. In the second case, the current is time-dependent and exhibits only activation processes while, in the third case, the time-dependent current exhibits both activation and inactivation processes.

In the Hodgkin-Huxley formulation for a particular cell, cell j, time-*independent* or background currents are often described by an equation of the form:

$$i = g(E_j)\ (E_j - E_{rev}) \tag{2.1}$$

where E_j is the transmembrane potential of the cell at a particular time and E_{rev} is the reversal potential at which the ionic current flowing across the cell membrane changes direction. The membrane conductance, $g(E_j)$, is often assumed to be constant.

For those components i which are time-*dependent*, the Hodgkin-Huxley formulation often describes their kinetics by an equation of the form:

$$i = g(E_j)\ x\ (E_j - E_{rev}) \tag{2.2}$$

if i is an activation current, and

$$i = g(E_j)\ x\ y\ (E_j - E_{rev}) \tag{2.3}$$

if i shows both activation and inactivation processes. Here $g(E_j)$, E_j, and E_{rev} are as in (2.1). The activation variable x and inactivation variable y are gating variables indicating the fraction of channels specific to a particular ion which are open at any time t. Both x and y take on values between 0 and 1 and follow the first-order equation, e.g., for x, given by:

$$\frac{dx}{dt} = \alpha_x\ (1 - x) - \beta_x\ (x). \tag{2.4}$$

The rate constants α_x and β_x are generally extremely complex nonlinear functions of the cell's membrane potential E_j. A similar equation holds for y but with α_x and β_x replaced by α_y and β_y, respectively. The rate constants for a particular gating variable determine the timing of its activation and/or inactivation. For an activation variable, the rate constants cause the variable to *increase* as the membrane potential becomes less negative (depolarizes) while, for an inactivation variable, they cause a *decrease* in the variable with increases in membrane potential.

Assuming there are no external current sources and that the changes in membrane potential are the result of the ionic current components, the Hodgkin-Huxley formulation describes the rate of change of the transmembrane potential of a cell by a governing equation of the form:

$$\frac{dE_j(t)}{dt} = -\frac{1}{C} i_{ionic} \tag{2.5}$$

where t is the time in msec, j denotes the cell type and, in this thesis, is one of: s, a, p, or v indicating SA node, AV node, Purkinje fibre, and ventricular myocardial cells respectively, $E_j(t)$ is the membrane potential in mV (expressed as the inside potential minus the outside potential) of cell j at time t, C is the membrane capacitance in μF/cm^2, and i_{ionic} is the total ionic current in μA/cm^2 flowing out of cell j.

There are many Hodgkin-Huxley-type models for cardiac cells in existence today. In this thesis, the electrical activity of the SA node cell has been modelled using equations devised by Yanagihara et al. (1980) [38]. Because of the relative complexity of Denis Noble's 1984 model for the Purkinje fibre cell, the 1975 model devised by McAllister, Noble, and Tsien [28] is used. For the ventricular myocardial cell, the model employed is due to Beeler and Reuter (1977) [1]. Finally, due to the lack of an existing model, and motivated by the fact that action potentials of an AV node cell are very similar to those of an SA node cell (Figure 1.2), a model for an AV node cell was created by modifying

the model equations for an SA node cell.

2.2.1 The SA Node Cell

Yanagihara et al. [38] modelled the electrical activity of an SA node cell using four dynamic currents and a time-independent leak current denoted i_l. The dynamic currents are: a slow inward current, i_{si}[1], a sodium current, i_{Na}, a delayed inward current activated by hyperpolarization, i_h, and a potassium current, i_K. Both i_{si} and i_{Na} involve activation and inactivation, while i_h and i_K involve only activation processes. The governing equation is given by (2.5) with:

$$i_{ionic} = i_{si} + i_{Na} + i_K + i_h + i_l. \tag{2.6}$$

The model exhibits spontaneous action potentials where the depolarization (phases 4 and 0) of the cell membrane is primarily due to the transient flow of i_{si} and repolarization (phases 1, 2, and 3) is caused by the combination of a decrease in i_{si} and an increase in i_K. A large fraction of the total ionic current is provided by i_{si}, i_K, and i_l, as i_h and i_{Na} are much smaller in magnitude. The equations describing each of these components of the ionic current are given in the Appendix, A.1.

2.2.2 The AV Node Cell

The action potentials of AV node cells are very similar in shape to the action potentials of SA node cells (Figure 1.2); therefore, a model for an AV node cell was created using the equations for an SA node cell [38]. Minor changes were made to slow the rate of depolarization which is not as fast as for SA node cells. The total ionic current for the AV node cell is given by (2.6) and the individual current components are described in the Appendix, A.2.

[1]In the original paper [38], the slow inward current is denoted i_s rather than i_{si}.

2.2.3 The Purkinje Fibre Cell

The McAllister, Noble, and Tsien model for the Purkinje fibre cell [28] describes the transmembrane potential by (2.5) where:

$$i_{ionic} = i_{Na} + i_{si} + i_{qr} + i_{K_2} + i_{x_1} + i_{x_2} + i_{K_1} + i_{Na_b} + i_{Cl_b} \tag{2.7}$$

and, as in the original paper, the outward (time-independent) background current, i_{K_1}, is listed *after* the time-dependent pacemaker potassium current, i_{K_2}.

Just as in the previous models, this model also exhibits spontaneous action potentials. The upstroke (phase 0) is mainly due to the activation of the sodium current, i_{Na}, in contrast to the SA and AV node cell models where i_{Na} plays only a minor role. The initial repolarization from the peak of the action potential (phase 1) is primarily caused by the transient chloride current, i_{qr}. The role of the slow inward current, i_{si}, is to slow this rapid repolarization and to produce the plateau (phase 2). Phase 3 repolarization is triggered by the onset of one of the plateau potassium currents, i_{x_1}, which becomes activated over the plateau range of potentials. Two other potassium currents, i_{x_2} and i_{K_2}, which also activate over this range, have only a minor influence on the repolarization. However, i_{K_2} is responsible for the slow phase 4 depolarization. The remaining currents, i_{K_1}, an outward potassium current component, and i_{Na_b} and i_{Cl_b}, time-independent background currents carried by sodium and chloride ions respectively, all play a relatively minor role. The equations describing the individual components of the ionic current are given in the Appendix, A.3.

2.2.4 The Ventricular Myocardial Cell

The model, due to Beeler and Reuter [1], for the ventricular muscle cell describes the total ionic current using three dynamic currents and one time-independent current, i_{K_1}. The dynamic currents are: a sodium current, i_{Na}, an outward current, i_{x_1}, primarily

carried by potassium ions, and a slow inward current, i_{si}[2], primarily carried by calcium ions. The governing equation is given by (2.5) where:

$$i_{ionic} = i_{Na} + i_{K_1} + i_{x_1} + i_{si}. \tag{2.8}$$

Most muscle cells of the ventricles are nonspontaneous; therefore, unlike the previous three model cells, the ventricular myocardial cell model does not exhibit spontaneous action potentials. When excitation does occur, due to an external stimulus, then, as for the Purkinje fibre cell model, the sodium current, i_{Na}, is primarily responsible for the rapid phase 0 depolarization. The early phase 1 repolarization is due to the continued activation of i_{si}. The plateau is determined by the antagonism between the outward currents, i_{K_1} and i_{x_1}, and the slow inward current, i_{si}. Individual current components are described in detail in the Appendix, A.4.

2.2.5 Control of Pacemaker Periodicity

Pacemaker cells from different regions of the heart have characteristically different intrinsic frequencies. For example, cells in the AV node have an inherent firing rate of $45-60$ cycles/min while Purkinje fibre cells have an intrinsic frequency between 20 and 40 cycles/min. In a healthy heart, all cells discharge at the intrinsic SA node frequency which is between 60 and 100 cycles/min. Furthermore, under pathological conditions, the heart rate can vary dramatically and cells can fire at frequencies as high as 650 cycles/min [6]. In order for the model of the heart to be able to accommodate such a wide variation, it was necessary to devise a means of altering the frequencies of the *spontaneous* cells of the model. The frequency of a particular cell is defined as the number of times per minute that its transmembrane potential crosses its threshold potential in

[2]In the original paper [1] the slow inward current is denoted i_s rather than i_{si}.

a depolarizing direction (Figure 1.1). The threshold potential for the ventricular myocardial and Purkinje fibre cells is -60 mV [1,28]. For the SA and AV node cells, the thresholds were estimated by analyzing the rate of change of the membrane potentials and were set at -30 mV for both.

Since most cells of the ventricular myocardium are *non*spontaneous [1,6], the model cell used for all simulations did not fire spontaneously. The Beeler and Reuter equations [1], as presented in the previous section, model such a nonpacemaker muscle cell. The resting membrane potential is constant at approximately −84 mV and remains at this value until some external stimulus of sufficient strength causes the cell's excitation. In contrast, the SA and AV node and Purkinje fibre cells are all spontaneous; therefore, each exhibits a wide range of oscillation rates. To model the behavior of a real SA node cell, 5 *model* SA node cells each having a different intrinsic frequency were created by altering certain constants in the SA node model equations. The frequencies of the 5 model cells were chosen to span a range which includes both the normal healthy range of oscillation rates for an SA node cell and a range of rates which commonly occur in pathological situations. Similarly, once the appropriate ranges had been determined for the frequencies of the AV node and Purkinje fibre cells, 5 model cells of each type, with intrinsic frequencies spanning those ranges, were created by altering the appropriate constants in the equations of both models.

SA node cells in a healthy adult heart typically have an oscillation rate which is between 60 and 100 cycles/min. Under certain pathological conditions this rate can increase dramatically; however, in the majority of cases the rate remains less than 200 cycles/min. Model SA node cells were created with intrinsic frequencies from approximately 80 to 180 cycles/min, a range which includes much of the normal and pathological behavior of an SA node cell. There are two currents primarily responsible for the pacemaker activity of the SA node cell: the potassium current, i_K, and the slow

Figure 2.1	$\overline{E_{\alpha_p}}$ (mV)	$\overline{E_{\beta_p}}$ (mV)	Frequency (cycles/min)	Period (msec)
(a)	-6.7	-65.0	79.65	753.25
(b)	-6.0	-62.0	100.08	599.53
(c)	-5.0	-58.0	119.42	502.44
(d)	-4.0	-49.7	149.63	401.00
(e)	-3.8	-39.0	178.26	336.58

Table 2.1: Parameter values and resulting frequencies for model SA node cells.

inward current, i_{si} [2,3]. The slow inward current is responsible for the relatively sharp upstroke in the action potential but contributes only during the last 30% of the time course (the latter part of phase 4 and phase 0) of depolarization. The decay of i_K, however, has a much longer time course, and is responsible for the preceding slow rise. Slight changes in the parameters, $\overline{E_{\alpha_p}}$ and $\overline{E_{\beta_p}}$ of i_K (A.17), produce a significant change in frequency. Figure 2.1 demonstrates the sensitivity of the cell frequency on the values of these parameters (Table 2.1). With $\overline{E_{\alpha_p}} = -6.7$ mV and $\overline{E_{\beta_p}} = -65$ mV (top trace) the frequency is 79.65 cycles/min. As both parameters are shifted to less negative potentials, the frequency increases (lower traces) and the action potential moves slightly upward on the voltage axis. The range of frequencies produced is typical of the range found in a human heart, where 80 cycles/min is a normal healthy rate for SA node cells and 180 cycles/min is representative of an arrhythmia known as sinus tachycardia.

In a normal heart, AV node cells have an intrinsic frequency which is slightly less than that of the SA node; therefore, to produce AV node cell models the five SA node models were modified to reduce their rate of spontaneous depolarization. Using the same adjustments in $\overline{E_{\alpha_p}}$ and $\overline{E_{\beta_p}}$ as for the model SA node cells, the maximum value of the slow inward current, i_{si}, was reduced in each by multiplying it by a constant fraction,

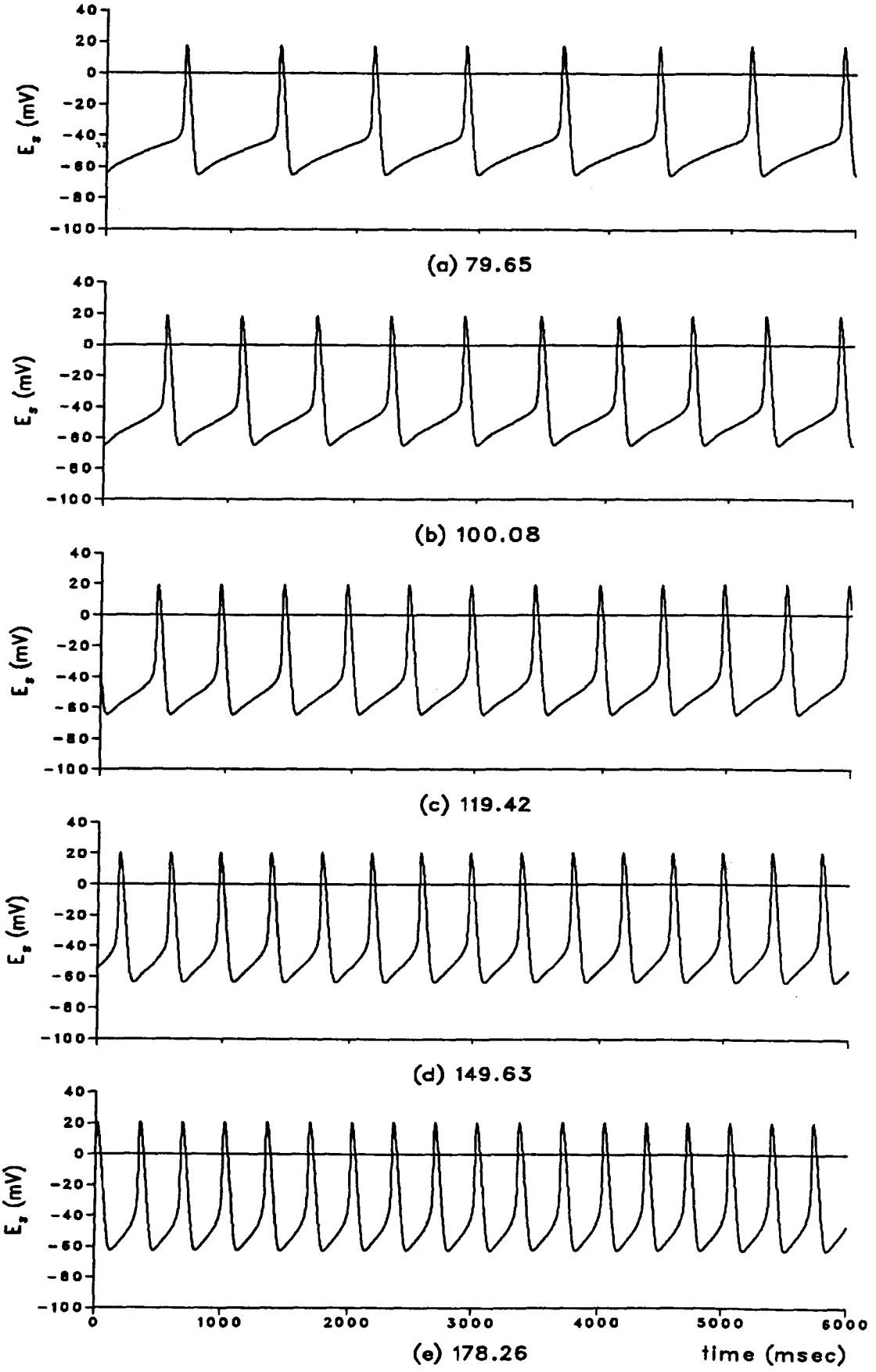

Figure 2.1: Model **SA node** cells (numbers indicate cell frequency in cycles/min).

Figure 2.2	$\overline{E_{\alpha_p}}$ (mV)	$\overline{E_{\beta_p}}$ (mV)	$\overline{i_{si}}$	Frequency (cycles/min)	Period (msec)
(a)	-6.7	-65.0	0.99	75.66	793.00
(b)	-6.0	-62.0	0.94	87.81	683.31
(c)	-5.0	-58.0	0.90	103.12	581.84
(d)	-4.0	-49.7	0.80	121.21	495.00
(e)	-3.8	-39.0	0.75	146.32	410.07

Table 2.2: Parameter values and resulting frequencies for model AV node cells.

$\overline{i_{si}}$. This is one of the methods used by Michaels et al. in their study of the interaction of SA node cells [30]. Table 2.2 lists the scaling values of $\overline{i_{si}}$ used and the resulting cell frequencies. Figures 2.2 a-e show the resulting action potentials which are modifications to the action potentials of Figures 2.1a-e, respectively. In the top trace, with $\overline{E_{\alpha_p}} = -6.7$ mV, $\overline{E_{\beta_p}} = -65$ mV, and $\overline{i_{si}} = 0.99$ the resulting reduction in i_{si} produces a model for an AV node cell with a period of 793 msec which is slightly longer than the 753.25 msec period of the corresponding SA node cell (Figure 2.1a). There is also a small decrease in the maximum membrane potential which accompanies the scaling of i_{si}. Similarly, lower traces show AV node cell models with intrinsic frequencies and maximum membrane potentials slightly less than that of the respective model SA node cells.

Purkinje fibre cells in a healthy adult heart have an intrinsic frequency between 20 and 40 cycles/min; however, this rate can increase significantly during many arrhythmias. Model cells with frequencies ranging from 40 to 120 cycles/min were produced by shifting the parameter, $\overline{E_k}$, of the pacemaker potassium current, i_{K_2} (A.34). Figure 2.3 shows the corresponding action potentials for the various values of $\overline{E_k}$ given in Table 2.3. In the top trace, with $\overline{E_k} = -54.7$ mV, the intrinsic period is 1506 msec. This corresponds to a firing frequency of approximately 40 cycles/min which is a typical

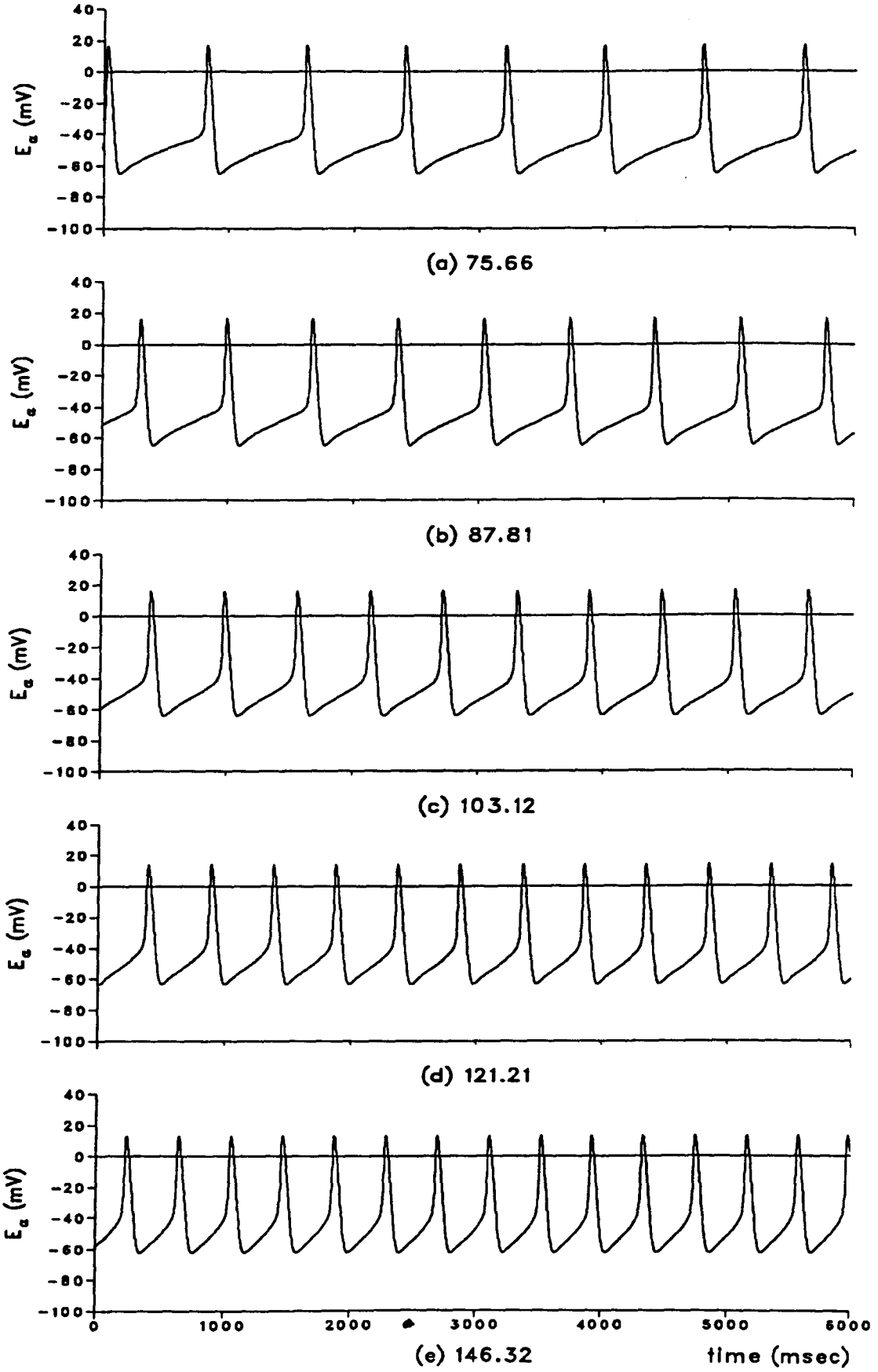

Figure 2.2: Model **AV node** cells (numbers indicate cell frequency in cycles/min).

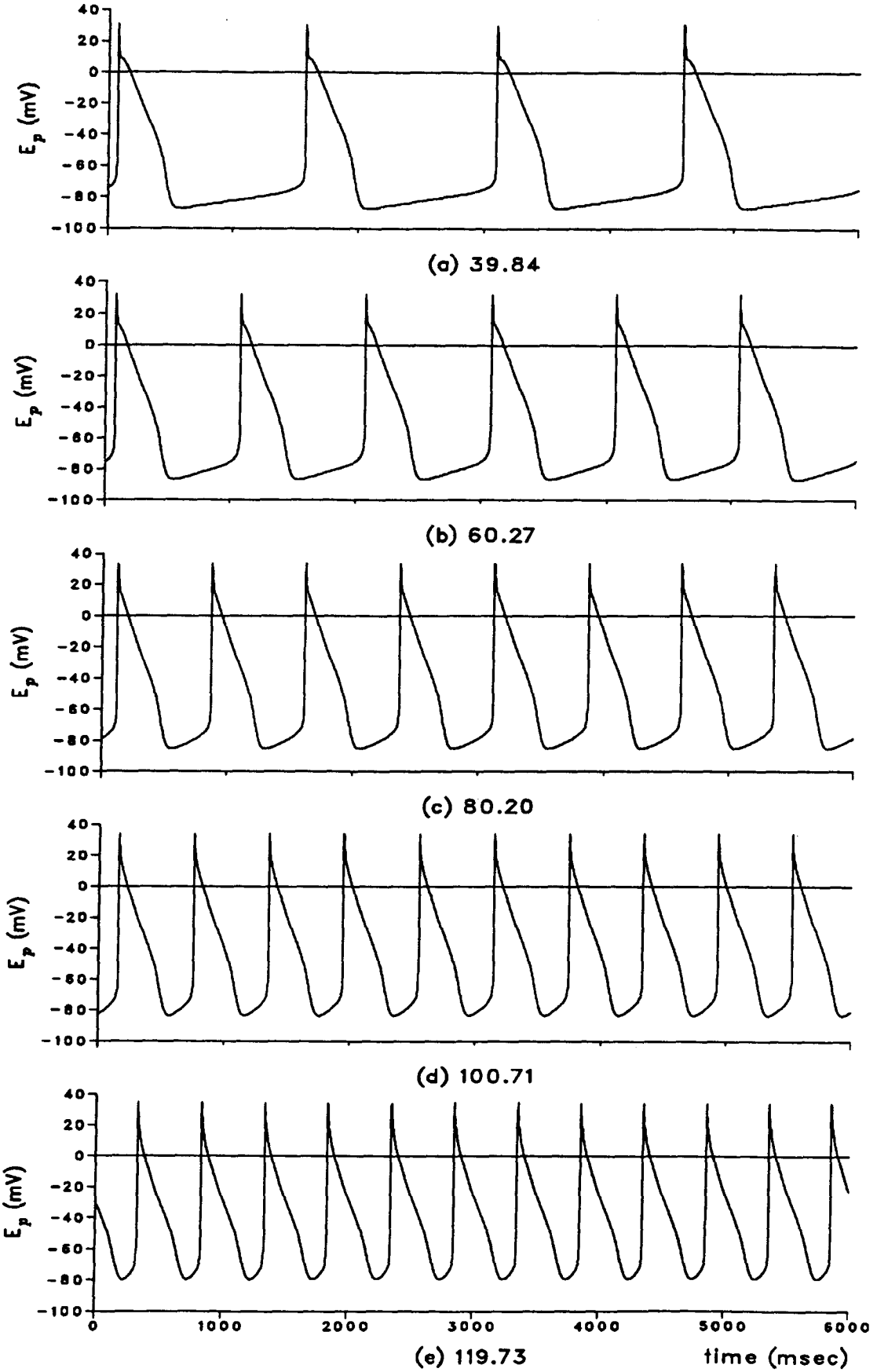

Figure 2.3: Model **Purkinje fibre** cells (numbers indicate cell frequency in cycles/min).

Figure 2.3	$\overline{E_k}$ (mV)	Frequency (cycles/min)	Period (msec)
(a)	-54.7	39.84	1506.00
(b)	-45.0	60.27	995.50
(c)	-35.0	80.20	748.13
(d)	-25.0	100.71	595.75
(e)	-15.0	119.73	501.11

Table 2.3: Parameter values and resulting frequencies for model Purkinje fibre cells.

value for a Purkinje fibre cell in a healthy human heart. As $\overline{E_k}$ is progressively shifted towards zero (lower traces) the frequency increases. As for the SA node cell, this increase is accompanied by a slight upward shift of the action potentials along the voltage axis. The five resulting models allow simulation of the electrical activity of Purkinje fibre cells with frequencies of approximately $40, 60, 80, 100$, and 120 cycles/min.

It should be noted that similar control of pacemaker periodicity can be obtained by the application of an external current to each of the models. A hyperpolarizing (outward) current decreases, while a depolarizing (inward) current increases, cell frequency [30].

2.3 Modelling Adjacent Cell Interaction

Action potentials propagate within the heart by moving from cell to cell over regions of close membrane association called *gap junctions* which exist between adjacent cells (Figure 2.4). These junctions provide a low resistance pathway through which electric current can easily flow [17,30,39].

To describe the interaction of two adjacent cells, cell i and cell j, it is assumed that coupling currents flow between the cells. For two neighbouring cells, these coupling currents simply describe the movement of action potentials over the gap junction between

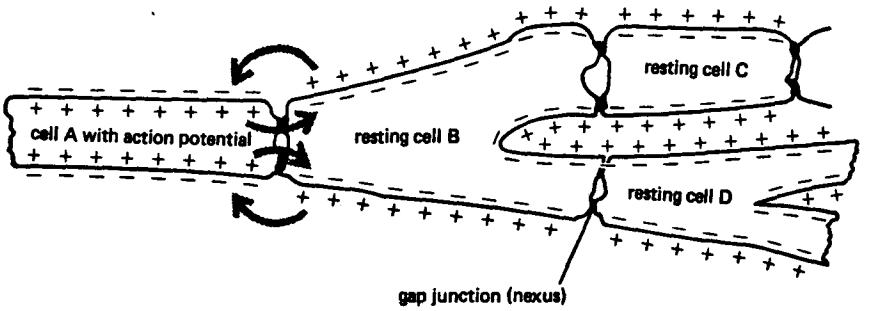

Figure 2.4: Schematic diagram depicting the flow of an action potential between two adjacent cells across a gap junction (taken from [17], p.20).

the cells. This gap junction constitutes the entire propagation path for impulses travelling in both directions; therefore, the influence of one cell on the other will be almost immediate. This influence of cell i on cell j is described by a coupling current, i_{c_j}, which is a function of intercell membrane conductance, g, and voltage difference as follows:

$$i_{c_j} = g\,[E_j(t) - E_i(t)]. \tag{2.9}$$

Similarly, the influence of cell j on cell i is given by:

$$i_{c_i} = g\,[E_i(t) - E_j(t)]. \tag{2.10}$$

These currents, (2.9) and (2.10), are included in the models for cell j and cell i, respectively, and integrated along with the other ionic currents. Also, (2.9) and (2.10) have the same magnitude but are of opposite sign implying that, for two adjacent cells, the same current that flows *out* of one cell flows *in* to the other. This is the form of the coupling currents employed in the previous studies by both Michaels et al. [30] and Lambert and Chay [5] where only *adjacent* cell interactions were modelled.

2.4 Modelling Nonadjacent Cell Interaction

Certain types of cardiac cells, e.g., an SA node cell and a Purkinje fibre cell, are never physically adjacent. Even two cells of the same type, such as two ventricular muscle

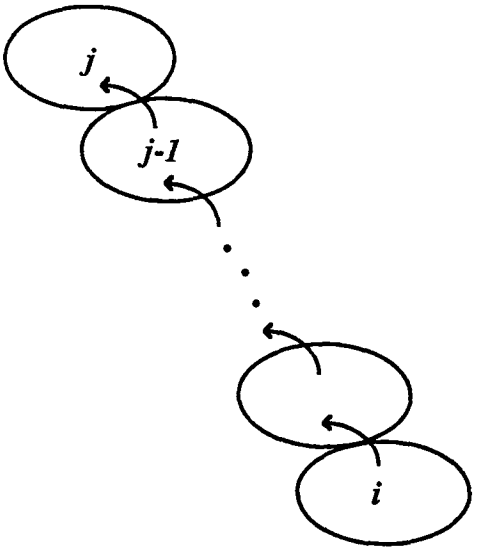

Figure 2.5: Schematic diagram depicting the flow of an action potential from cell i to cell j.

cells, may be located some distance from each other. For two such *nonadjacent* cells, cell i and cell j, the time required for action potential propagation between them will be significant relative to the duration of their action potentials. Furthermore, the path taken by an impulse from one to the other may not be the same as the path taken in the reverse direction. Consequently, in this case, the cells may not exert equal influences on each other and the coupling currents must be direction dependent.

An impulse originating at a particular cell, cell i, eventually reaches another distant cell, cell j, by travelling cell-to-cell crossing gap junctions over a path from cell i to cell j. Finally, the impulse will arrive at cell j from an adjacent cell denoted cell $j-1$ (Figure 2.5).

The coupling current flowing between the adjacent cells, cell $j-1$ and cell j, is analogous to (2.9) with subscripts changed and is described by:

$$i_{c_j} = g_{j-1,j}\,[E_j(t) - E_{j-1}(t)] \tag{2.11}$$

where $g_{j-1,j}$ is a constant representing the conductance in mS/cm^2 of the gap junction between cells $j-1$ and j.

In describing the influence of cell i on cell j it is the electrical activities of these two cells which are of concern in the model; therefore, the coupling current flowing between cell i and cell j should be expressed in terms of parameters describing only these two cells. In order to accomplish this, it is assumed that the impulse generated at cell i is not affected by its propagation to cell j or, in other words, that the membrane potential at cell i reaches cell j through cell $j-1$, after a finite amount of time, without a change in magnitude. Mathematically,

$$E_{j-1}(t) = E_i(t - \tau_{i,j-1})$$

where $\tau_{i,j-1}$ is a constant representing the time in msec required for the conduction of an impulse from cell i to cell $j-1$. With this assumption, (2.11) becomes:

$$i_{c_j} = g_{j-1,j}\,[E_j(t) - E_i(t - \tau_{i,j-1})]. \tag{2.12}$$

To remove any reference to cell $j-1$ in the above expression we let $g_{i,j} = g_{j-1,j}$ and $\tau_{i,j} = \tau_{i,j-1}$. With this new notation, $g_{i,j}$ should be interpreted as the conductance of the gap junction between cell j and the cell adjacent to it in the conductance path from cell i to cell j. Similarly, $\tau_{i,j}$ is the time required for an impulse to travel from cell i to the cell immediately preceding cell j along a path to cell j. Consequently, the coupling current which represents the influence of cell i on cell j can be written:

$$i_{c_j} = g_{i,j}\,[E_j(t) - E_i(t - \tau_{i,j})]. \tag{2.13}$$

This coupling current is included in the model for cell j and integrated along with the ionic currents. The governing equation for cell j, (2.5), becomes:

$$\frac{dE_j(t)}{dt} = -\frac{1}{C}\,(i_{ionic} + i_{c_j}) \tag{2.14}$$

with

$$i_{c_j} = \sum_i g_{i,j} \left[E_j(t) - E_i(t - \tau_{i,j})\right] \tag{2.15}$$

being the sum of coupling currents over all cells i which influence cell j.

This form of the coupling currents for modelling nonadjacent cell interaction is consistent with (2.9) for adjacent cells. For two adjacent cells, cell i and cell j, the gap junction between the cells constitutes the entire propagation path for impulses travelling in either direction; therefore, letting g be the conductance of this intercell membrane, the following is true:

$$g = g_{i,j}.$$

Furthermore, the impulse propagation times between the cells will be negligible; therefore, the following assumption can be made:

$$\tau_{i,j} = 0.$$

Then (2.13) which describes the influence of cell i on cell j becomes:

$$i_{c_j} = g \left[E_j(t) - E_i(t)\right]. \tag{2.16}$$

which is (2.9) given earlier.

2.5 Range of Coupling Conductances

Numerical computations of cell interaction were run over a range of coupling conductances from $g_{i,j} = 0$ mS/cm^2 (no coupling) to $g_{i,j} = 0.1$ mS/cm^2. Ypey [39], in a study of interactions between general cardiac cells uses a value of 0.003 mS/cm^2 for the maximum coupling conductance while Lambert and Chay [5] use values as high as 3.5 mS/cm^2 in coupling their simple 2-variable model cells. The upper limit used throughout this paper, $g_{i,j} = 0.1$ mS/cm^2, corresponds to a gap junction membrane

resistance of 10 $k\Omega/cm^2$ and is the value used by Michaels et al. [30] in their study of the interactions of SA node cells modelled using the same Yanagihara et al. equations [38] as are used here.

2.6 Propagation Time Delays

Propagation time delays appropriate to the types of cells coupled in a particular computation are incorporated into the coupling currents flowing between the cells. For example, for studies involving the influence of an SA node cell on an AV node cell, $\tau_{s,a}$ is assigned a value representative of the time required for impulse conduction from the SA node to the AV node. This is the time required for atrial depolarization which, according to Section 1.1.3, has an average value of between 80 and 120 msec in a healthy heart. Similarly, in a computation of normal behavior, $\tau_{a,p}$ might be assigned a value corresponding to the time required for the passage of an impulse through the AV node from which it emerges to the Purkinje fibre network. Under pathological conditions, such as with damaged tissue, the transmission times between different regions of the heart can be much longer than their average values and, in severe cases, the damaged tissue may create a blockage so that impulses are not conducted at all from one region to another. The propagation time delays can be chosen according to the particular situation being modelled.

Chapter 3

Phasic Interactions of Pacemaker Cells

3.1 Phase Resetting

When two pacemaker cells interact, impulses which originate at one cell may induce subthreshold depolarizations in another causing all subsequent action potentials of the latter cell to be advanced or delayed in comparison with its undisturbed oscillation [28,39]. These alterations, or phase shifts, in the rhythms of interacting cells are a prerequisite to entrainment and have been observed both experimentally and theoretically. Phase resetting has been demonstrated by Jalife and Antzelevitch [22] for rabbit SA node cells and by Guevara, Shrier, and Glass [13] for embryonic chick ventricular heart cell aggregates. Numerous computer simulations have also been done. Winfree [37] has studied phase resetting for a wide variety of biological oscillators. Michaels et al. [30] using the Yanagihara et al. [38] SA node cell model and McAllister, Noble, and Tsien [28] using their Purkinje fibre cell model have reproduced experimental results quite closely. These studies, however, have been based on the interactions of *similar adjacent* cells. For the present model, the phenomenon of phase resetting will be analyzed for various pairs of the three different types of pacemaker cells. Because these cells are not necessarily physically adjacent, the propagation time between them will be significant and the strength of the coupling will be direction dependent.

The effect of an incoming pulse on the cycle length of an oscillator depends not only on the intensity and duration of the stimulus but also on its timing. If the arrival of

the impulse occurs while the cell is in a refractory state, its next action potential will be delayed. If, on the other hand, the impulse arrives at a time when the membrane impedance is low, e.g., during phase 0 or the latter part of phase 4, then the subsequent action potential may be advanced. The arrival time of an impulse from one cell at another cell is determined by two factors: the relative frequencies of the cells and the impulse propagation time between them. In the remainder of this chapter, impulse propagation times will be systematically adjusted to study the effects of the arrival time of one cell's action potentials on the firing times of another cell.

When a relatively fast cell (one with a shorter period of oscillation) is coupled to a slower cell, more than one action potential of the fast cell will occur in each cycle of the slow cell. Therefore, to study the effects of a *single* action potential of one cell on the cycle length of another cell, the two cells were permitted to interact only during a single action potential phase (Figure 1.1) of the cell providing the stimulus. The action potential phase of a cell is defined as the period beginning when the membrane potential crosses its threshold value during phase 0 depolarization and ending when the potential first reaches its minimum value. For consistency, this type of *pulsed* coupling was also used for studies of the effects of slow cells on fast cells. *Continuous* coupling (the continuous interaction of cells from the time of onset of the stimulus to the end of the computation), however, probably reflects the true physical situation in a real heart more closely. Michaels et al. [30] consider the influence of one cell on another as consisting of two parts: the "phasic" influence during the action potential phase and the continuous or "tonic" influence over the period of phase 4 depolarizaton. Using both pulsed and continuous coupling to study phase resetting of SA node cells, they found that, qualitatively, the results were similar for both types of coupling and concluded that the entrainment phenonema observed during continuous coupling were "primarily a function of the phasic influence"...."of one pacemaker on the activity of the other". The

primary method of coupling in this chapter will be pulsed coupling although continuous coupling will also be done to compare results.

3.2 Methods

To study the effects of a single action potential of model cell i on the intrinsic cycle length of model cell j, the cells were coupled as follows. First, the influence of j on i was eliminated, i.e., the conductance $g_{j,i}$ was set to zero so that no coupling current would flow from j to i. Thus i would oscillate unperturbed. On the other hand, the coupling conductance $g_{i,j}$ was maintained at a sufficiently high value during the action potential phase of i and set equal to zero otherwise. This achieved the desired pulsed coupling. The propagation time $\tau_{i,j}$ was then adjusted in steps so the action potential of i was 'felt' at different times, or phases, ϕ_j within a cycle of j. A cycle of j begins from the peak or maximum potential of one action potential and ends with the peak of the subsequent action potential. The phases, ϕ_j, were measured relative to the time corresponding to the peak of the first action potential of the perturbed cycle of j. Denoting this time by t_j and the time at which the potential of i crosses its threshold value by $t_{i_{threshold}}$, the phase ϕ_j satisfies:

$$\phi_j = (t_{i_{threshold}} + \tau_{i,j}) - t_j \qquad \text{where } 0 \leq \phi_j \leq T_j.$$

Figure 3.1 indicates the terminology used to describe phase interactions and shows an action potential of i which causes an abbreviation of the perturbed cycle of j. Computations were caried out for numerous values of the propagation time $\tau_{i,j}$ such that the resulting phases ϕ_j assumed values ranging from 0 to T_j, the intrinsic cycle length of j ($\phi_j = 0$, indicates that the action potential of i reached j at exactly the time, t_j, corresponding to the peak of the first action potential of the perturbed cycle of j). In this way the effect of the arrival of an action potential from i at *any* time within a cycle

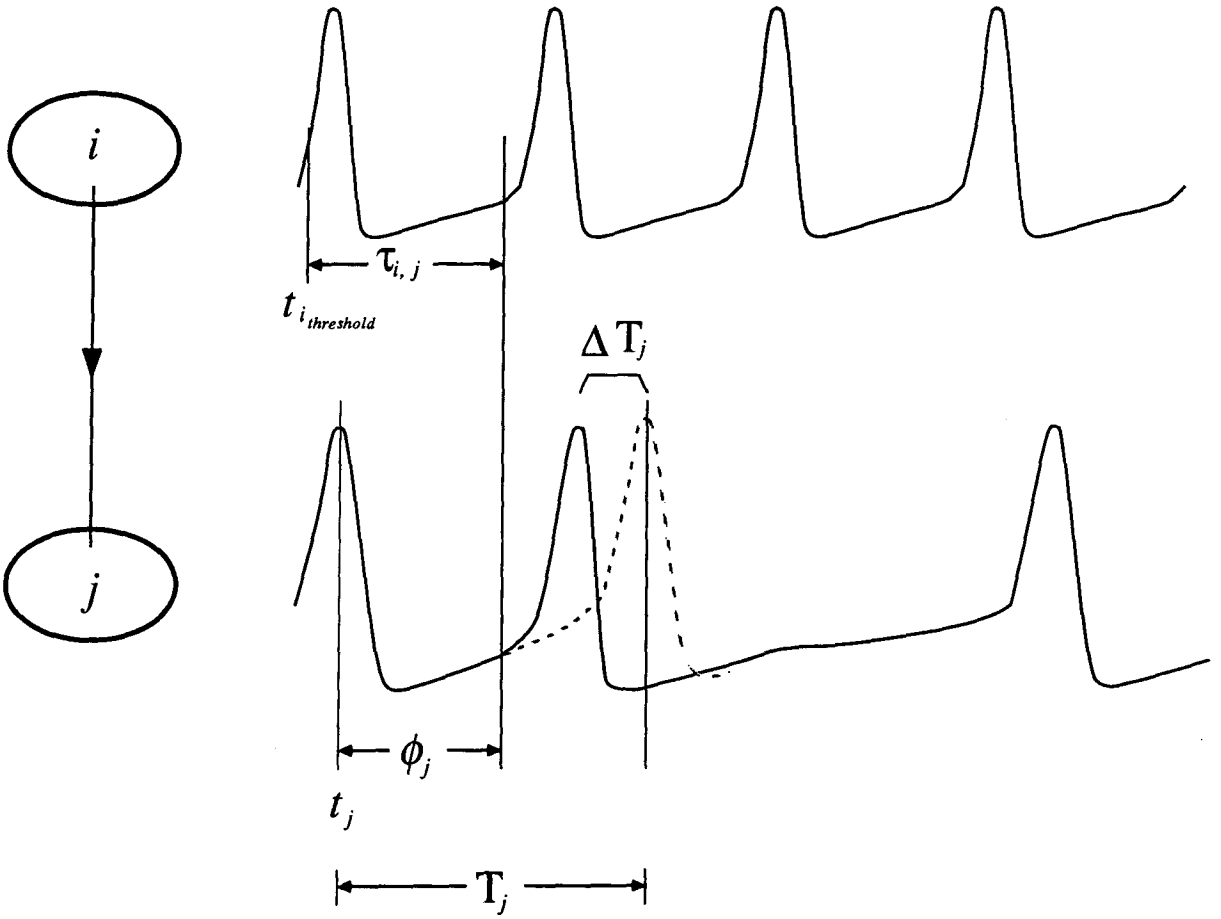

Figure 3.1: Terminology used to describe the influence of an action potential of cell i on cell j. Schematic on left shows unidirectional coupling from i to j. Dashed trace indicates control action potential (no interaction). Solid traces indicate activity when cells are coupled. Cell i oscillates unperturbed and stimulates cell j causing its second action potential to be advanced. Terminology used for delays (not shown) is analogous.

of j could be analyzed. After each computation, it was possible to scan the cycle in which the stimulus occurred and measure the phase shift ΔT_j in the cycle length. These phase shifts were measured as the perturbed cycle length minus the intrinsic length; therefore, a positive phase shift (positive ΔT_j) corresponds to a delay while a negative phase shift (negative ΔT_j) corresponds to an advance in the occurrence of the subsequent action potential of j. The shifts ΔT_j were then plotted against ϕ_j (where both were expressed as percent of the intrinsic cycle length, T_j) in what is known as a phase response curve (PRC). Some sample PRCs were obtained for various values of coupling conductances between different types of cells with different intrinsic cycle lengths. The coupling conductance values were chosen from the range of conductances of this study (0.0-0.1 mS/cm^2) and were sufficiently high to cause a measurable phase shift in the perturbed cell's cycle length.

3.3 An SA Node Cell and a Purkinje Fibre Cell

Although in a real heart an SA node cell is never physically adjacent to a Purkinje fibre cell, the activity of one may affect the activity of the other through the cell-to-cell propagation of impulses. With the present model, this type of interaction is studied by the incorporation of propagation time delays in the coupling currents flowing between the cells. This form of coupling and the method of the preceding section were used to study the phasic interactions of a model SA node cell (s) and model Purkinje fibre cell (p). The intrinsic periods of the cells were $T_s = 599.53$ msec and $T_p = 748.13$ msec which correspond to frequencies of approximately 100 and 80 cycles/min, respectively. These values represent a normal healthy oscillation rate for an SA node cell and a significantly high oscillation rate for a Purkinje fibre cell. This is a situation which is common in arrhythmias such as ventricular tachycardia and fibrillation.

The phase response curves of Figure 3.2 summarize, for two different values of the coupling conductance $g_{p,s}$, the effects of an action potential of p on the cycle length of s. Although PRCs were obtained for several values of $g_{p,s}$, only two have been included. These PRCs use values of $g_{p,s}$ which are large enough to induce measurable phase shifts in the cycle of s and produce PRCs which demonstrate, by the differences in their shapes, the effect of the coupling conductance. For $g_{p,s} = 0.005$ mS/cm^2, the PRC shows that action potentials from p which arrive during approximately the first one-third of the cycle of s cause a delay, whereas those which arrive later cause an advance of the subsequent firing of s. When the coupling conductance was decreased to $g_{p,s} = 0.002$ mS/cm^2 the shape of the PRC was maintained. Also, during this first one-third of the cycle of s where *both* curves indicate delays (positive $\Delta\ T_s$), they are less for the case of coupling with the smaller conductance. Similarly, where both curves show advances, the magnitudes of the phase shifts are less for weaker coupling. These results are expected, since with decreased conductance, p has less influence on the cycle length of s. For this reason also, with the smaller conductance, delays occur over a larger portion of the cycle (up to 40%). With the larger value of $g_{p,s}$, an action potential of p is able to cause an advancement of the excitation of s, but a weaker stimulus still may cause only subthreshold depolarizations. These subthreshold depolarizations do not excite the cell and are followed by a period of repolarization to a more negative membrane potential from which the increase to the threshold value must begin again. The time required for this depolarization and subsequent repolarization delays the occurrence of the next action potential of s. Conversely, a stronger stimulus will be capable of exciting s while it is relatively more refractory which occurs early in its peak-to-peak cycle, thus advances occur for lower ϕ_s with a larger conductance.

The lower graph of Figure 3.2 shows the membrane potential of s plotted as a function of percent of its intrinsic cycle length over a complete peak-to-peak cycle prior to

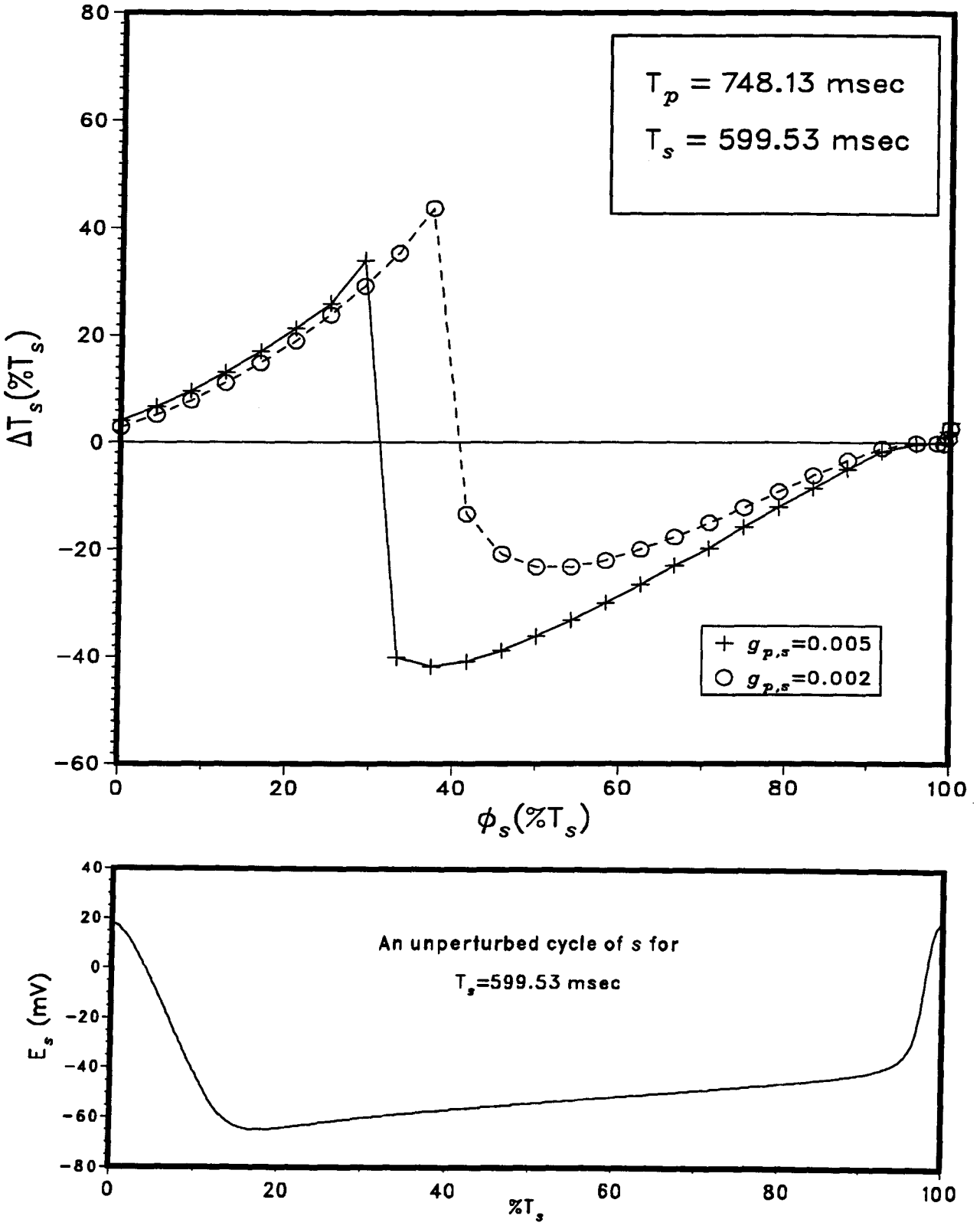

Figure 3.2: Upper graph shows phase response curves summarizing the effects of a single action potential from p on the cycle length of s for two values of $g_{p,s}$ (mS/cm^2). Lower graph shows the intrinsic electrical activity of s over a complete peak-to-peak cycle.

coupling. This plot provides a means of associating the cell's intrinsic electrical activity with any value of ϕ_s of the corresponding PRC. For example, it is clear that for both values of $g_{p,s}$ the earliest phase advance of the action potential of s does not occur until s is undergoing phase 4 depolarization and membrane impedance is low.

For the same two model cells, the PRCs of Figure 3.3 demonstrate the effect of an action potential of s on the cycle length of p for two values of the coupling conductance $g_{s,p}$. As for the previous case, PRCs were obtained for several values of $g_{s,p}$, however, only two have been included. The values shown are sufficiently high that, in both cases, s induces a measurable influence on the cycle length of p, yet the effects are different enough in each case to demonstrate the effect of the coupling conductance on the shape of the PRC. Again, for smaller conductance, corresponding to a decrease in the influence of s on p, the general shape of the PRC is maintained and, where either both curves show delays or both show advances, the corresponding phase shifts are smaller in magnitude for the smaller value of $g_{s,p}$. Also, as in the preceding case with stronger coupling, delays occur over a smaller portion of p's cycle because the larger the conductance, the more easily and the earlier in p's cycle an action potential of s can cause the advancement of a subsequent action potential of p. Comparing the electrical activity of p (lower graph of Figure 3.3) at various phases to its PRC indicates that the largest phase delays occur during phase 3 repolarization when the cell is in a highly refractory state following its excitation. Furthermore, the transition from maximal delay to maximal advance occurs near the end of phase 3 repolarization and beginning of phase 4 depolarization when the refractory period comes to an end. Action potentials of s arriving early in p's cycle, at a time corresponding to the initial rapid rate of repolarization from the peak (phase 1), cause slight delays. McAllister, Noble, and Tsien [28] suggest that these delays might be due to a delayed repolarization. Following this region, there is an interval over which the rate of decrease in the membrane potential of p lessens and during which a stimulus

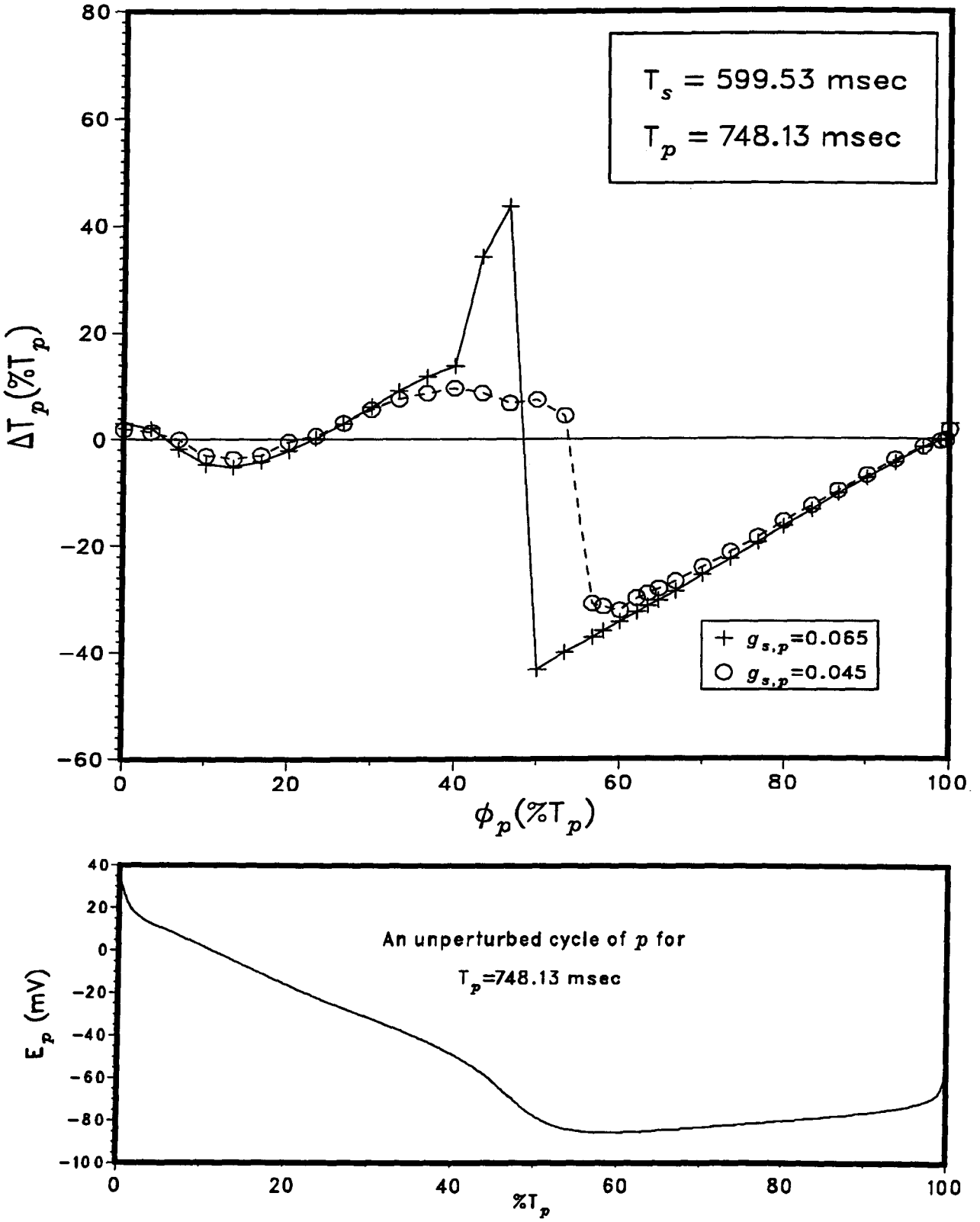

Figure 3.3: Upper graph shows phase response curves summarizing the effects of a single action potential from s on the cycle length of p for two values of $g_{s,p}$ (mS/cm^2). Lower graph shows the intrinsic electrical activity of p over a complete peak-to-peak cycle.

from s causes slight advances. The magnitude of these phase shifts which occur early in p's cycle are small, in agreement with the fact that a cardiac cell is most immune to stimulii immediately after excitation when it is in its absolute refractory state.

The biphasic response curves obtained here are similar in shape to those obtained experimentally by, amongst others, Jalife et al. [22] and numerically by Michaels et al. [30]. When either p stimulates s or vice-versa, the resulting PRCs (Figures 3.2, 3.3) demonstrate that, as the interaction between the cells is strengthened by increasing the coupling conductance, the transition from maximal delays to maximal advances occurs over a narrower range of phase values. This behavior was also found experimentally by Guevara et al. [13] for embryonic chick ventricular heart cells. When aggregates of these cells were stimulated by increasingly strong current pulses, the transition from maximal delay to maximal advance occurred much more abruptly.

3.4 An SA Node Cell and an AV Node Cell

Phase response curves were also obtained for the case of interaction between an SA node cell (s) and an AV node cell (a) where the same model SA node cell with an intrinsic oscillation period given by $T_s = 599.53$ msec as in the preceding simulations was used and coupled to a model AV node cell with $T_a = 793.00$ msec. These cycle lengths correspond to frequencies of approximately 80 and 75 cycles/min, respectively and represent normal rates for healthy SA node and AV node cells. The PRC of Figure 3.4 summarizes the effects of an action potential of s on the intrinsic cycle length of a for $g_{s,a} = 0.05$ mS/cm^2 while the PRC of Figure 3.5 demonstrates, for the same two cells and $g_{a,s} = 0.05$ mS/cm^2, the effects of the excitation of a on the cycle length of s (this value of the coupling conductances is one of several values which causes measurable changes in the perturbed cell's cycle length and for which PRCs were obtained). The PRCs are almost identical

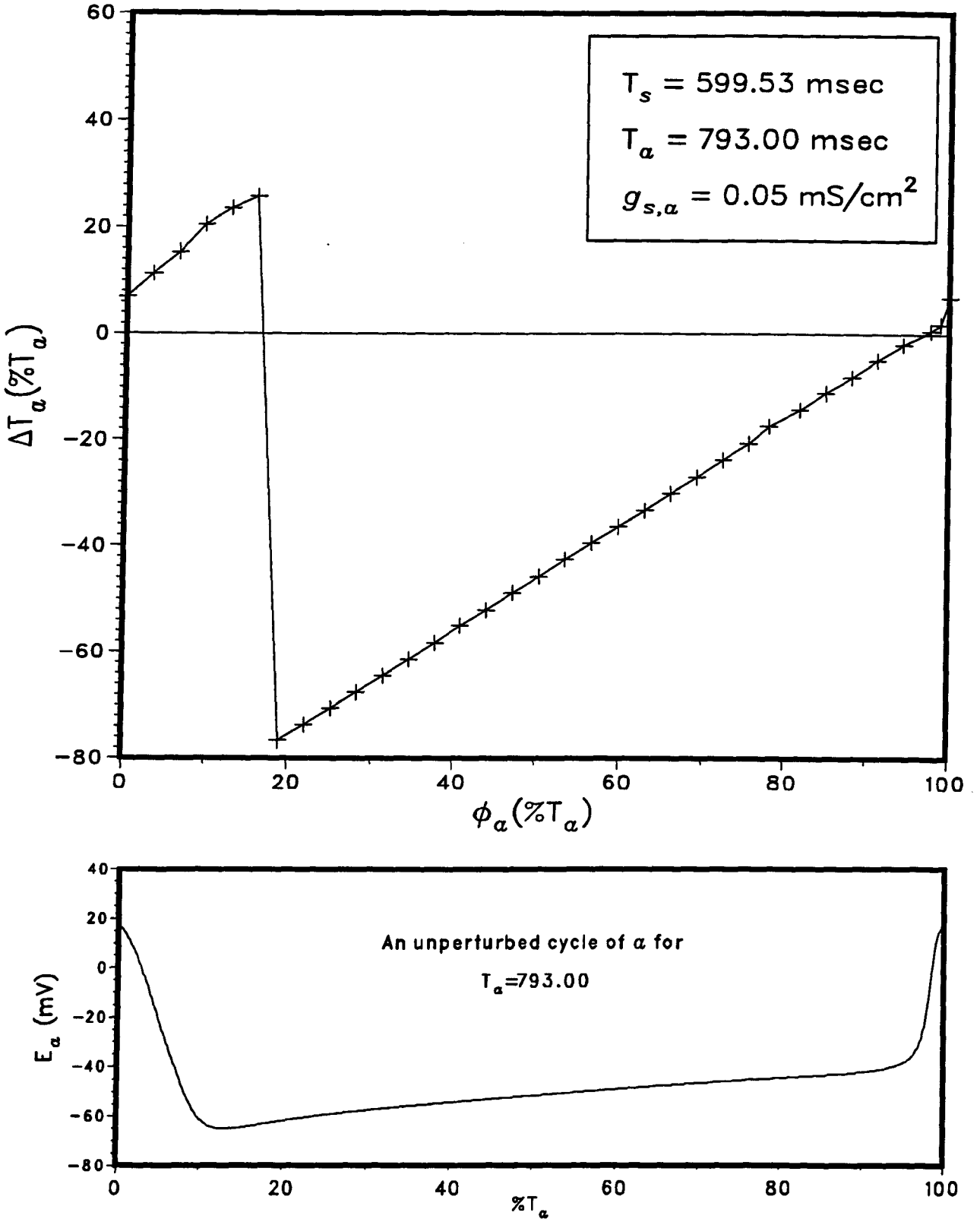

Figure 3.4: Upper graph shows phase response curve summarizing the effects of a single action potential from s on the cycle length of a. Lower graph shows the intrinsic electrical activity of a over a complete peak-to-peak cycle.

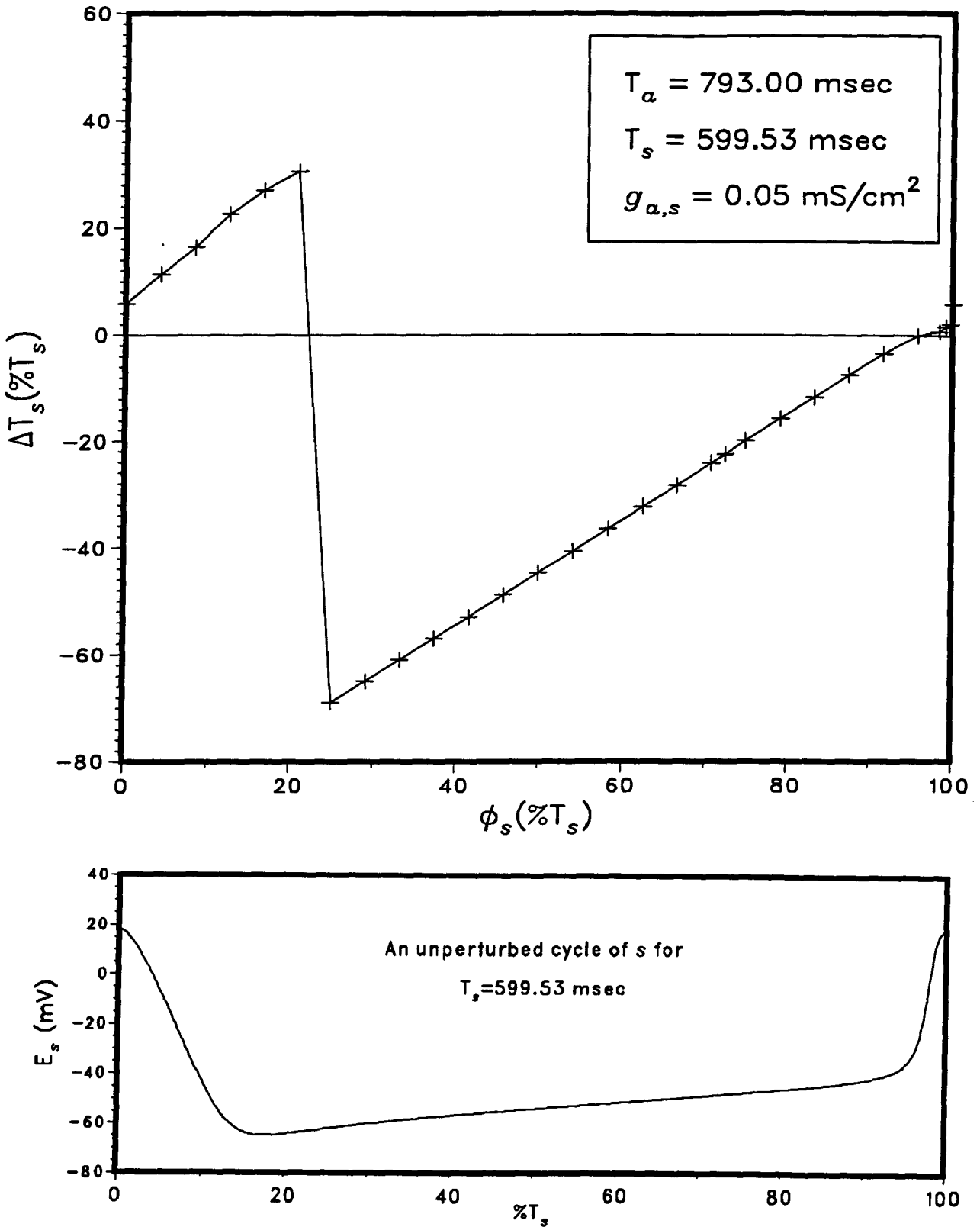

Figure 3.5: Upper graph shows phase response curve summarizing the effects of a single action potential from a on the cycle length of s. Lower graph shows the intrinsic electrical activity of s over a complete peak-to-peak cycle.

in shape. This is not unexpected since, except for the slower rate of depolarization of the AV node cell, the action potentials of the two cells are very similar (Figure 1.2). In both cases, discharges arriving early prolong, while those arriving later shorten, the cycle in which the stimulus occurs. As for the preceding PRCs, the transition from delay to advance occurs early in the phase 4 depolarization portion of the cycles in both cases. A further observation is that Figure 3.5 which shows the effects of the action potentials of a on s is very similar to Figure 3.2 which shows the effects of action potentials of p on s. This indicates, as one would expect, that the source of the stimulus is not as important in determining the form of the resulting PRC as the type of cell being stimulated.

3.5 Fast and Slow Cells

Previous studies [30,39] have obtained phase response curves showing that slower cells were much more affected by depolarizing currents than faster cells and that the phase shifts induced in a slow cell by a faster cell were always greater than those induced in the fast cell by the slower cell. These studies also indicated that the common entrained period for coupled fast and slow pacemakers firing in synchrony was always closer to the intrinsic period of the fast cell than of the slow cell. Thus, the changes in cycle length and subsequent phase shifts of the PRC were necessarily greater for the slower cell. These results; however, were obtained for *similar* cells coupled using *adjacent*-cell-coupling (Section 2.3) where the same current flowing *out* of one cell flows *in* to the other. For the present model, which allows the coupling of nonadjacent cells, the coupling currents flowing between the cells are direction dependent and are characterized by values of the coupling conductances and propagation time delays. The PRCs obtained here indicate that, with this direction dependent coupling, the phase shifts are not necessarily greater for the slower cell.

Comparing Figure 3.2 with Figure 3.3 reveals that the maximal advance of the slower Purkinje fibre cell (p) may be larger or smaller than the maximal advance of the faster SA node cell. Similarly, the maximal delay of p may be greater or less than the maximal delay of s. The shape of the PRCs, and subsequently the cell which shows the greater phase shifts, is dependent on the values of the conductances $g_{p,s}$ and $g_{s,p}$. Thus, either cell can exert the larger influence.

Behavior similar to that of previous studies *was* obtained when a particular cell with a fixed period was coupled to another cell whose period of oscillation was then altered. As an example, Figure 3.6 shows the phase dependent effects of an action potential of an SA node cell on the cycle lengths of two Purkinje fibre cells, one with a period of 748.13 msec and the other with a period of 995.50 msec. The coupling conductance $g_{s,p}$ remained constant at 0.065 mS/cm^2, a value that is sufficiently high that action potentials at s were able to cause measurable phase-shifts in p's cycle in both cases. At any given phase, the phase shifts are greater in magnitude for the slower Purkinje fibre cell. Furthermore, both the maximal delay and maximal advance are greater for the slower cell (although the maximal delays of the two cells differ only very slightly).

3.6 Phase Response Curves and Zones of Entrainment

The phase response curve gives some insight into the synchronization properties of an excitable cell oscillator since it determines the limits of the zones of stable entrainment for unidirectional coupling [39]. An action potential of one pacemaker can only advance or delay an action potential of another cell by a maximum amount indicated by the PRC. If the periods of the two oscillators differ by more than the maximum possible phase shift, the cells will not be entrained to a common frequency. For example, if a relatively fast cell is providing the stimulus to a slower cell and the corresponding PRC

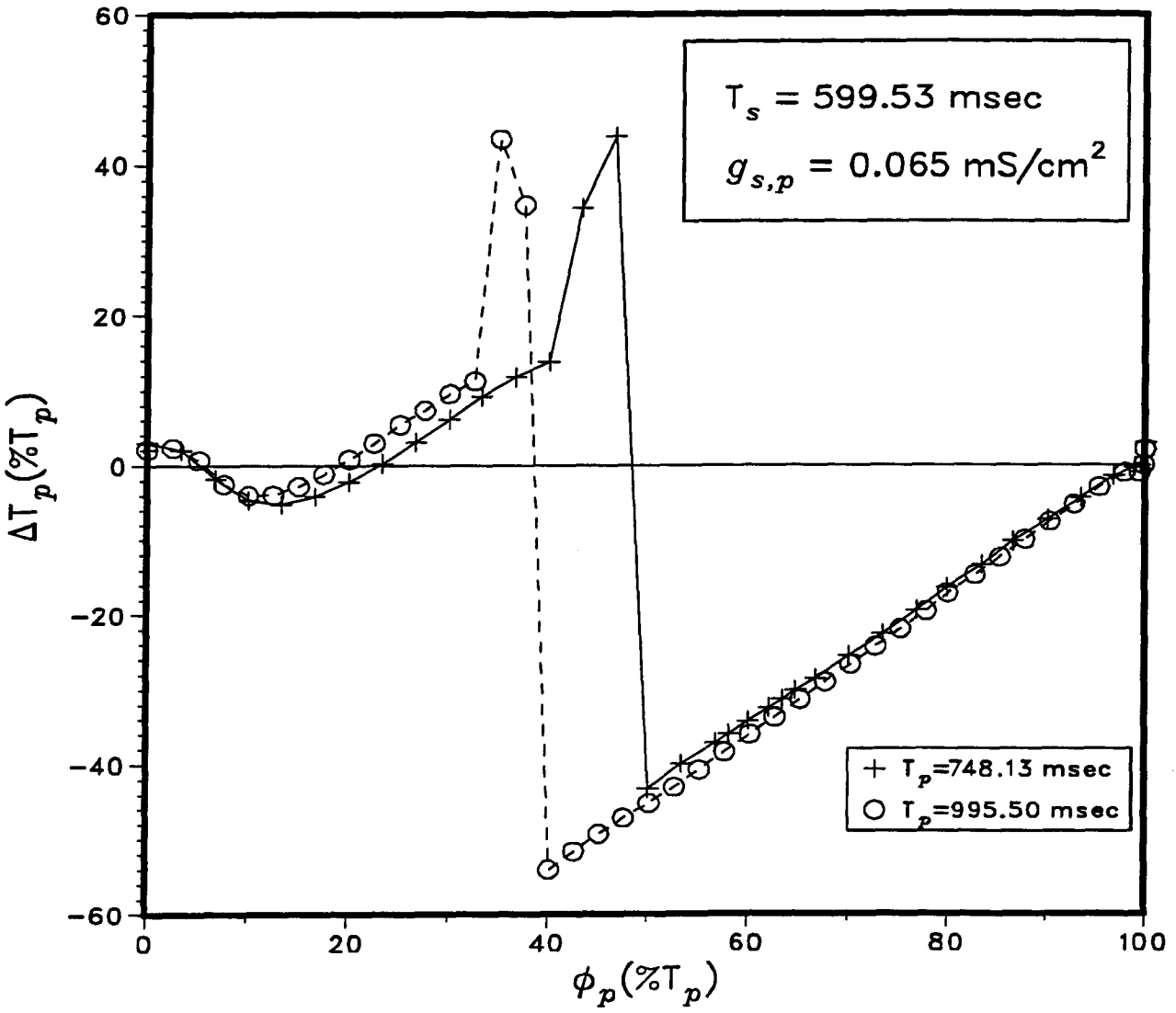

Figure 3.6: Phase response curves summarizing the effects of a single action potential from s on two different Purkinje fibre cells with periods as shown.

predicts that the maximal advance of the slower cell is less than the difference in the cycle lengths of the cells then the slow cell cannot be entrained to beat synchronously to the fast cell. Thus, a phase response curve provides a means of determining bounds on the cycle lengths of the cells for which entrainment can occur.

3.7 Pulsed versus Continuous Coupling

When pacemaker cells of the heart interact, the interaction is not restricted to the action potential phase. Consequently, the pulsed coupling used in obtaining the preceding PRCs does not reflect the true physiological situation. However, it was mentioned earlier that previous studies have concluded that the phasic interactions during an action potential were most important in determining the ultimate shape of the phase response curve and, therefore, the ultimate rhythm of coupled cells. This section will investigate some of the differences in PRCs obtained under conditions of pulsed and continuous coupling. Continuous coupling refers to a simulation allowing the interaction of the cells from the time of onset of the stimulus until the occurrence of the subsequent action potential of the perturbed cell at which time the computation was usually terminated.

Figure 3.7a shows the phase shifts induced in an SA node cell with period $T_s = 599.53$ msec due to continuous stimulation by a Purkinje fibre cell with period $T_p = 748.13$ msec. The coupling conductance used was $g_{p,s} = 0.005$ mS/cm^2. This value of $g_{p,s}$ and the same two cells were also used to obtain one of the PRCs shown in Figure 3.2 under conditions of pulsed coupling. Qualitatively, the results are similar in both cases. The general shape of the PRCs is the same with delays occurring for action potentials arriving early and advances occurring for action potentials arriving late in the cycle of s. The striking similarity between the PRCs is expected because the slower Purkinje fibre cell fires only once during any cycle of the faster SA node cell and coupling only during

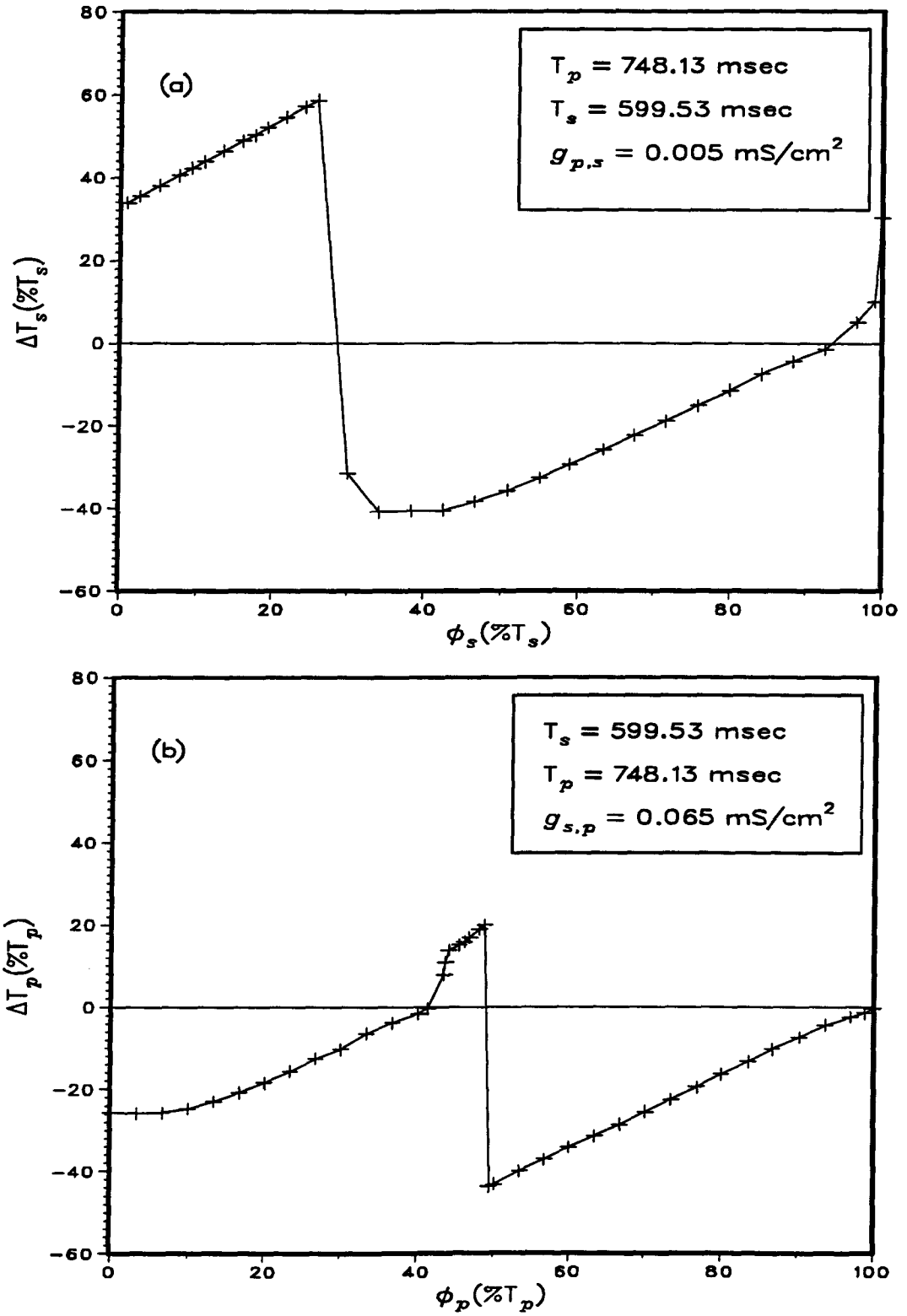

Figure 3.7: Phase response curves summarizing the effects of p on s (a) and s on p (b) under conditions of continuous coupling.

the action potential phase of p simply eliminates the remaining weaker influence during phase 4 depolarization. Quantitatively, there are differences in the results obtained under conditions of pulsed and continuous coupling. Although the portion of the curves showing advances are almost identical, the delays are greater in magnitude for the case of continuous coupling. This is due to the continuous 'pull' of the slower Purkinje fibre cell on the faster SA node cell during phase 4 depolarization.

When a fast cell provides the stimulus for a slower cell, the results obtained for the two methods of coupling are somewhat different. Figure 3.7b shows, for the same SA node and Purkinje fibre cells, the effects of the activity of s on the cycle length of p under conditions of continuous coupling. The corresponding PRC obtained using pulsed coupling is shown in Figure 3.3 with $g_{s,p} = 0.05$ mS/cm^2. As in the previous case, the portion of the curves after the transition from delay to advance are almost identical. However, for small values of ϕ_p the PRCs are quite different. When the coupling is continuous the cycle length of p is significantly shortened, whereas under pulsed coupling the phase shifts were small for small values of ϕ_p. These advances which occur for continuous coupling are due to the fact that if an action potential of the faster cell (s) arrives early in p's cycle then a second action potential will also arrive within the same cycle of p. In addition, since $T_s = 599.53$ msec and $T_p = 748.13$ msec this second action potential of s will occur for $\phi_p > 80\%$, at a time when p is in the latter stages of phase 4 depolarization and membrane impedance is low. Consequently, the firing of p will be advanced in comparison to its unperturbed oscillation. A further observation is that the phase delays under continuous coupling are smaller due to the 'pull' of the faster SA node cell during phase 4 of its cycle than under conditions of pulsed coupling.

Chapter 4

Behavior of a Healthy Heart

4.1 Activation of a Nonspontaneous Cell

Under normal conditions muscle cells of the ventricles are not capable of spontaneous depolarization. These cells are excited by action potentials which are initiated by pacemaker cells and arrive through neighbouring Purkinje fibre cells (Figure 4.1) or other muscle cells. Since Purkinje fibre cells are spontaneous they can act as independent pacemakers and fire at their own intrinsic frequencies or they can fire in response to the activity of another pacemaker site. Figure 4.2 demonstrates the activation of a ventricular myocardial cell (v) by an adjacent Purkinje fibre cell (p) with an intrinsic period of 748.13 msec (approximate frequency of 80 cycles/min). This period represents an approximate frequency of 80 cycles/min, a rate which is above the normal range of frequencies of healthy Purkinje fibre cells; however, the results are qualitatively similar to results obtained for several other values of the Purkinje fibre cell period which were within the normal range. Results are shown only for the shorter period (748.13 msec) in order that a shorter time scale can be used to demonstrate the behavior of the two cells. Because the two cells are contiguous, the action potential propagation time between them is negligible and the conductance path is simply the intercell membrane (Section 2.3); therefore, the following are assumed:

$$\tau_{p,v} = \tau_{v,p} = 0,$$

$$g_{p,v} = g_{v,p}.$$

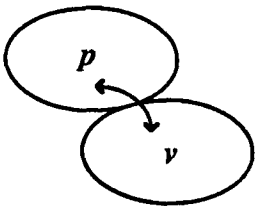

Figure 4.1: Schematic representation of the interaction of a Purkinje fibre cell (p) and an adjacent ventricular myocardial cell (v). Arrows indicate flow of coupling current between cells.

Letting $g = g_{p,v} = g_{v,p}$, the coupling current added to the model for the Purkinje fibre cell is analogous to (2.9) and is, therefore, given by:

$$i_{c_p} = g\,[E_p(t) - E_v(t)].$$

The negative of this current is added to the muscle cell model to describe the influence of the pacemaker cell.

When there is no interaction between the cells, $g = 0$ (Figure 4.2a), the nonpacemaker ventricular myocardial cell is completely silent. Its membrane potential remains at its rest value of approximately -84 mV while the Purkinje fibre cell fires independently at its own rate. When the coupling is weak (Figure 4.2b) subthreshold responses are induced in the muscle cell. These responses grow in amplitude with increased coupling strength. With still stronger coupling, each cell influences the other in such a way that a form of arrhythmia develops. Under these circumstances entrainment may occur as in (Figure 4.2d) where, for every 2 cycles of the Purkinje fibre cell there is 1 cycle of the muscle cell so that a 2:1 ratio exists between the frequencies of the cells. When the coupling is strong enough, the cells beat synchronously (Figure 4.2e); however, the action potential of the ventricular myocardial cell is slightly delayed and continues to differ in shape from the action potential of the Purkinje fibre cell. With further increases in g, the delay gradually disappears, the nonspontaneous cell begins to exhibit phase 4

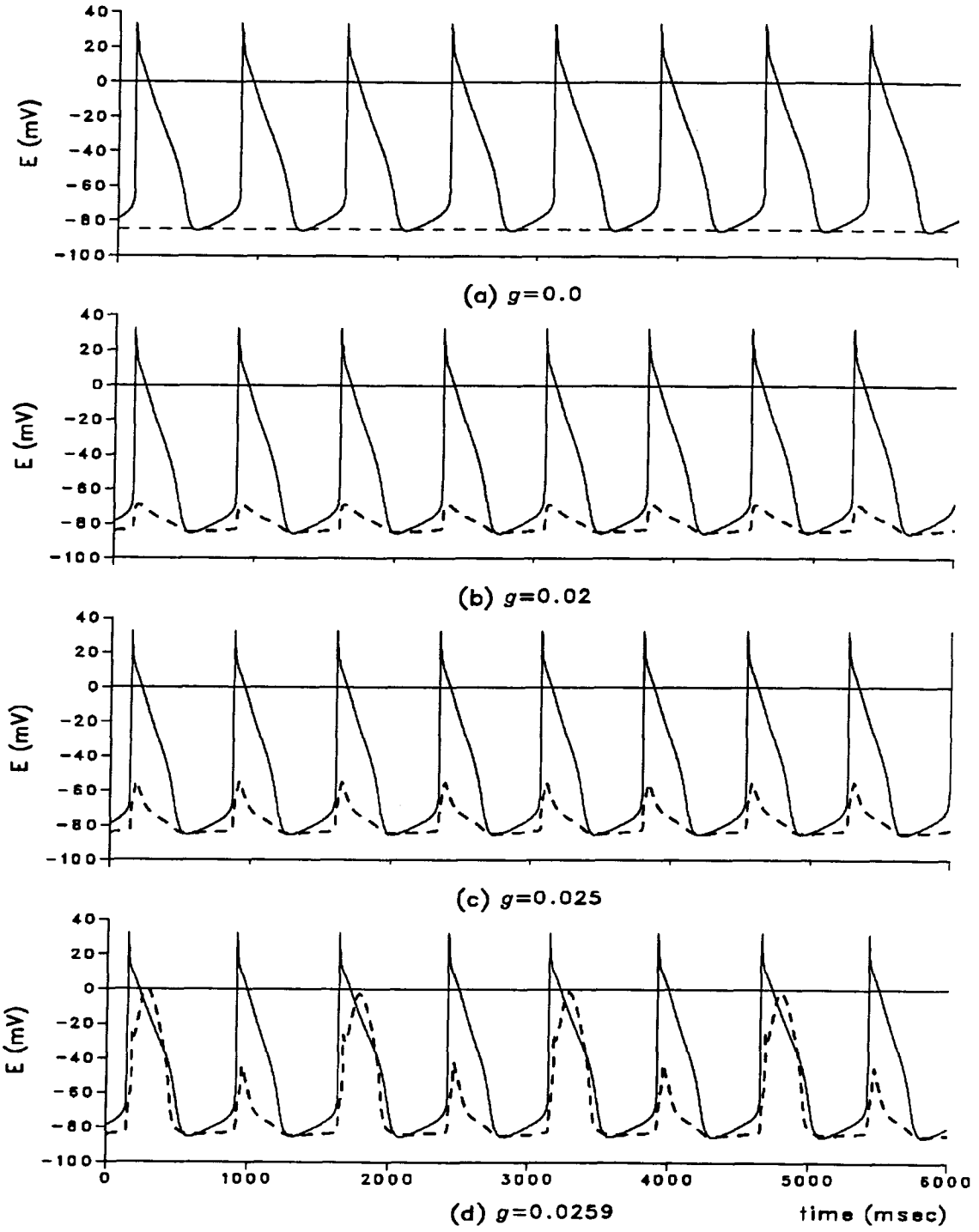
E (mV)
40
20
0
-20
-40
-60
-80
-100
(a) g=0.0
(b) g=0.02
(c) g=0.025
(d) g=0.0259
0
1000
2000
3000
4000
5000
6000
time (msec)

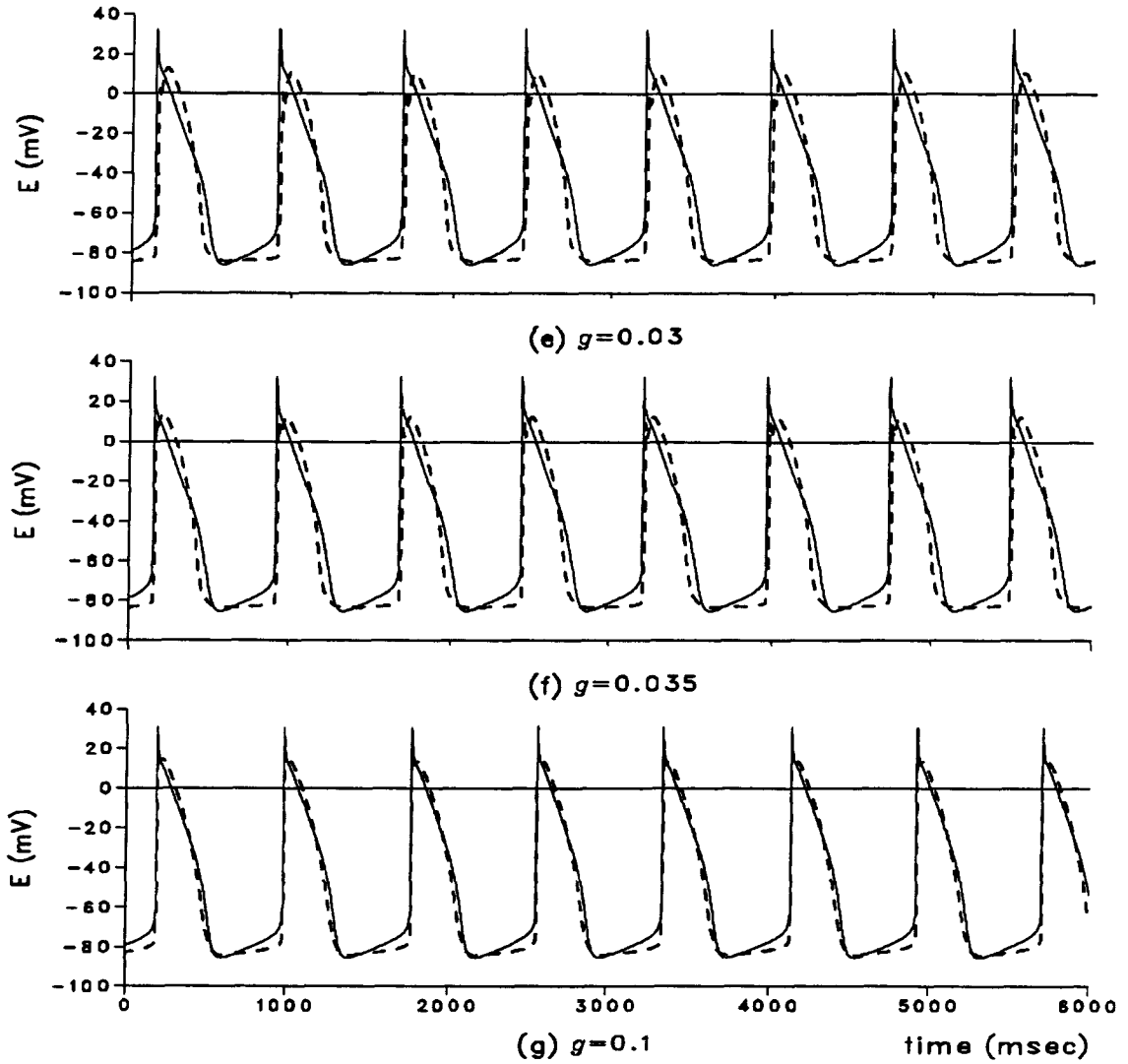

Figure 4.2: Transmembrane potentials of a Purkinje fibre cell (solid trace) and a ventricular myocardial cell (dashed trace) for increasing values of the coupling conductance g (mS/cm^2).

depolarization of its resting membrane and the action potentials of the two cells become increasingly similar (Figure 4.2f).

While the changes in cycle length which accompany the increases in coupling strength are not as pronounced for the Purkinje fibre cell as for the nonspontaneous muscle cell, they are significant. Figure 4.3 shows the period of oscillation of the Purkinje fibre cell as a function of the coupling conductance g. For weak coupling, $0 < g < 0.0255$ (approximately), the period is less than it was prior to cell interaction due to the subthreshold depolarizations which the ventricular myocardial cell induces in the pacemaker cell. The period continues to decrease with increases in g until g reaches a critical value of approximately 0.0255 mS/cm^2. At this point, an action potential is, for the first time, induced in the nonspontaneous cell and there is a sharp increase in the pacemaker cell's period to a value somewhat higher than the cycle length prior to coupling. This sharp rise continues over a small range of g where the muscle cell is periodically activated but does not yet oscillate at the same frequency as p. When g reaches approximately 0.026 mS/cm^2, the cells fire at the same rate and for $g > 0.026$ mS/cm^2 the period plotted in Figure 4.3 is the common period of both cells. Further increases in coupling strength produce a short interval of decrease followed by a region of slow increase in the entrained cycle length. Although not shown, the cycle length approaches an upper limit of approximately 850 msec.

These results are in close agreement with those of van Capelle et al. [34] who, using a simple two state variable model of excitable elements, studied the interaction of a pacemaker cell and a nonpacemaker cell and also noted that when the cells beat synchronously the common oscillation period is somewhat longer than the intrinsic rate of the pacemaker cell. This increase in cycle length is caused by a hyperpolarizing (outward) current flowing from the ventricular myocardial (nonpacemaker) cell to the

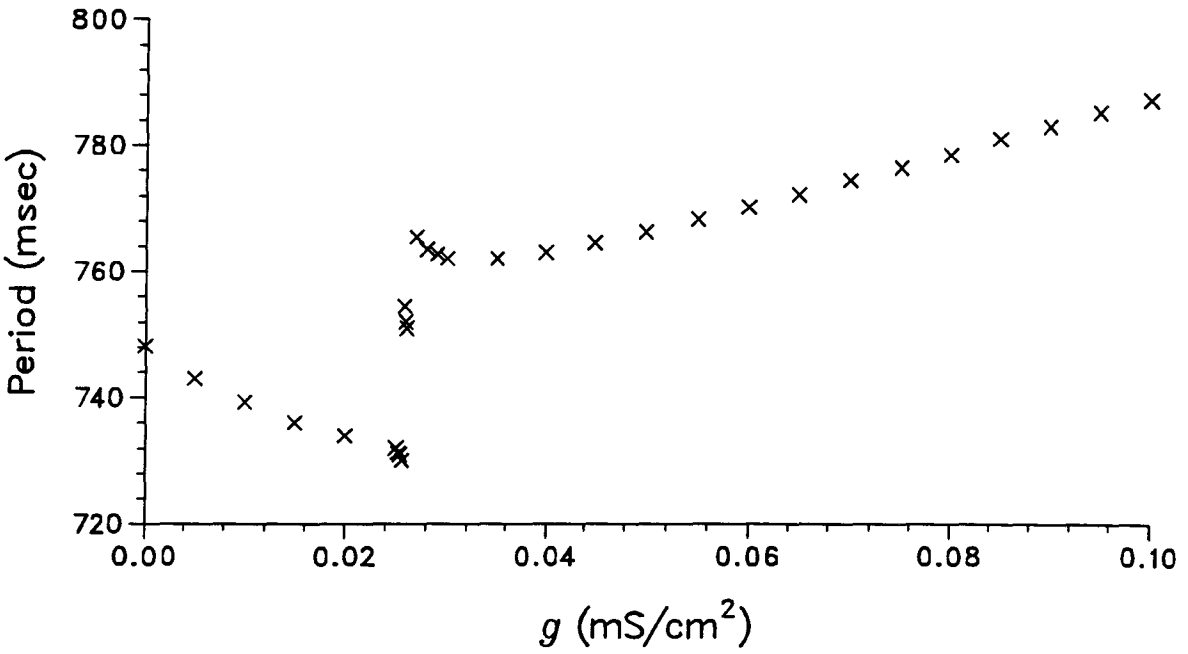

Figure 4.3: Period of oscillation of the Purkinje fibre cell as a function of coupling conductance g (mS/cm^2).

Purkinje fibre (pacemaker) cell. This occurs during the latter part of phase 4 depolarization when the membrane potential of the nonpacemaker cell is more negative than the membrane potential of the pacemaker cell.

4.2 The Production of a Heartbeat

Immediately and for a short time after the production of an action potential, a cell is in an absolute refractory state where no stimulus, no matter what its strength, can cause a second discharge; therefore, when an impulse reaches a cell and causes its excitation, the action potential generated cannot cause neighbouring cells which immediately preceded it in the conduction path to fire. For this reason, in a healthy heart, where action potentials are generated at, and spread radially from, the SA node, these impulses travel through the atria to the AV node, then to the Purkinje fibre network and finally to the muscles cells of the ventricles where the refractory nature of the surrounding tissue

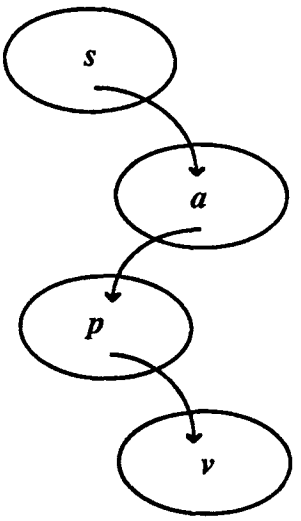

Figure 4.4: Schematic representation of the model used to simulate the production of a heartbeat. Arrows indicate flow of coupling currents between cells.

causes them to die out. There is no retrograde conduction of impulses in the reverse direction back towards the SA node.

In simulating this generation and propagation of action potentials which produces each heartbeat (where a heartbeat consists of the spread of an action potential from the SA node throughout the entire heart causing the atria and ventricles to contract in turn), cells representing the major components of the heart's conduction system were coupled as follows. An SA node cell (s) with an intrinsic frequency of 79.65 cycles/min was coupled to an AV node cell (a) with an intrinsic frequency of 75.66 cycles/min. The AV node cell was coupled to a Purkinje fibre cell (p) which had a frequency of 39.84 cycles/min and which, in turn, was coupled to a nonpacemaker ventricular myocardial cell (v) (Figure 4.4). These particular frequencies were chosen as they are representative of average rates in a healthy heart (Section 2.2.5). The coupling conductance $g_{a,s}$ was set to zero so that no coupling current would flow from the AV node back to the SA node. Similarly, $g_{p,a}$ and $g_{v,p}$ were set to zero. While preventing reverse conduction, the

simulation had to, at the same time, ensure that impulses originating at the SA node did in fact reach the cells of the ventricles. Setting $g_{s,a}$ to a value high enough for an action potential conducted from the SA node cell to depolarize the AV node cell membrane potential to at least its threshold value guaranteed AV node excitation. Similarly, $g_{a,p}$ and $g_{p,v}$ were given sufficiently high values to ensure impulse propagation to the Purkinje fibre cell and the ventricular myocardial cell.

To completely characterize the coupling currents, delays corresponding to action potential conduction times between pairs of interacting cells must be specified. Because the simulation is for a healthy heart, the information in Section 1.1.3 can be used to assign values to $\tau_{s,a}$, $\tau_{a,p}$, and $\tau_{p,v}$. The duration of atrial depolarization, which has an average value of between 60 and 120 msec, is the time required for an impulse generated at the SA node to spread over the atria and reach the AV node. In the current simulation, this corresponds to the conduction time $\tau_{s,a}$. Passage through the AV node requires approximately 50 msec and is indicative of the conduction time $\tau_{a,p}$ between cells of the AV node and the Purkinje fibre system. Finally, the propagation time between a Purkinje fibre cell and a ventricular myocardial cell varies considerably from a value near zero, when the two cells are adjacent, to a maximum in the range of $60 - 100$ msec corresponding to the average duration of ventricular depolarization. Table 4.4 reports the actual values of the coupling conductances and propagation time delays used in the simulation.

Results of the simulation are demonstrated in Figure 4.5 which shows the electrical activity of each model cell. The temporal displacement of phase 0 in the action potentials of Figures 4.5a-d is indicative of the propagation times between the cells. The SA node cell fires independently at its intrinsic frequency of approximately 80 cycles/minute (top trace). After the production of each impulse there is a delay due to atrial depolarization before the impulse reaches the AV node cell causing it to fire in response. After a further

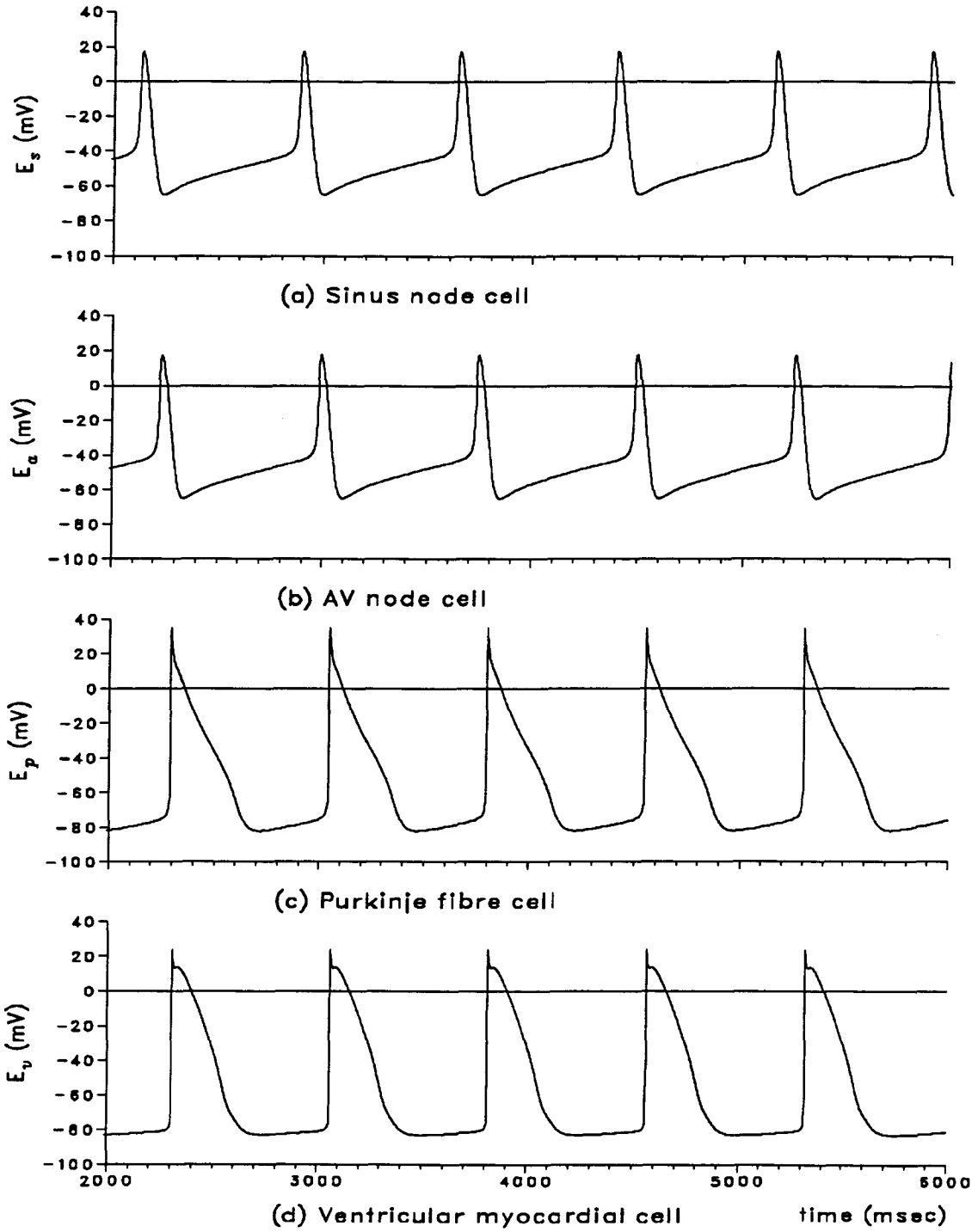

Figure 4.5: Electrical activity of SA node, AV node, Purkinje fibre, and ventricular muscle cells (traces (a) - (d), respectively) during the simulation of a heartbeat. Traces show the activity of the cells beginning 2 sec after coupling was introduced when the cells have settled into a regular rhythm.

Cells i, j	$g_{i,j}$ (mS/cm^2)	$\tau_{i,j}$ (msec)
s, a	0.03	100
a, p	0.05	50
p, v	0.10	10

Table 4.4: Coupling conductance and delay values.

delay, representing the propagation time through the AV node to the Purkinje fibre network, an action potential is produced in the Purkinje fibre cell and finally, when the impulse reaches the nonspontaneous ventricular myocardial cell it too fires. Each cell is excited in turn as the impulse spreads. This process is repeated for every action potential produced at the SA node. Consequently, the AV node and Purkinje fibre cells no longer fire at their own intrinsic frequencies of approximately 75 and 40 cycles/min, respectively, but are entrained to the SA node with its faster rate of spontaneous depolarization. Similarly, the nonspontaneous muscle cell which, prior to coupling produced no action potentials, now fires at the SA node frequency.

Figure 4.6 plots the time corresponding to the peak or maximum membrane potential of each cell along the horizontal axis, and the time *between* the peak of an action potential at the SA node and the peak of the subsequent action potential of each of the other three model cells along the vertical axis. The time corresponding to the peak of an action potential of a particular cell, cell i, is denoted t_i. For each action potential initiated at the SA node there is a corresponding action potential induced in each of the other three cells indicating that all cells beat synchronously. The common cycle length (given by the horizontal distance between the firings of each cell) is approximately 753 msec which is the intrinsic oscillation period of the SA node cell. For two cells, cell i and cell j, the latency between the activation of cell i and the *next* activation of cell j is denoted

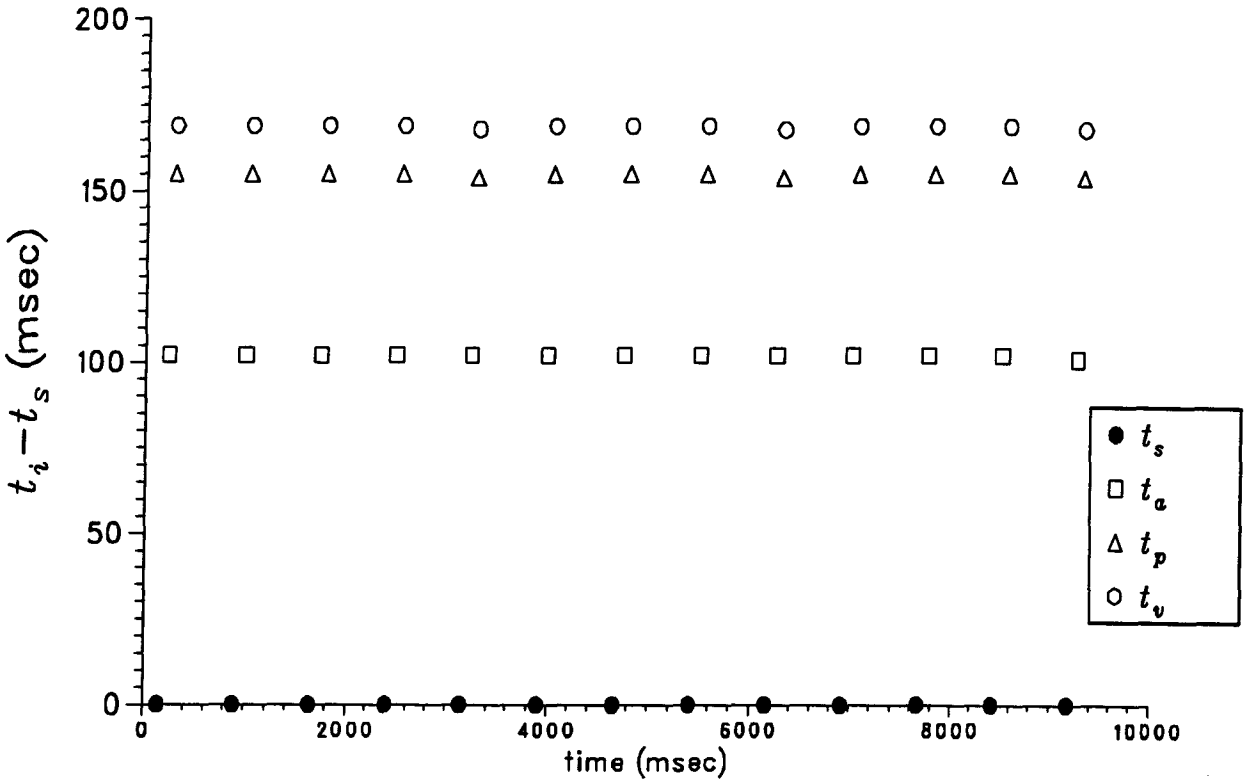

Figure 4.6: Peak action potential times of the AV node, Purkinje fibre, and ventricular myocardial cells relative to the peak action potential times of the SA node during a simulation of the production of a heartbeart. t_i is the time corresponding to the peak of an action potential of cell i, where i is one of s, a, p, or v.

$l_{i,j}$ and is represented by the vertical distances between cell firing times. The values of these peak-to-peak delays are approximately:

$$\begin{aligned} l_{s,a} &= t_a - t_s &= 102, \\ l_{a,p} &= t_p - t_a &= 53, \\ l_{p,v} &= t_v - t_p &= 14. \end{aligned}$$

These values are slightly higher than the action potential propagation times used in the simulation (Table 4.4) due to the fact that once an impulse reaches a cell there is a small delay before the cell is excited and its membrane potential reaches its maximum.

Chapter 5

Modulated Ventricular Parasystole

5.1 Cardiac Arrhythmias and Ectopic Pacemakers

Arrhythmias or irregular cardiac rhythms, are caused by abnormalities in both impulse initiation and conduction. Abnormal impulse initiation may refer to an alteration in the rate of the primary pacemaker or the initiation of impulses at a nonsinus location (ectopic focus). Subsidiary pacemaker cells normally remain latent because the SA (sinus) node produces impulses at a rate faster than other cardiac cells; however, under various pathological conditions a cell or group of cells other than those of the SA node can become a site of pacemaker activity. For example, when the rate of impulse production at the SA node is reduced significantly so that it is smaller than the rate of a secondary pacemaker, the ectopic focus can exhibit its spontaneous activity.

When an ectopic pacemaker produces an action potential in addition to the primary pacemaker, there will be a collision of the two impulses. The action potentials may collide while propagating in opposite directions causing both to be extinguished. They also may travel in similar directions in which case the second impulse will be delayed because of the refractory nature of the tissue. This interaction and competition between pacemaker sites for control of the myocardium results in various arrhythmias.

5.2 Modulated Ventricular Parasystole

Many of the more serious cardiac arrhythmias result from a situation known as *parasystole* which involves the simultaneous activity of two (rarely more) pacemaker sites. In *pure* parasystole one pacemaker functions completely independently of the other, while in *modulated* parasystole each pacemaker is affected by the activity of the other. Usually, one of the pacemaker sites is the SA node and the other an ectopic focus which, although it can be located anywhere in the heart, is usually found in the ventricles. This is known as *modulated ventricular parasystole.*

Figure 5.1 shows a schematic representation of a simple model used to simulate modulated ventricular parasystole. Since most muscle cells are not capable of spontaneous depolarization, the ventricular ectopic focus is assumed to be located in the Purkinje fibre system. Thus, the simulation involves a model SA node cell (s) coupled to a model Purkinje fibre cell (p). Atrial depolarization has an average duration of between 80 and 120 msec and an impulse requires, on average, a further 50 msec to pass through the AV node (Section 1.1.3). The sum of these two durations gives an indication of the time required for an action potential generated at the SA node to reach the Purkinje fibres of the ventricles, thus, in these simulations $\tau_{s,p}$ is given a value of 150 msec. Making the assumption that impulses propagating in the reverse direction are slowed somewhat, perhaps due to the refractory nature of the tissue, $\tau_{p,s}$ was assigned a value of 160 msec. The interaction of the cells for various values of the coupling conductances, $g_{s,p}$ and $g_{p,s}$, were studied and simulations repeated using model cells with different intrinsic cycle lengths, T_s and T_p.

When two pacemakers of different intrinsic oscillation periods are coupled, and the strength of the coupling is increased, the ratio of their periods approaches unity [30,39]. For the present simulation, this means that as one (or both) of $g_{s,p}$ and $g_{p,s}$ is increased,

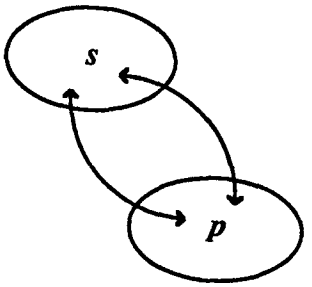

Figure 5.1: Schematic diagram of the model used to simulate modulated ventricular parasystole. A model SA node cell (s) is coupled to a nonadjacent model Purkinje fibre cell (p). Arrows indicate flow of coupling currents between cells.

the ratio T_p/T_s approaches 1. Near certain values of the coupling conductances, $g_{s,p}$ and $g_{p,s}$, the cells become entrained so that their mean cycle lengths are related as simple integral values. This type of entrainment in which there are m periods of s to every n periods of p is denoted m:n entrainment and is a commonly occurring form of cardiac arrhythmia. If the influence of one cell on the other is strong enough, the cells will beat synchronously (1:1 entrainment). Furthermore, the cell with the stronger influence will *lead* the other and determine the entrained oscillation period. In all computations of modulated ventricular parasystole, the cells were allowed to interact for at least 6 seconds or until a definite pattern of $s : p$ firings could be recognized. The average time between the action potentials of each cell was calculated for each cycle of the pattern. The period of the cell was then calculated as the mean of these averages over all observed cycles of the pattern.

5.3 The Lead Cell

In a simulation involving two cells, i and j, the latency, denoted $l_{i,j}$, between their impulses is defined as the time from the peak or maximum voltage of an action potential

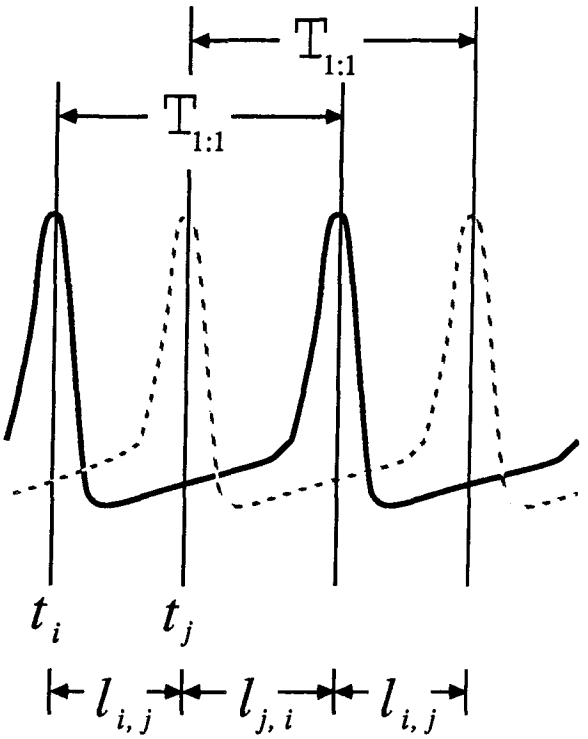

Figure 5.2: Action potentials of cells i and j at 1:1 entrainment. The solid and dashed curves represent the activities of cell i and cell j, respectively.

of i to the peak of the *next* action potential of j. When the cells have synchronized to 1:1 entrainment their action potentials alternate and they oscillate with a common fixed period denoted $T_{1:1}$. That is, $T_i = T_j = T_{1:1}$. In addition, the time, $l_{i,j}$, between every action potential of i and subsequent action potential of j is constant over the entire simulation. Similarly, the latency, $l_{j,i}$, between every action potential of j and subsequent action potential of i is constant throughout the simulation (Figure 5.2). In a two-cell interaction, the lead cell at 1:1 entrainment is that cell whose action potentials cause the excitation of the other most quickly after their arrival at the other cell. If an action potential induced in j is caused by the arrival of the preceding impulse originating

at i then the excitation of j must occur *after* the impulse from i reaches j. That is,

$$l_{i,j} \geq \tau_{i,j}. \tag{5.1}$$

If j is activated *before* the arrival of the impulse from i then its excitation cannot have been caused by the arrival of the incoming current from i; therefore, (5.1) constitutes a necessary condition for i to be the lead cell.

Over the range of coupling conductances studied ($g_{s,p} \in [0, 0.1]$ (mS/cm^2), $g_{p,s} \in [0, 0.01]$ (mS/cm^2)) in the computations of modulated ventricular parasystole, it was found that the entrained period $T_{1:1}$ was always greater than the round-trip propagation time from one cell to the other and back again. That is,

$$T_{1:1} = l_{s,p} + l_{p,s} \geq \tau_{s,p} + \tau_{p,s}. \tag{5.2}$$

Thus, *at least one* of the following must be true:

$$l_{p,s} \geq \tau_{p,s} \tag{5.3}$$

and/or

$$l_{s,p} \geq \tau_{s,p}. \tag{5.4}$$

The lead cell is determined by comparing the peak-to-peak times between the action potentials of the two cells with the impulse propagation times $\tau_{s,p}$ and $\tau_{p,s}$. If $l_{s,p} < \tau_{s,p}$ then s violates (5.1) and is not the lead cell; however, from (5.3), p *will* satisfy the necessary condition (5.1). Each activation of s occurs after the arrival of an impulse from p. In this case p is said to be the lead cell and the entrainment is referred to as **1:1 p entrainment**. Similarly, if $l_{p,s} < \tau_{p,s}$ then p violates the necessary condition (5.1) and so cannot be the lead cell; however, s *will* satisfy (5.1) and the entrainment is referred to as **1:1 s entrainment**.

Finally, if both

$$l_{s,p} \geq \tau_{s,p} \tag{5.5}$$

and

$$l_{p,s} \geq \tau_{p,s}, \tag{5.6}$$

then, in this case, the lead cell is the one which causes the other to be activated the *most* quickly after the arrival of its impulse. If

$$l_{s,p} - \tau_{s,p} \quad < \quad l_{p,s} - \tau_{p,s} \tag{5.7}$$

then s is designated as the lead cell (1:1 s entrainment). On the other hand, if

$$l_{p,s} - \tau_{p,s} \quad < \quad l_{s,p} - \tau_{s,p} \tag{5.8}$$

then p is said to be the lead cell (1:1 p entrainment).

5.4 $T_p/T_s = 3$

For the first set of simulations of modulated ventricular parasystole, a model SA node cell with an intrinsic cycle length T_s = 502.44 msec (frequency = 119.42 cycles/min) was coupled to a model Purkinje fibre cell with an intrinsic cycle length T_p = 1506 msec (frequency = 39.84 cycles/min) so that an approximate 3:1 ratio existed between the periods T_p and T_s prior to coupling.

5.4.1 Regions of Synchronous and Asynchronous Behavior

Figure 5.3 shows the regions of synchronous and asynchronous behavior for a range of the coupling conductances $g_{s,p}$ and $g_{p,s}$ where $0 \leq g_{s,p} \leq 0.1$ mS/cm^2 and $0 \leq g_{p,s} \leq 0.01$ mS/cm^2. For reasons to be outlined in Section 5.7, the Purkinje fibre cell exerts a greater influence on the SA node cell for equal values of the coupling conductances $g_{s,p}$ and $g_{p,s}$ than vice-versa; therefore, to obtain a comparable level of influence of p on s, the range

of values of $g_{p,s}$ used in the simulations of modulated parasystole was smaller than the range of values of $g_{s,p}$. The four curves represent cubic spline interpolations of discrete data points given by coupling conductance pairs ($g_{s,p}$, $g_{p,s}$). Approximately 200 such coupling conductance pairs were used to obtain the curves separating the regions of entrainment. Each computation was run until a definite pattern of $s : p$ firings could be recognized and there was little or no variation in the periods of the cells between cycles of the pattern. Much of the curves were obtained by fixing $g_{s,p}$ at a particular value and then systematically increasing $g_{p,s}$. If two values of $g_{p,s}$ were found, one for which the cells beat synchronously and one for which they did not, a third computation using the average $g_{p,s}$ value was done. This method of bisection was continued until the boundary separating the regions of synchrony and asynchrony was located within approximately 0.0001 mS/cm^2. The dashed curves indicate values of the conductances which resulted in 1:1 entrainment while the solid curves represent values of the conductances for which the cells beat asynchronously. The actual boundaries of the regions lie somewhere between the pairs of dashed and solid curves. The lower plot of Figure 5.3 shows a particular area of the larger plot at a scale which emphasizes the existence of the four curves.

When there is no interaction between s and p ($g_{s,p} = 0 = g_{p,s}$) the cells fire at their own intrinsic frequencies of 119.42 and 39.06 cycles/minute, respectively. At weak coupling ($g_{s,p} < 0.05192$ mS/cm^2, $g_{p,s} < 0.004$ mS/cm^2 (approximately)), corresponding to the region labelled 'not 1:1', neither cell exhibits enough influence on the other to cause 1:1 entrainment.

When $g_{p,s} = 0$ mS/cm^2, p has no influence on s so that when $g_{s,p}$ is sufficiently high (> 0.05192 mS/cm^2) to cause synchrony, p is entrained to s. The positive slope of the curves defining the left boundary of the 1:1 s region indicates that as $g_{p,s}$ is increased, the effects which p begins to exert on s require that $g_{s,p}$ also increase in order that the influence of s on p is sufficient to maintain the 1:1 s entrainment. Conversely, as $g_{s,p}$ is

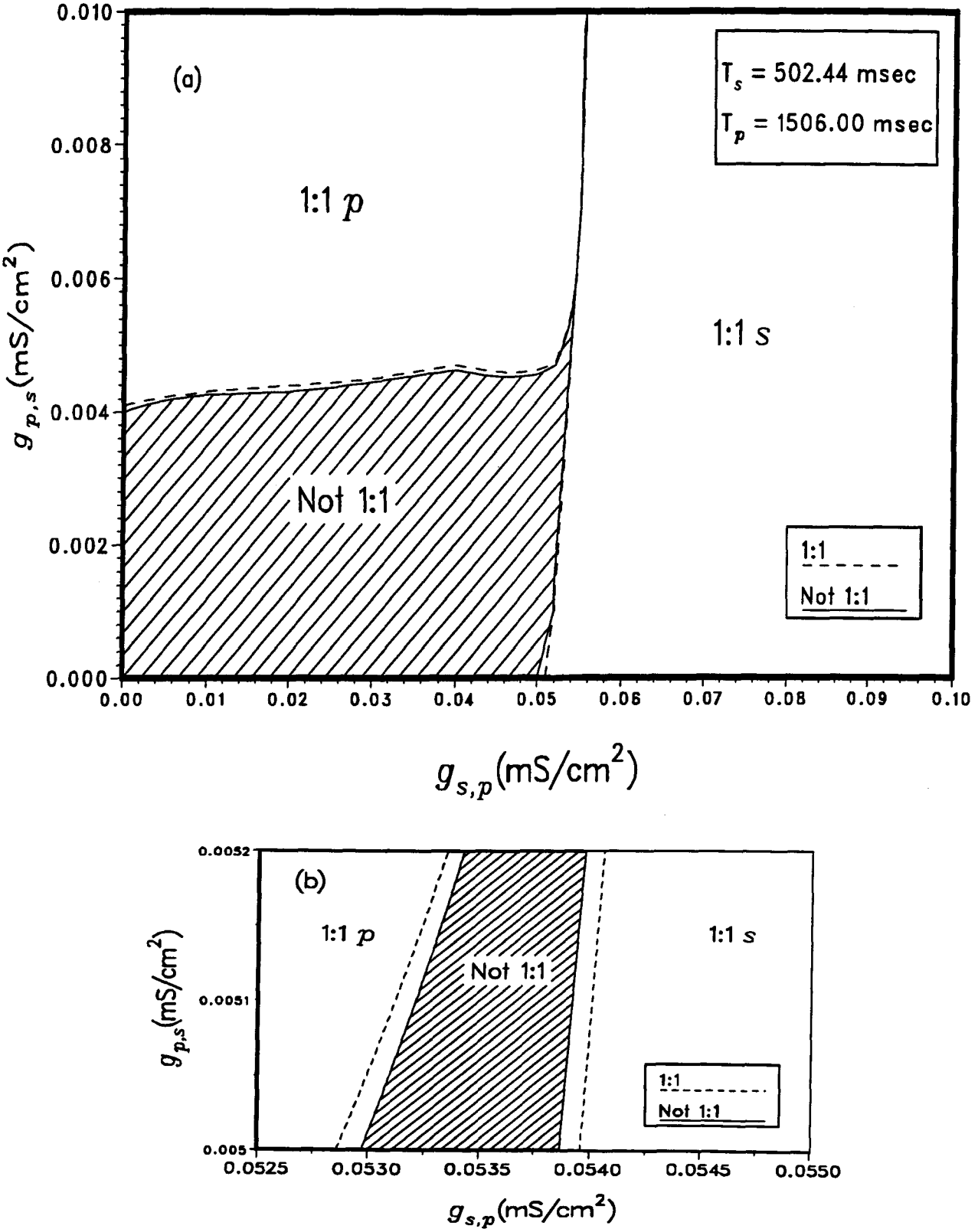

Figure 5.3: Regions of entrainment for $T_p/T_s = 3$.

increased over the range $[0.05192, 0.055495]$, the stronger influence s exerts on p results in an expansion of the region of 1:1 s entrainment. Finally, when the coupling current from s to p is strong enough ($g_{s,p} > 0.0555$ mS/cm^2) the cells are at 1:1 s entrainment over the entire range of $g_{p,s}$ from 0 to 0.01 mS/cm^2.

The Purkinje fibre cell also can be the lead cell. When $g_{p,s}$ is greater than some critical minimum value near 0.004 mS/cm^2 and the ratio $g_{p,s}/g_{s,p}$ is sufficiently high, s fires synchronously with p (region labelled 1:1 p).

For high values of $g_{p,s}$, the regions of synchrony to p and to s appear to be almost contiguous. Moving horizontally along a fixed value of $g_{p,s}$ from the 1:1 p region to the 1:1 s region by increasing $g_{s,p}$ causes dramatic changes in the periods T_p and T_s. For example, with $g_{p,s}$ at its maximum value of 0.01 mS/cm^2 and $g_{s,p} = 0.55495$ mS/cm^2, the common cycle length is 1255 msec. The time between each action potential at s and each action potential at p is given by $l_{s,p} = 1063$ msec while the latency from the activation of p to the activation of s is given by $l_{p,s} = 172$ msec; therefore, from Section 5.3, p is the lead cell. Keeping $g_{p,s}$ fixed at 0.01 and increasing $g_{s,p}$ by only 0.000005 to a value of 0.0555 results in 1:1 s entrainment with a common cycle length of only 409.5 msec and latencies given by $l_{s,p} = 204.0$ msec and $l_{p,s} = 205.5$ msec. It is hypothesized that between these two values, $g_{s,p} = 0.055495$ mS/cm^2 and $g_{s,p} = 0.0555$ mS/cm^2, which correspond to two very different types of 1:1 entrainment with the cycle length differing by approximately 745.5 msec, there are values of $g_{s,p}$ for which the cells are not synchronized and that the region marked 'not 1:1' extends upwards separating the 1:1 p and 1:1 s regions.

5.4.2 1:1 s Entrainment

When s is the lead cell in 1:1 entrainment (5.3), the entrained oscillation period is closer to the intrinsic cycle length of s than to the intrinsic cycle length of p. Figure 5.4 demonstrates the changes which occur in T_p and T_s as the cells approach 1:1 s entrainment for the specific case where $g_{p,s}$ is fixed at 0.001 mS/cm^2 and $g_{s,p}$ is increased from 0 to 0.1 mS/cm^2. This corresponds to moving along a horizontal line at $g_{p,s} = 0.001$ mS/cm^2 in Figure 5.3a. When $g_{s,p} = 0$ mS/cm^2, the cycle lengths of s and p are 530.25 msec and 1505.8 msec, respectively, so that $T_p/T_s = 2.84$ (Figure 5.4b). As $g_{s,p}$ is increased the mean cycle lengths decrease although the changes are much more pronounced in T_p than in T_s. When $g_{s,p}$ reaches 0.051919 mS/cm^2, there is an abrupt decrease in T_p and finally, for $g_{s,p} = 0.05192$ mS/cm^2, p fires with the same period (474 msec) as s and $T_p/T_s = 1$. The latency $l_{s,p}$ between an action potential of s and subsequent activation of p is 219 msec while $l_{p,s} = 255$ msec; therefore, s is the lead cell. With further increases in $g_{s,p}$ to 0.1 mS/cm^2, 1:1 s entrainment continues with slight decreases in the entrained cycle length to a value of 454 msec, a value which is less than the intrinsic oscillation periods of both s and p.

Figure 5.5 shows, for $g_{p,s}$ fixed at 0.001 mS/cm^2, the effects of increases in $g_{s,p}$ on the action potentials of the two cells. In (a) with $g_{s,p} = 0$ there are almost three complete action potentials of s for each action potential of p while in (b), where $g_{s,p} = 0.03$ mS/cm^2, there is 2:1 entrainment. Increasing $g_{s,p}$ to 0.051918 mS/cm^2 results in 3:2 entrainment and for $g_{s,p} = 0.1$ mS/cm^2 the cells exhibit 1:1 s entrainment.

5.4.3 1:1 p Entrainment

When the Purkinje fibre cell is the lead cell in 1:1 entrainment (5.3), the entrained oscillation period is closer to the intrinsic cycle length of p than to the intrinsic cycle

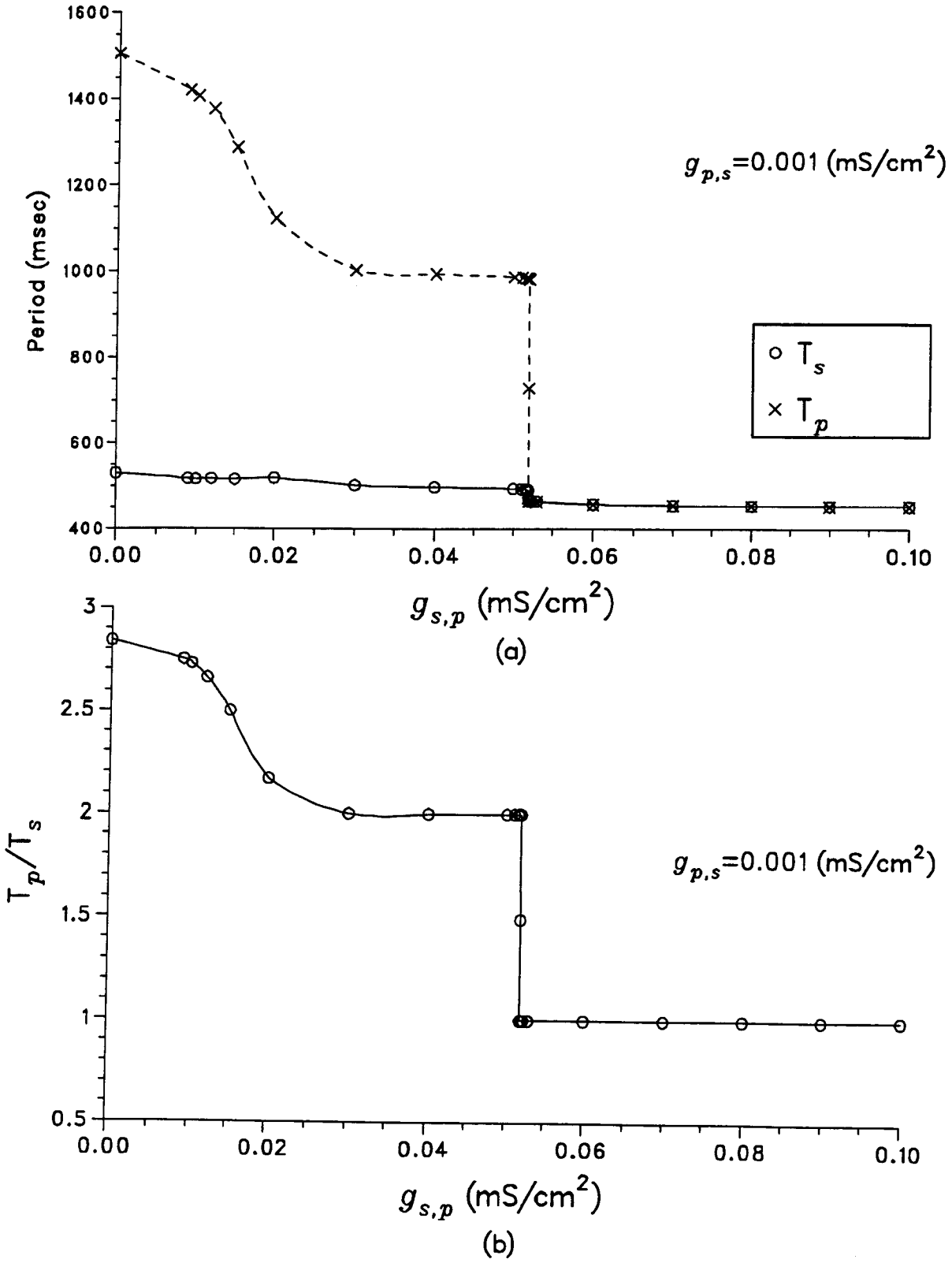

Figure 5.4: Changes in cycle lengths T_p and T_s for $g_{p,s} = 0.001$ mS/cm^2 and increasing $g_{s,p}$ (mS/cm^2).

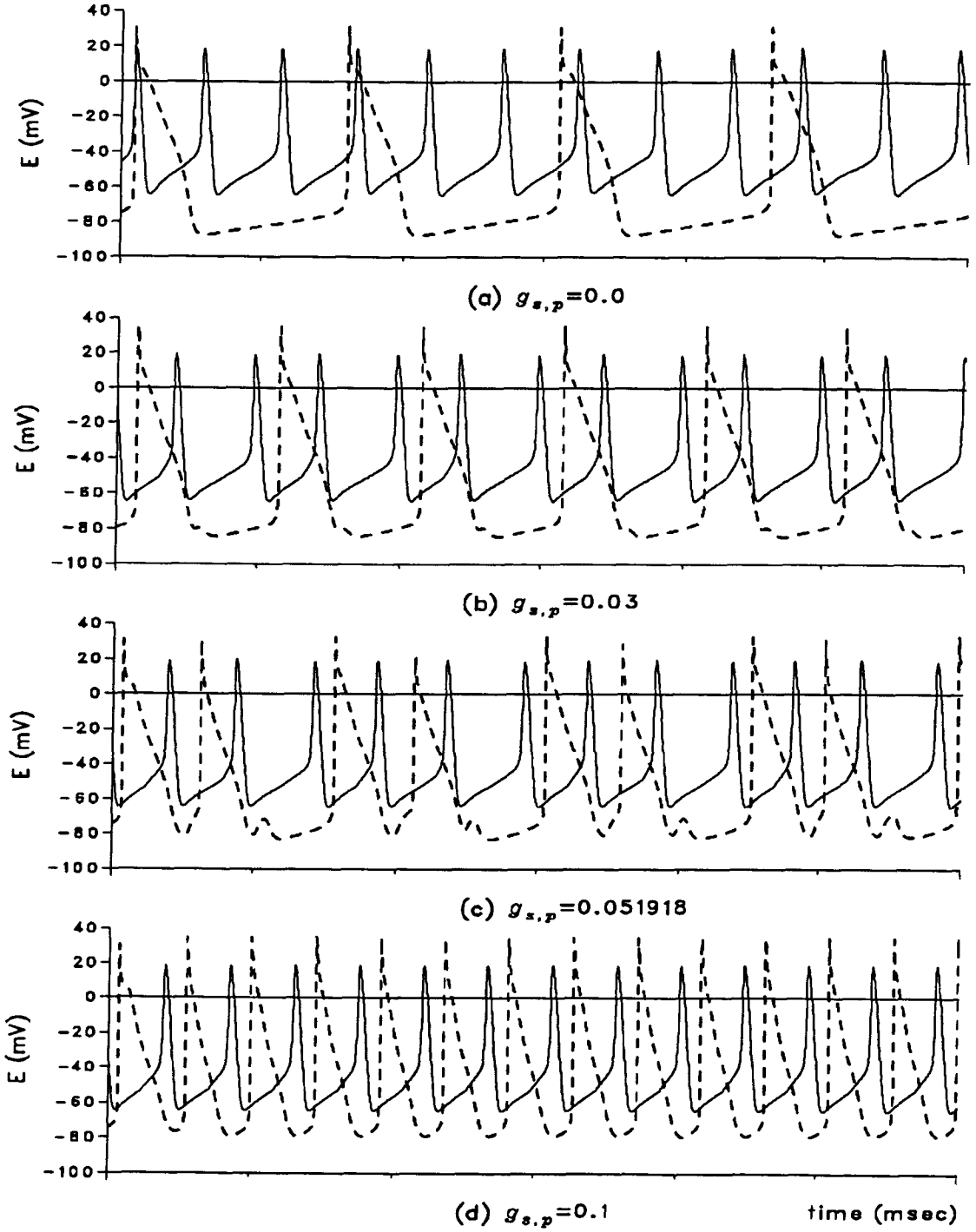

Figure 5.5: Action potentials of cells s and p for $g_{p,s} = 0.001$ mS/cm^2 and increasing $g_{s,p}$ (mS/cm^2). Solid curve is the SA node cell. Dashed curve is the Purkinje fibre cell.

length of s. Figure 5.6 shows the changes which occur in T_p and T_s as the cells approach 1:1 p entrainment. Here, as a specific example, $g_{s,p}$ is fixed at a value of 0.04 mS/cm^2 and $g_{p,s}$ is increased over the range [0,0.01] mS/cm^2. This corresponds to moving upward along a vertical at $g_{s,p} = 0.04$ mS/cm^2 in Figure 5.3.

When $g_{p,s} = 0$ mS/cm^2 the mean cycle lengths of s and p are 502.71 and 1005.3 msec, respectively, and the cells exhibit 2:1 entrainment. As $g_{p,s}$ increases, the cycle lengths T_p and T_s *increase* (in contrast to the previous case of 1:1 s entrainment where increased coupling caused *decreased* cycle lengths). The ratio T_p/T_s, however, remains constant at approximately 2 until $g_{p,s}$ reaches a value near 0.004 mS/cm^2 when, due to an abrupt increase in the period of s, there is a corresponding decrease in T_p/T_s. With another slight increase to $g_{p,s} = 0.00465$ mS/cm^2, the cycle lengths become equal and s fires synchronously with p with a common period of 1186 msec. At this point, the latencies $l_{s,p}$ and $l_{p,s}$ are 982 and 204 msec, respectively; therefore, p is the lead cell. With additional increases in $g_{p,s}$, 1:1 p entrainment continues with corresponding increases in the entrained cycle length which reaches a value of 1261.5 msec when $g_{p,s} = 0.01$ mS/cm^2. Throughout the region of 1:1 p entrainment the common cycle length is closer to the intrinsic cycle length of p than to the intrinsic cycle length of s. Furthermore, in this case, the entrained period takes on values *between* the intrinsic cycle lengths ($T_s = 502.44$ msec, $T_p = 1506$ msec) in contrast to the case of 1:1 s entrainment where the common period at synchrony was always less than the intrinsic cycle lengths of s and p.

Figure 5.7 shows the changes in the action potentials of s and p for $g_{s,p}$ fixed at 0.04 mS/cm^2 and increasing values of $g_{p,s}$. In (a) there is 2:1 entrainment. In (b) and (c) the cells undergo 5:3 and 4:3 entrainment patterns, respectively. Finally, (d), with $g_{p,s} = 0.0047$ mS/cm^2, demonstrates 1:1 p entrainment.

Earlier it was noted that these patterns of m:n entrainment are common in clinical

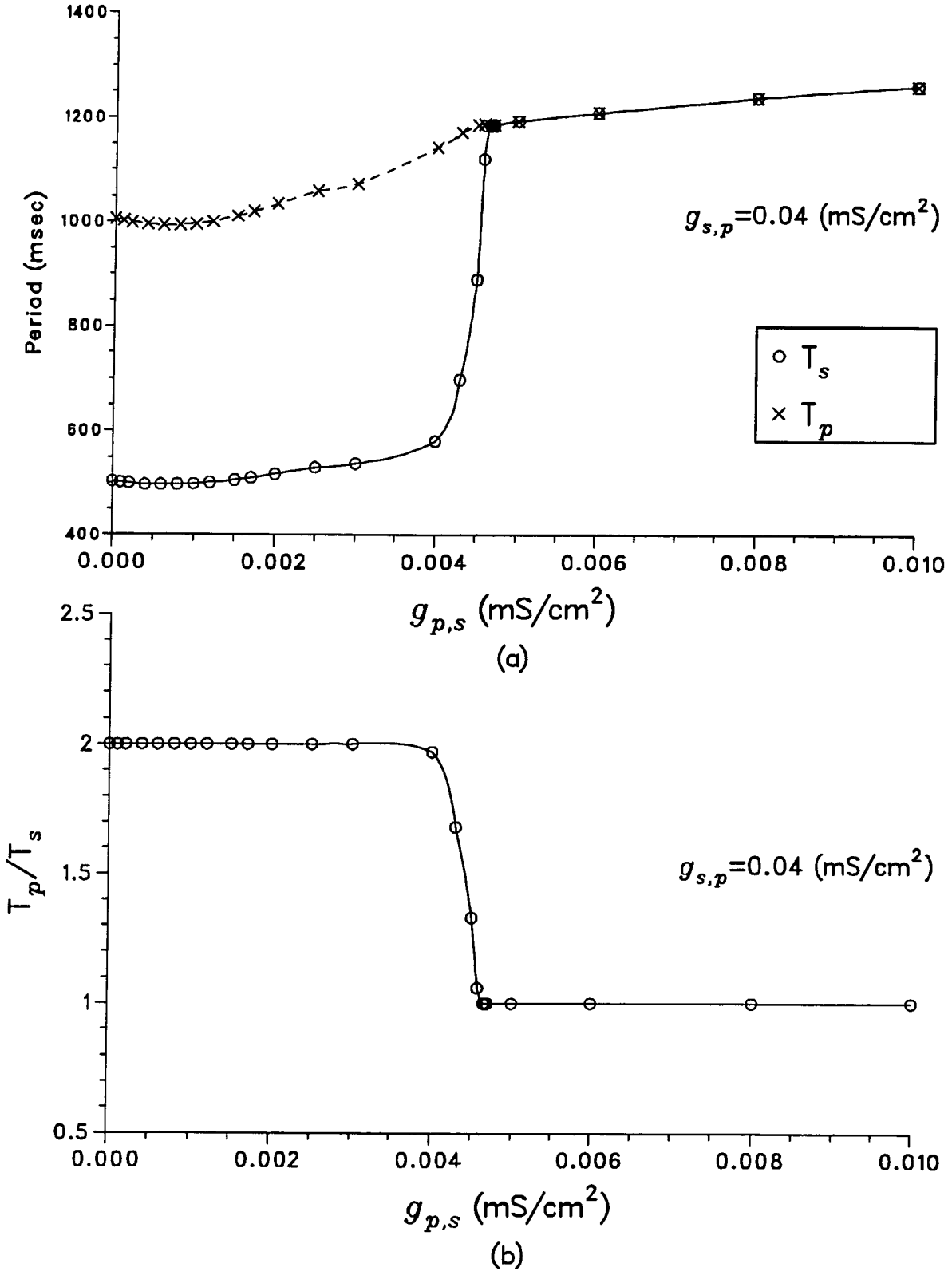

Figure 5.6: Changes in cycle lengths T_p and T_s for $g_{s,p} = 0.04$ mS/cm^2 and increasing $g_{p,s}$ (mS/cm^2).

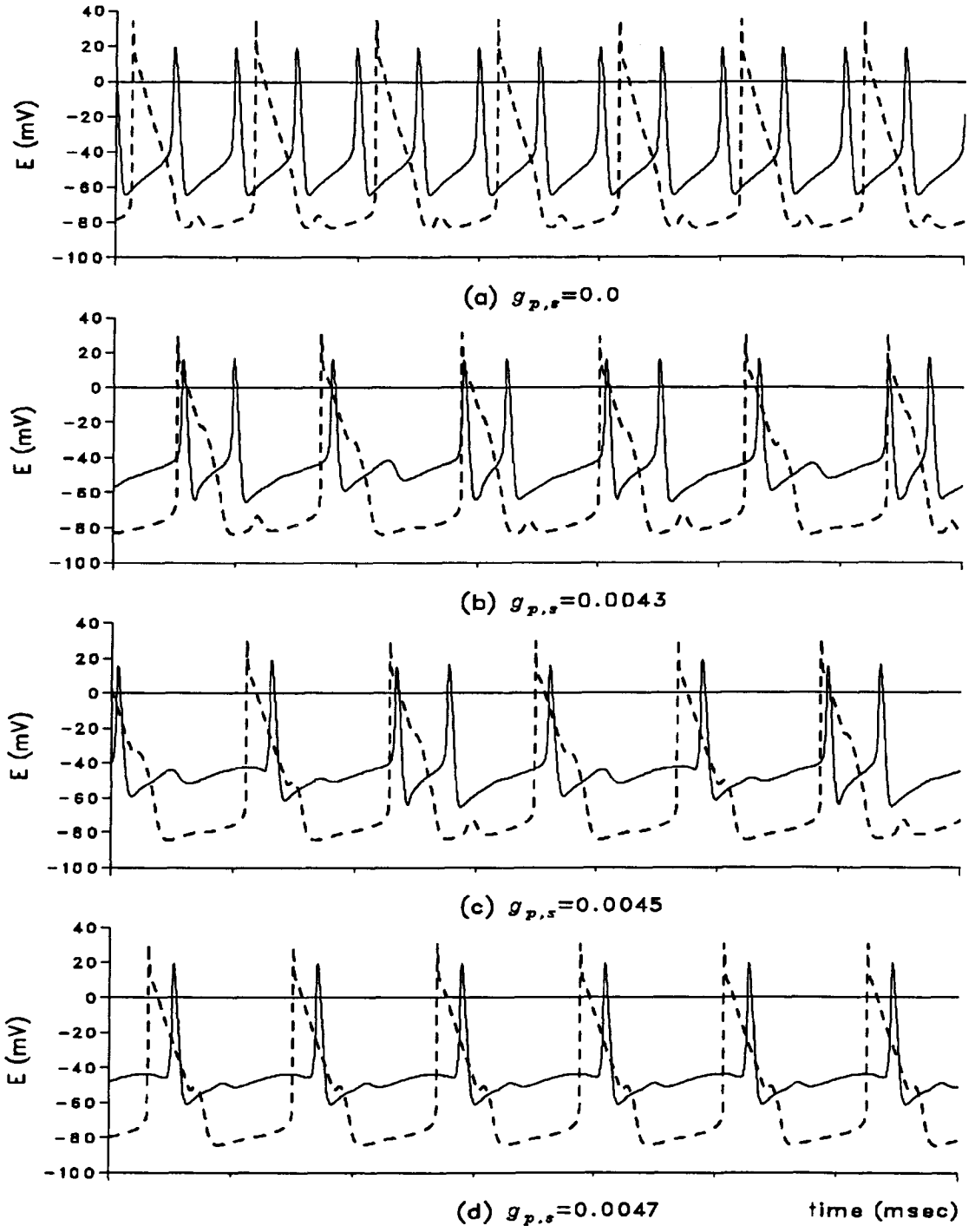

Figure 5.7: Action potentials of cells s and p for $g_{s,p} = 0.04$ mS/cm^2 and increasing $g_{p,s}$ (mS/cm^2). Solid curves indicate SA node cell. Dashed curves indicate Purkinje fibre cell.

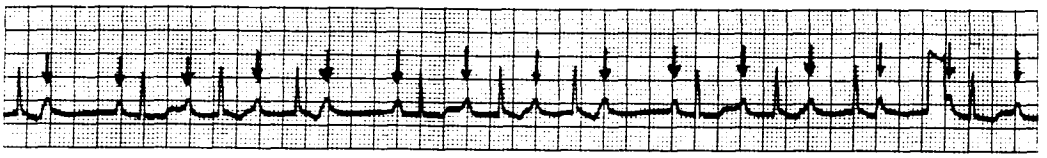

Figure 5.8: ECG recording showing 4:3 entrainment. Arrows indicate atrial contractions and the large spikes indicate ventricular contractions (taken from [6], p.284).

electrocardiography (ECG). Figure 5.8 shows an ECG recording from a patient experiencing a 4:3 entrainment arrhythmia. The arrows indicate atrial depolarization while the large peaks correspond to ventricular depolarizations. This is analogous to the result of Figure 5.7c where there are 4 SA node action potentials (atrial contractions) for every 3 Purkinje fibre action potentials (ventricular contractions).

5.5 $T_p/T_s = 2$

For the second set of calculations of modulated ventricular parasystole the same model Purkinje fibre cell was coupled to an SA node cell with a period of oscillation 1.25 times longer than in Section 5.4, i.e., the intrinsic cycle lengths of p and s were $T_p = 1506.0$ and $T_s = 753.25$ msec respectively. Hence, the ratio of the intrinsic periods T_p/T_s was approximately 2. These cycle lengths correspond to approximate intrinsic frequencies of 80 and 40 cycles/min which are normal healthy rates for Purkinje fibre and SA node cells, respectively.

5.5.1 Regions of Synchronous and Asynchronous Behavior

Figure 5.9 shows the regions of synchronous and asynchronous behavior of the two cells for the coupling conductances $g_{s,p}$ and $g_{p,s}$ over the same range of values as in Section 5.4.

A comparison with Figure 5.3 shows that the behavior is very similar to the case where $T_p/T_s = 3$. Again, for small values of $g_{s,p}$ and $g_{p,s}$ the cells fire asynchronously. For sufficiently high values of $g_{s,p}/g_{p,s}$ with $g_{s,p}$ greater than some critical value near 0.036 mS/cm^2, the cells exhibit 1:1 s entrainment. Also when $g_{p,s}$ is greater than some minimum value near 0.0004 mS/cm^2 and the ratio $g_{p,s}/g_{s,p}$ is sufficiently large, p becomes the lead cell and 1:1 p entrainment occurs. As for the previous set of computations, it appears that the region of asynchronous behavior extends upward to separate the regions of 1:1 s and p entrainment.

The main difference between this and the previous case lies in the relative sizes of the regions of synchronous and asynchronous behavior of the cells. The 1:1 s region has expanded over lower values of $g_{s,p}$ to include a region defined only for very small $g_{p,s}$ and where the slope of the curves defining its boundary are almost zero. The slope remains near zero until $g_{s,p}$ reaches approximately 0.055 mS/cm^2, (a value only slightly higher than the corresponding value in the previous set of calculations with $T_p/T_s = 3$) when the boundary becomes almost vertical. More noticeably, the 1:1 p region has also expanded from the previous case. Here entrainment to p occurs for sufficiently high values of the ratio $g_{p,s}/g_{s,p}$ where $g_{p,s}$ is greater than some critical value near 0.0004 mS/cm^2 whereas previously, for $T_p/T_s = 3$, the critical value was almost ten times larger ($\approx$ 0.004 mS/cm^2). This expansion of the regions of 1:1 entrainment suggests the well-known result that the closer the intrinsic cycle lengths of the cells, the more easily (for weaker coupling) synchronization is obtained [39].

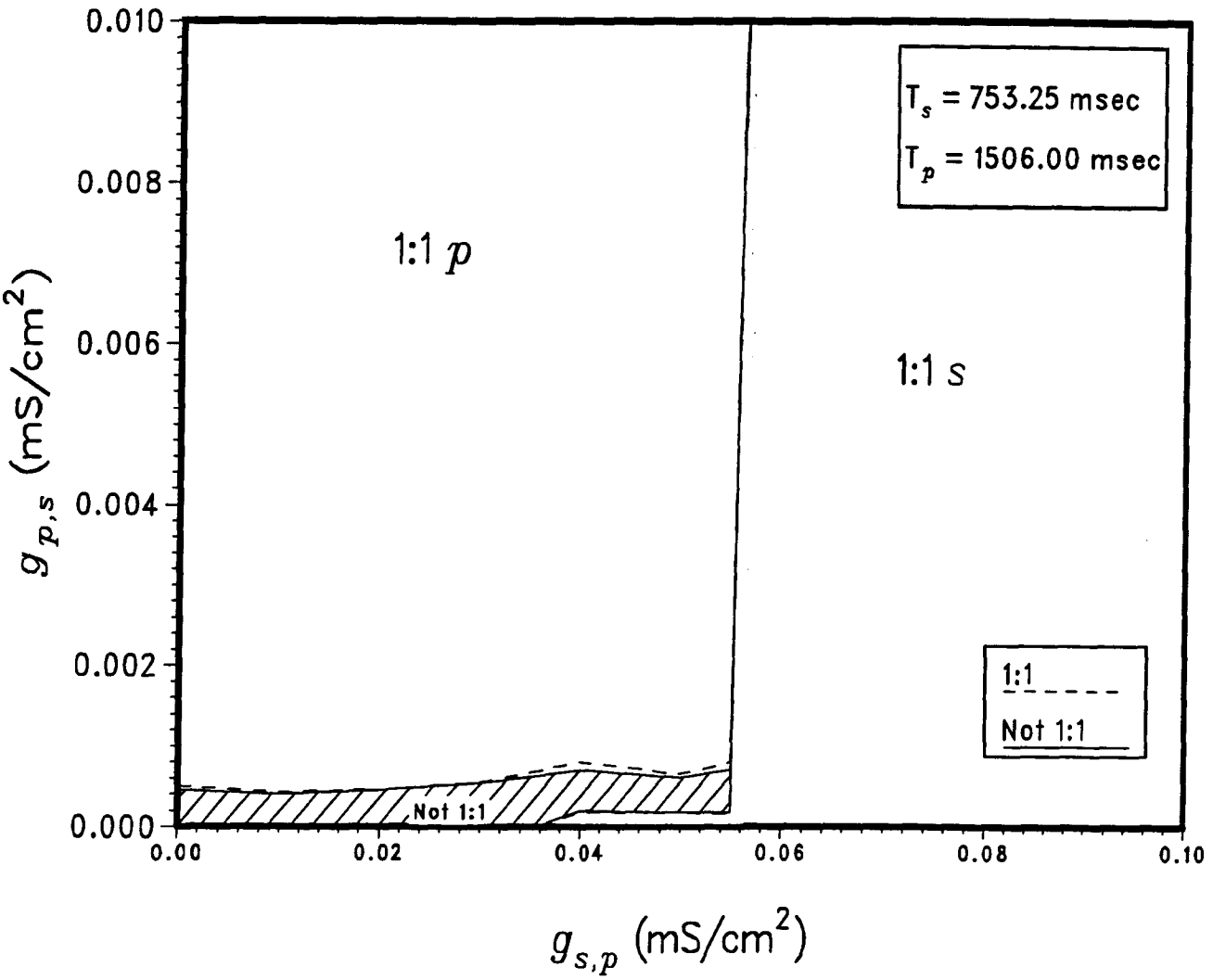

Figure 5.9: Regions of entrainment for $T_p/T_s = 2$.

5.6 $T_p/T_s = 0.75$

In each of the previous two sets of computations of modulated ventricular paraystole, a model Purkinje fibre cell with an intrinsic period of oscillation of 1506 msec was coupled to an SA node cell with a shorter period so that $T_p/T_s > 1$. For the final set of simulations a model Purkinje fibre cell with an intrinsic cycle length of 501.11 msec (frequency = 120 cycles/minute) was allowed to interact with a model SA node cell with an intrinsic cycle length of 753.25 msec (This is the same model SA node cell used in Section 5.5 with $T_p/T_s = 2.$). In this case, the ratio of the intrinsic periods of the cells is given by $T_p/T_s = 0.75$.

5.6.1 Regions of Synchronous and Asynchronous Behavior

Figure 5.10 illustrates the values of the coupling conductances $g_{s,p}$ and $g_{p,s}$ for which the cells fire synchronously and asynchronously. For the values of $g_{s,p}$ and $g_{p,s}$ studied, the cells do not exhibit 1:1 s entrainment at all and the 1:1 p entrainment region has expanded over the full range of $g_{s,p}$ shown. The positive slope of the lower boundary defining this region demonstrates that, as the influence of p on s increases, so does the range of values of $g_{s,p}$ for which s is entrained to p; or, conversely, as the strength of the coupling from s to p increases so must the coupling from p to s in order for p to remain the lead cell in 1:1 p entrainment.

5.7 The Greater Influence of the Purkinje Fibre Cell

For the three sets of computations corresponding to $T_p/T_s = 3$, 2, and 0.75, synchrony to the Purkinje fibre cell occurs for much smaller values of $g_{p,s}$ than the values of $g_{s,p}$ required to cause synchrony to s. For example, when $T_p/T_s = 3$ (Figure 5.3) 1:1 p entrainment occurs for $g_{p,s} \geq 0.0043$ mS/cm^2, whereas, 1:1 s entrainment does not occur

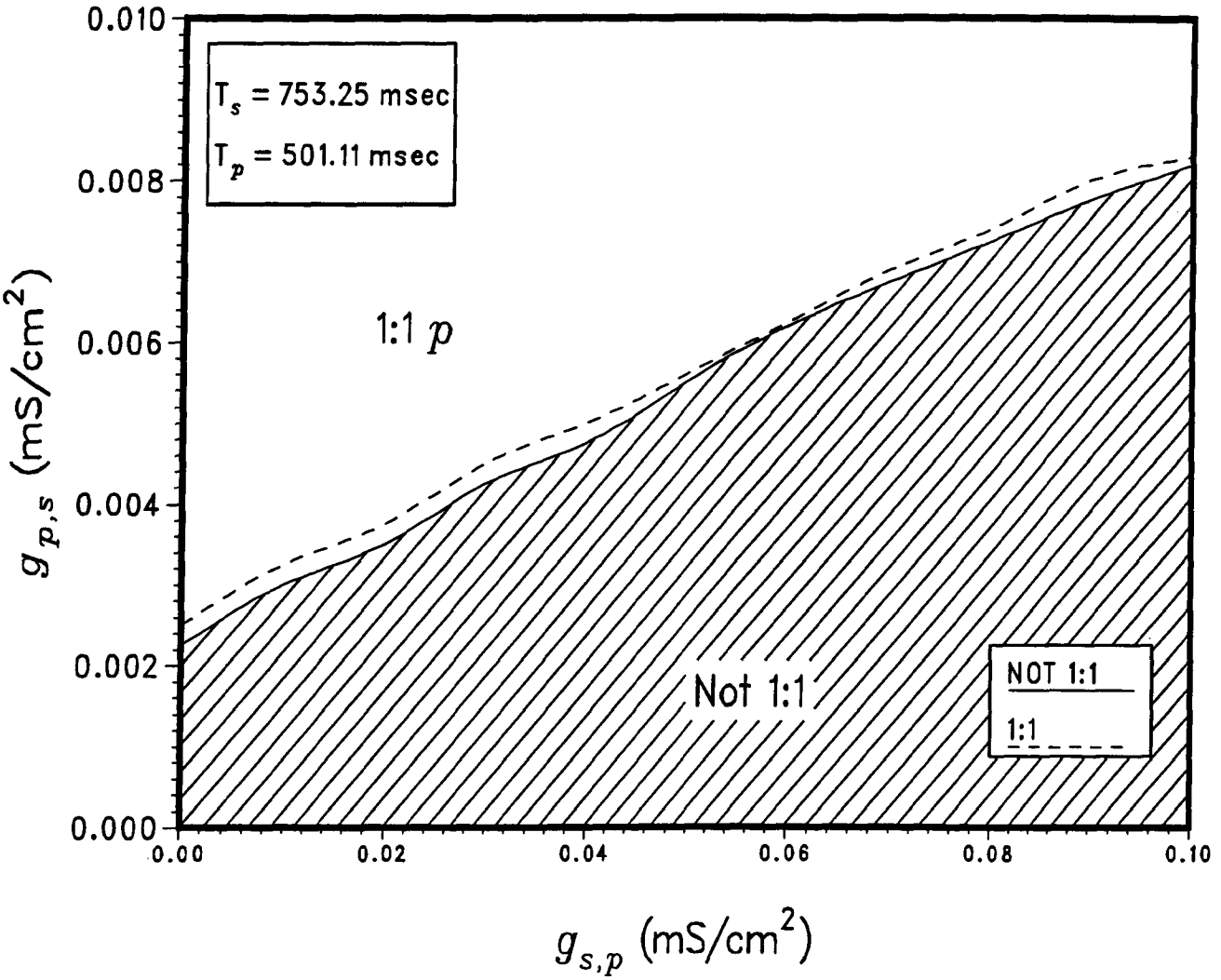

Figure 5.10: Regions of entrainment for $T_p/T_s = 0.75$.

unless $g_{s,p} > 0.05192$ mS/cm^2. Similarly, in the case when $T_p/T_s = 2$ (Figure 5.9), synchrony to p occurs for $g_{p,s}$ just slightly greater than 0.0004 mS/cm^2; however, synchrony to s occurs only when $g_{s,p} > 0.036$ mS/cm^2. Lastly, when $T_p/T_s = 0.75$ (Figure 5.10), 1:1 s entrainment does not occur for any of the values of $g_{s,p}$ studied. In all cases, for s to be the lead cell at 1:1 s entrainment, $g_{s,p}$ must be over ten times greater than the value of $g_{p,s}$ required for p to be the lead cell. These findings indicate that for equal values of the conductances, p has a much stronger influence on s than s has on p. Two factors which affect the activation of a cell by an external current are the strength and duration of the stimulus. Because the most negative potential of the Purkinje fibre cell (≈ -85 mV) is much less than the minimum potential of the SA node cell (≈ -64 mV) and because the threshold for p is -60 mV, the potential of p will be less than the potential of s for almost the entire duration of phase 4 depolarization of p. This will induce in s a depolarizing current which will contribute to its excitation. Furthermore, the rate of depolarization of the Purkinje fibre cell's membrane potential during phase 0 is very rapid and will have a more pronounced effect on s than the slower rate of depolarization of s will have on p.

5.8 The Lead Cell and the Entrained Oscillation Period

In previous studies, Ypey et al. [39] used a simple Hodgkin-Huxley-type model of a pacemaker cell, and Michaels et al. [30] used the same SA node model due to Yanagihara et al. [38] to study interactions of identical adjacent cells with different intrinsic periods. They found that at 1:1 entrainment the cell with the shorter intrinsic cycle length was always the lead cell. Furthermore, the entrained cycle length was, not only closer to the intrinsic period of oscillation of the lead cell, but had a value *between* the intrinsic cycle lengths of the coupled cells. For the present model, the results also suggest that the

entrained period of oscillation is closer to that of the lead cell; however, here *either* cell can be the lead cell. This result is also supported by the phase response curves obtained in Chapter 3. There it was found that the shape of the PRCs, and subsequently the cell which undergoes the smaller phase shifts (from the results of the current chapter, this cell is the lead cell), was dependent on the values of the conductances $g_{p,s}$ and $g_{s,p}$. The computations of modulated ventricular parasystole also demonstrated that the cycle length at 1:1 entrainment was not restricted to values *between* the intrinsic periods of s and p. For example, for the case where $T_p/T_s = 3$ and $g_{s,p} = 0.04$ mS/cm^2, the entrained period in the 1:1 s region was smaller than the intrinsic cycle lengths of both s and p (Figure 5.4).

5.9 The Effect of Changes in T_p and T_s

A comparison of Figure 5.3 where $T_p/T_s = 3$ and Figure 5.9 where $T_p/T_s = 2$ indicates that for $T_p > T_s$ the closer the intrinsic periods of s and p, the more easily the cells are synchronized. Both regions of 1:1 s entrainment and 1:1 p entrainment became larger with the decrease in T_p/T_s suggesting that the closer the intrinsic periods of oscillation the weaker the coupling strength required for synchrony. Decreasing the ratio T_p/T_s to 0.75 resulted in a further increase in the size of the 1:1 p region; however, the 1:1 s region ceased to exist for the range of $g_{s,p}$ studied. The difference here is that p fires at a faster rate than s and combining this with the fact that p exerts a greater influence on s than s on p, means that 1:1 s entrainment is more difficult to achieve.

Chapter 6

Discussion

6.1 Summary of the Heart Model

Various aspects of the electrophysiology of the heart, such as phase resetting and mutual entrainment, due to the initiation and conduction of cardiac action potentials have been investigated through the dynamic interactions of model cells representing the major components of the heart's conduction system. These cells of the SA node, AV node, Purkinje fibre system, and ventricular myocardium were modelled using Hodgkin-Huxley-type oscillators. The electrical activities of the SA node, Purkinje fibre, and ventricular myocardial cells were simulated using the models devised by Yanagihara et al. [38], McAllister et al. [28], and Beeler and Reuter [1], respectively. Because the action potentials of an AV node cell are very similar to those of an SA node cell, the electrical activity of the AV node cell was simulated using a model derived from the Yanagihara et al. model for the SA node cell. In order that the model heart be capable of simulating the wide range of both normal and pathological functionings typical of a real heart, certain physiologically based parameters in the model equations were altered to produce model cells which exhibit a wide range of frequencies. The model allowed the coupling of any number of the four types of cells where the frequencies of the pacemaker cells were chosen from predetermined sets of values. Cell interaction was simulated by the addition of purely resistive coupling currents flowing between interacting cells where the form of the coupling current was dependent on whether or not the cells were assumed

to be physically adjacent. An action potential travelling from one cell to another *non-adjacent* cell will likely take a different path over the tissue separating the cells than an impulse travelling in the reverse direction. Furthermore, the time required for this impulse propagation between such nonadjacent cells is significant relative to the duration of the action potentials. These facts were incorporated into the model by means of direction dependent coupling conductances and conduction time delays. For *adjacent* cells, where the intercell membrane constitutes the entire propagation path, the conduction times are negligible and the coupling conductances simply represent the conductance of the gap junction membrane. Consequently, in this case, the coupling currents were reduced to the form used in previous studies of adjacent cell interaction [5,30,39] where the coupling currents flowing between two model cells were of opposite sign but equal magnitude. Then with the four types of model cells of varying frequencies and a method of coupling them, various aspects of cell interaction were investigated throughout the chapters of this thesis.

6.2 Discussion of Results

The changes in cycle length caused by the subthreshold depolarizations induced in one pacemaker by another are a prerequisite to the entrainment of the cells. This phase-resetting phenomenon was investigated in Chapter 3 through the use of phase-response curves for various pairs of interacting cells using pulsed-coupling. Biphasic response curves similar to those obtained experimentally were produced. As in previous studies, the shape of a PRC was maintained with a decrease in coupling conductance. Also, as expected, over most of the cycle, the phase shifts were less with weaker cell interaction. The exception was a small range of phase values where delays occur for lower conductances and the transition to advances had already been made with the stronger stimulus.

It also was found that with an increase in conductance the transition from maximal cycle prolongation to maximal cycle abbreviation occurred over a much narrower range of phases. This is analogous to previous experimental results obtained for chick heart cells [13]. The PRCs for fast and slow cells were also studied. In contrast to previous works studying interactions of similar cells, the phase shifts induced in a slow cell by a faster one were not necessarily larger than the corresponding phase shifts induced in the same fast cell by the slower one. Again this is due to the direction dependent coupling currents and the unequal influences exerted by different types of cells. Behavior demonstrating the greater sensitivity of a slower cell *was* obtained, however, when a particular cell was coupled to another cell whose intrinsic frequency was subsequently altered. In this case, the phase shifts were indeed greater at a given phase for the slower cell. Finally, comparisons were made between phase response curves obtained under conditions of pulsed and continuous coupling with expected results. PRCs summarizing the effects of a slower cell on a faster cell were similar for both methods of coupling. The differences lie in the size of the phase delays which were greater under continuous coupling due to the continuous 'pull' of the slower cell. For the case of a fast cell stimulating a slower one, the PRC obtained under continuous coupling was somewhat different from the corresponding pulsed-coupling PRC. This is due to the fact that for certain phases more than one discharge of the faster cell will occur during the perturbed cycle of the slower cell. Also, the continuous influence of the fast cell caused delays to be less for the PRC obtained under conditions of continuous coupling.

Most muscle cells are nonspontaneous and are only activated by the external stimulation of neighbouring cells. For ventricular muscle cells the external stimulation may be provided by Purkinje fibre cells. This activation of a nonpacemaker cell was computed for the present model in Chapter 4 and it was found that the level of activation of the muscle cell was dependent on the strength of the interaction. Also, as in an earlier study

by van Capelle [34] which uses a simple two-state variable model, the common cycle length at synchrony was somewhat lower than the intrinsic period of oscillation of the pacemaker cell.

A second property of a healthy heart is that the SA node acts as the primary pacemaker and other cells are entrained to its regular rhythm. Impulses generated at the SA node spread throughout the atria and then the ventricles causing first atrial and then ventricular contraction. This production of a heartbeat was mimicked for the present model in Chapter 4 by the coupling of one of each type of model cell with intrinsic frequencies and propagation time delays representative of those in a healthy heart. Results demonstrated that each impulse initiated at the SA node was transmitted from one model cell to another causing the excitation of each shortly after its stimulation. Each cell fired at the SA node rate. Also, the time between the activation of one cell and a succeeding cell in the conduction path was within milliseconds of the specified action potential propagation time between the same cells.

Both of the functions of a healthy heart discussed in Chapter 4 are possible because of the ability of cardiac cells to become entrained to a common frequency. Entrainment, however, can also be the cause of many irregular rhythms of the heart. A particular pathological situation known as modulated ventricular parasystole which is characterized by the formation of a ventricular ectopic focus (site of pacemaker activity other than the SA node) was studied in Chapter 5. A simple two-cell model in which an SA node cell (s) was coupled to a Purkinje fibre cell (p) was used throughout the computations. The results confirmed the well-known result that when two pacemakers of different intrinsic oscillation periods are coupled and the strength of the coupling increased, the ratio of their periods approaches unity [30,39]. Furthermore, around certain values of the coupling conductances, stable patterns of m:n entrainment (m cycles of one pacemaker

for every n cycles of the other) which are common in the clinical analysis of electrocardiograms were observed. The results differed from previous studies of similar adjacent cell interaction, in that the faster cell did not always determine the cycle length at 1:1 entrainment. This is due to the fact that the coupling currents are characterized by direction dependent conductances, $g_{s,p}$ and $g_{p,s}$, and also that different cells do not exert equal influences on each other. For example, it was found that for equal values of $g_{s,p}$ and $g_{p,s}$ the Purkinje fibre cell exerts a much greater influence on the SA node cell than vice-versa. Cells of different intrinsic oscillation periods were made to interact for different values of the coupling conductances and regions of synchronous and asynchronous behavior plotted. It was found that when $g_{p,s}$ was greater than some minimum value and the ratio of the coupling conductances $g_{p,s}/g_{s,p}$ was sufficiently high (indicating that the influence of p on s was greater than the influence of s on p), then p became the lead cell and the common period at synchrony was closer to the intrinsic cycle length of p than of s. Similarly, when $g_{s,p}$ was greater than some minimum value and the ratio $g_{s,p}/g_{p,s}$ was sufficiently high then 1:1 s entrainment occurred and the common cycle length was closer to the intrinsic cycle length of s than of p. For the case of interactions between similar adjacent cells, previous studies [30,39] have found that the common cycle length was, both closer to the intrinsic period of the faster cell, and always *between* the intrinsic periods of the two cells. For the present model, the common cycle length was always closer to the intrinsic oscillation period of the lead cell but was not restricted to values between the periods of the two cells. When the intrinsic period of s was less than that of p (s firing at a faster rate than p) and the ratio T_p/T_s decreased, the regions of 1:1 s and 1:1 p entrainment increased in size, supporting the general rule: the closer the intrinsic periods of interacting cells the less coupling is required for synchrony [39]. However, the increase in size of the region of entrainment to p was greater than the increase in size of the 1:1 s entrainment region. This exemplified the fact that the Purkinje fibre cell

exerts a stronger influence on the SA node cell than vice-versa. Further evidence of this was discovered when the ratio T_p/T_s was decreased to a value less than 1. In this case, p fires at a faster rate than s and it was found that, over the range of conductances studied, p was never 1:1 s entrained.

6.3 Suggestions for Future Research

Due to the vast number of cardiac arrhythmias and entrainment phenomena readily observable in a real heart, the present study has only begun to explore the properties of impulse initiation and conduction among interacting cells. As a result, the following also are just a few of the ways the model can be used to investigate further the electrophysiology of the heart.

The AV node provides the only passage for impulses travelling between the atria and the ventricles; therefore, its malfunction may completely dissociate atrial and ventricular contraction. Studies of arrhythmias caused by the malfunction of the AV node have been done using simplified models, for example by Keener [25]. The present model which uses the more physiologically realistic Hodgkin-Huxley-type oscillators and provides a method of coupling nonadjacent cells could be used to study these arrhythmias which lead to the independent functioning of cells of the atria and ventricles.

Ventricular fibrillation, an arrhythmia which occurs under conditions of ventricular parasystole (at least two ventricular ectopic foci discharging independently of the SA node), has been of much interest in recent years. This arrhythmia, which leads to rapid death, has often been associated with aperiodic dynamics and chaos. There has been much controversy over the existence of chaotic modes separating the stable modes of m:n entrainment [24,15]. Glass et al. [9], using circle maps to simulate ventricular parasystole, have theoretically predicted regions of aperiodic dynamics which also have

been observed experimentally. They claim that, even if experimental noise were not present, these regions would still exist. Ypey et al. [39]; however, state that their results on the mutual entrainment of pacemaker cells suggest that chaotic modes do not exist between the regions of stable m:n entrainment. For the present model, the existence of aperiodic dynamics, also could be investigated for ventricular parasystole. For the simple model of Chapter 6, this would require subdividing the regions of asynchronous behavior (labelled 'not 1:1') of the various synchrony diagrams into zones of m:n entrainment. The difficulty lies in the fact that some stable m:n entrainment patterns, such as, say, 1021 : 1019 entrainment, require long simulation runs to detect and may be mistakenly classified as aperiodic.

Simulations involving larger numbers of model cells would allow the study of the spread of the cardiac action potential over a *tissue* as well as provide some insight into the mechanisms which cause the mutual synchronization of small clusters of adjacent cells. However, the computational cost and time of such an endeavor could become exorbitant.

The use of the highly nonlinear Hodgkin-Huxley-type oscillators to represent the cells of the model meant that extensive numerical computations were required to solve the systems of equations. One of the long range objectives of this research is to reduce the system of cell model equations to a form which is more tractable analytically and yet retains physiological relevancy. A possible approach is to adapt the averaging technique employed by Ermentrout and Kopell [27] in their studies of coupled biological oscillators.

Finally, it was briefly mentioned that the phase response curve may be useful in predicting zones of entrainment for unidirectional interaction [39]. This, as well as its potential use in studies of mutual entrainment, is an area worthy of further investigation.

Bibliography

[1] Beeler, G.W. and Reuter, H. Reconstruction of the action potential of ventricular myocardial fibres. *J. Physiol. Lond.*, **268**, 177-210, 1977.

[2] Brown, H.F., Kimura, J., Noble, D., Noble, S.J., and Taupignon, A. The ionic currents underlying pacemaker activity in rabbit sino-atrial node: experimental results and computer simulations. *Proc. R. Soc. Lond.*, **B222**, 329-347, 1984.

[3] Brown, H.F., Kimura, J., Noble, D., Noble, S.J., and Taupignon, A. The slow inward current, i_{si}, in the rabbit sino-atrial node investigated by voltage clamp and computer simulation. *Proc. R. Soc. Lond.*, **B222**, 305-328, 1984.

[4] Burne, R.M. and Levy, M.N. *Cardiovascular Physiology.* 5th ed., C.V. Mosby Company, 1986.

[5] Lambert, M.H. and Chay, T.R. Cardiac arrhythmias modelled by Ca_i-inactivated Ca^{2+} channels. *Biol. Cybern.*, **61**, 21-28, 1989.

[6] Chung, P.F. *Principles of Cardiac Arrhythmias.* 4th ed., Williams & Wilkins, Baltimore, 1989.

[7] Cranfield, P.F. *The Conduction of the Cardiac Impulse.* Futura Publishing Company, Inc., New York, 1975.

[8] DiFrancesco, D. and Noble, D. A model of cardiac electrical activity incorporating ionic pumps and concentration changes. *Phil. Trans. R. Soc. Lond.* [Biol.], **307**, 353-398, 1984.

[9] Glass, L., Goldberger, A.L., Courtemanche, M., and Shrier, A. Nonlinear dynamics, chaos and complex cardiac arrhythmias. *Proc. R. Soc. Lond.*, A**413**, 9-26, 1987.

[10] Glass, L., Hunter, P., and McCulloch, A., editors. *Theory of Heart, Biomechanics, Biophysics, and Nonlinear Dynamics of Cardiac Function.* Springer-Verlag, New York, 1991.

[11] Glass, L., Guevara, M.R., Bélair, J., and Shrier, A. Global bifurcations of a periodically forced biological oscillator. *Phys. Rev. A*, **29**, 1348-1357, 1984.

[12] Glass, L., and Mackey, M.C. *From Clocks to Chaos: The Rhythms of Life.* Princeton University Press, Princeton, 1988.

[13] Guevara, M.R., Shrier, A., and Glass, L. Phase resetting of spontaneously beating embryonic ventricular heart cell aggregates. *Am. J. Physiol.*, **251**, H1298-H1305, 1986.

[14] Guevara, M.R., Shrier, A., and Glass, L. Phase-locked rhythms of periodically stimulated heart cell aggregates. *Am. J. Physiol*, **254**, H1-H10, 1988.

[15] Goldberger, A.L., Bhargava, V., West B.J., and Mandell, A.J. Some observations on the question : Is ventricular fibrillation "chaos"?. *Physica* D, **19**, 282-289, 1986.

[16] Heethaar, R.M., Pao, Y.C., and Ritman, E.L. Computer aspects of three-dimensional finite element analysis of stresses and strains in the intact heart. *Comp. Biomed. Res.*, **10**, 271-285, 1977.

[17] Heller, L.J. and Mohrman, D.E. *Cardiovascular Physiology.* McGraw-Hill, Inc., New York, 1981.

[18] Honerkamp, J. The heart as a system of coupled nonlinear oscillators. *J. Math. Biol.*, **18**, 69-88, 1983.

[19] Horowitz, A., Lanir, Y., Yin, F.C.P., Perl, M., Sheinman, I., and Strumpf, R.K. Structural three-dimensional constitutive law for the passive myocardium. ASME J. Biomech. Eng., 200-207, 1988.

[20] Hunter, P.J., McCulloch, A.D., Nielsen, P.M.F., and Smaill, B.H. A finite element model of passive ventricular mechanics. *Computational Methods in Bioengineering* ASME, New York, 387-397, 1988.

[21] Ikeda, N., Yoshizawa, N.S., and Sato, T. Difference equation model of ventricular parasystole as an interaction of pacemakers based on the phase response curve. *J. Theor. Biol.*, **103**, 439-465, 1983.

[22] Jalife, J. and Antzelevitch, C. Phase resetting and annihilation of pacemaker activity in cardiac tissue. *Science*, **206**, 695-697, 1979.

[23] Janz, R.F. and Grimm, A.F. Finite element model for the mechanical behavior of the left ventricle. *Circ. Res.*, **30**, 244-252, 1972.

[24] Kaplan, D.T. and Cohen, R.J. Is fibrillation chaos?. *Circ. Res.*, **67**, 886-892, 1990.

[25] Keener, J.P. On cardiac arrythmias: AV conduction block. *J. Math. Biology*, **12**, 215-225, 1981.

[26] Keener, J.P. and Glass, L. Global bifurcations of a periodically forced oscillator. *J. Math. Biol.*, **21**, 175-190, 1984.

[27] Ermentrout, G.B. and Kopell, N. Multiple pulse interactions and averaging in systems of coupled oscillators. *J. Math. Biol.*, **29**, 195-217, 1991.

[28] McAllister, R.E., Noble, D., and Tsien, R.W. Reconstruction of the electrical activity of cardiac Purkinje fibres. *J. Physiol. Lond.*, **251**, 1-59, 1975.

[29] McCulloch, A.D. Deformation and stress in the passive heart. Ph.D. thesis, University of Auckland, New Zealand, 1986.

[30] Michaels, D.C., Matyas, E.P., and Jalife, J. Dynamic interactions and mutual synchronization of sinoatrial node pacemaker cells. *Circ. Res.*, **58**, 706-720, 1986.

[31] Noble, D. A modification of the Hodgkin-Huxley equations applicable to Purkinje fibre action and pacemaker potentials. *J. Physiol. Lond.*, **160**, 317-352, 1962.

[32] Noble, D. The surprising heart: A review of recent progress in cardiac electrophysiology. *J. Physiol. Lond.*, **353**, 1-50, 1984.

[33] Pao, Y.C., Ritman, E.L., and Wood, E.H. Finite-element analysis of left ventricular myocardial stresses. *J. Biomech.*, **7**, 469-477, 1974.

[34] van Capelle, Frans J.L. and Durrer, D. Computer simulation of arrhythmias in a network of coupled excitable elements. *Circ. Res.*, **47**, 454-466, 1980.

[35] van der Pol, B. and van der Mark, J. The heartbeat considered as a relaxation oscillation, and an electrical model of the heart. *Phil. Mag. (Series 7)*, **6**, 763-775, 1928.

[36] Vinsen, C.A., Gibson, D.G., and Yettram, A.L. Analysis of left ventricular behavior in diastole by means of finite element method. *Br. Heart. J.*, **41**, 60-67, 1979.

[37] Winfree, A.T. *The Geometry of Biological Time.* Springer, New York, 1980.

[38] Yanagihara, K., Noma, A., and Irisawa, H. Reconstruction of sino-atrial node pacemaker potential based on the voltage clamp experiments. *Jpn. J. Physiol.*, **30**, 841-857, 1980.

[39] Ypey, D.L., Van Meerwijk, W.P.M., Ince, C., and Groos, G. Mutual entrainment of two pacemaker cells. A study with an electronic parallel conductance model. *J. Theor. Biol.*, **86**, 731-755, 1980.

Appendix A

The Cell Models

The SA and AV nodes, Purkinje fibre, and ventricular myocardial cells have been modelled using the Hodgkin-Huxley formulation in which the rate of change of the transmembrane potential of a cell is described by a governing equation of the form:

$$\frac{dE_j(t)}{dt} = -\frac{1}{C}\, i_{ionic} \tag{A.1}$$

where t is the time in msec, j denotes the cell type and is one of: s,a,p, or v indicating SA node, AV node, Purkinje fibre, and ventricular myocardial cells, respectively, $E_j(t)$ is the membrane potential in mV (expressed as the inside potential minus the outside potential) of cell j at time t, C is the membrane capacitance in μF/cm^2, and i_{ionic} is the total ionic current in μA/cm^2 flowing out of cell j.

In the sections to follow, the equations describing the ionic current, i_{ionic}, of each of the four types of cells are given in detail. The equations for the SA node, Purkinje fibre, and ventricular myocardial cells are, for the most part, exactly as they are in the original papers [1,28,38] with the exception of a few minor changes in notation. The equations for the AV node cell are a modification of the equations for the SA node cell. In each of the models, ionic current components which are time dependent include gating variables for activation and/or inactivation. Such a gating variable x follows the first-order kinetics:

$$\frac{dx}{dt} = \alpha_x\,(1-x) - \beta_x\, x \tag{A.2}$$

A.1 The Sinus Node Cell

Yanagihara et al. [38] describe the total ionic current of the SA node cell by:

$$i_{ionic} = i_{si} + i_{Na} + i_K + i_h + i_l. \tag{A.3}$$

The individual components of the ionic current are given by the following equations where E_s is the transmembrane potential of the SA node cell at a particular time.

Slow inward current:

$$i_{si} = 12.5\,\{exp[(E_s - 30)/15] - 1\}\,(0.95d + 0.05)\,(0.95f + 0.05) \tag{A.4}$$

where the gating variables d and f satisfy (A.2) and the rate constants are given by:

$$\alpha_d = \frac{1.045 \times 10^{-2}(E_s + 35)}{1 - exp[-(E_s + 35)/2.5]} + \frac{3.125 \times 10^{-2} E_s}{1 - exp(-E_s/4.8)}, \tag{A.5}$$

$$\beta_d = \frac{4.21 \times 10^{-3}(E_s - 5)}{exp[(E_s - 5)/2.5] - 1}, \tag{A.6}$$

$$\alpha_f = \frac{3.55 \times 10^{-4}(E_s + 20)}{exp[(E_s + 20)/5.633] - 1}, \tag{A.7}$$

$$\beta_f = \frac{9.44 \times 10^{-4}\,|E_s + 60|}{1 + exp[-(E_s + 29.5)/4.16]}. \tag{A.8}$$

Sodium current:

$$i_{Na} = 0.5\,m^3 h\,(E_s - 30) \tag{A.9}$$

where the gating variables m and h satisfy (A.2) and the rate constants are given by:

$$\alpha_m = \frac{E_s + 37}{1 - exp[-(E_s + 37)/10]}, \tag{A.10}$$

$$\beta_m = 40\,exp[-5.6 \times 10^{-2}(E_s + 62)], \tag{A.11}$$

$$\alpha_h = 1.209 \times 10^{-3} exp[-(E_s + 20)/6.534], \tag{A.12}$$

$$\beta_h = \frac{1}{exp[-(E_s + 30)/10) + 1]}. \tag{A.13}$$

Hyperpolarization current:

$$i_h = 0.4\, q\, (E_s + 25) \tag{A.14}$$

where the gating variable q satisfies (A.2) and the rate constants are given by:

$$\alpha_q = \frac{3.4 \times 10^{-4}(E_s + 100)}{exp[(E_s + 100)/4.4] - 1} + 4.95 \times 10^{-5}, \tag{A.15}$$

$$\beta_q = \frac{5 \times 10^{-4}(E_s + 40)}{1 - exp[-(E_s + 40)/6]} + 8.45 \times 10^{-5}. \tag{A.16}$$

Potassium current:

$$i_K = \frac{0.7\, p\, \{exp[0.0277(E_s + 90)] - 1\}}{exp[0.0277(E_s + 40)]} \tag{A.17}$$

where the gating variable p satisfies (A.2) and the rate constants are given by:

$$\alpha_p = \frac{9 \times 10^{-3}}{1 + exp[-(E_s - \overline{E_{\alpha_p}})/9.71]} + 6 \times 10^{-4}, \tag{A.18}$$

$$\beta_p = \frac{2.25 \times 10^{-4}}{(E_s - \overline{E_{\beta_p}})\{exp[(E_s - \overline{E_{\beta_p}})/13.3] - 1\}}. \tag{A.19}$$

Since slight changes in $\overline{E_{\alpha_p}}$ and $\overline{E_{\beta_p}}$ produce significant changes in the oscillation frequency of the SA node cell, these parameters were used to produce model cells with varying cycle lengths. The actual values used along with the resulting frequencies are given in Section 2.2.5.

Leak current:

$$i_l = 0.8\,\{1 - exp[-(E_s + 60)/20]\}. \tag{A.20}$$

A.2 The AV Node Cell

A model for AV node cells was created from the equations for the SA node cells [38]. The total ionic current for the AV node cell is given by (A.3) where, with the exception of i_{si}, the individual current components are described by the same equations as for the SA node cell. The slow inward current, i_{si}, however, was scaled by the constant, $\overline{i_{si}}$, to slow the rate of depolarization which is not as fast for AV node cells as it is for SA node cells (Figure 1.2). Thus, for the AV node cell, i_{si} is given by:

$$i_{si} = \overline{i_{si}}\,12.5\,\{exp[(E_a - 30)/15] - 1\}\,(0.95d + 0.05)\,(0.95f + 0.05) \tag{A.21}$$

where E_a denotes the cell membrane potential and the subscript a indicates that the cell is an AV node cell. The gating variables d and f and their rate constants are as for the SA node cell. The intrinsic oscillation frequency of the model AV node cell is determined by the value of the scaling constant $\overline{i_{si}}$ and, as for the SA node cell, the values of the constants $\overline{E_{\alpha_p}}$ and $\overline{E_{\beta_p}}$ of i_K. The actual values used for these three constants are reported in Section 2.2.5.

A.3 The Purkinje Fibre Cell

The McAllister, Noble, and Tsien model for the Purkinje fibre cell [28] describes the membrane current by the following:

$$i_{ionic} = i_{Na} + i_{si} + i_{qr} + i_{K_2} + i_{x_1} + i_{x_2} + i_{K_1} + i_{Na_b} + i_{Cl_b}. \tag{A.22}$$

The ionic current components are described below where E_p denotes the membrane potential of the Purkinje fibre cell at a specific time.

Excitatory Sodium current:

$$i_{Na} = m^3 h\,(E_p - 40) \tag{A.23}$$

where the gating variables m and h satisfy (A.2) and the rate constants are given by:

$$\alpha_h = 1.13 \times 10^{-7} exp[-(E_p + 10)/5.43], \tag{A.24}$$

$$\beta_h = \frac{2.5}{exp[-0.082(E_p + 10)] + 1}, \tag{A.25}$$

$$\alpha_m = \frac{(E_p + 47)}{1 - exp[-0.1(E_p + 47)]}, \tag{A.26}$$

$$\beta_m = 9.86\, exp[-(E_p + 47)/17.86]. \tag{A.27}$$

Secondary inward current:

$$i_{si} = 0.8\,(E_p - 70)\,d\,f + 0.04\,(E_p - 70)\,d' \tag{A.28}$$

where the gating variables d and f satisfy (A.2) and the rate constants are given by:

$$\alpha_d = \frac{0.002\,(E_p + 40)}{1 - exp[-0.1(E_p + 40)]}, \tag{A.29}$$

$$\beta_d = 0.02\, exp[-0.0888(E_p + 40)], \tag{A.30}$$

$$\alpha_f = 0.000987\, exp[-0.04(E_p + 60)], \tag{A.31}$$

$$\beta_f = \frac{0.02}{exp[-0.087(E_p + 26)] + 1}, \tag{A.32}$$

$$d' = 1 + exp[-0.15(E_p + 40)]^{-1}. \tag{A.33}$$

Pacemaker potassium current:

$$i_{K_2} = \overline{i_{K_2}}\, k \tag{A.34}$$

where the gating variable k [1] satisfies (A.2) and the rate constants are given by:

$$\overline{i_{K_2}} = \frac{2.8\,\{exp[0.04(E_p + 110)] - 1\}}{exp[0.08(E_p + 60)] + exp[0.04(E_p + 60)]}, \tag{A.35}$$

$$\alpha_k = \frac{0.001(E_p - \overline{E_k})}{1 - exp[-0.2(E_p - \overline{E_k})]}, \tag{A.36}$$

$$\beta_k = 0.00005\, exp[-0.067(E_p - \overline{E_k})], \tag{A.37}$$

where the variable $\overline{E_k}$ is used to determine the oscillation frequency of the Purkinje fibre cell. The values used and the resulting oscillation frequencies are reported in Section 2.2.5.

Plateau potassium currents:

The first plateau potassium current is:

$$i_{x_1} = \frac{1.2\, x_1 \{exp[0.04(E_p + 95)] - 1\}}{exp[0.04(E_p + 45)]} \tag{A.38}$$

where the gating variable x_1 satisfies (A.2) and the rate constants are given by:

$$\alpha_{x_1} = \frac{0.0005\, exp[(E_p + 50)/12.1]}{1 + exp[(E_p + 50)/17.5]}, \tag{A.39}$$

$$\beta_{x_1} = \frac{0.0013\, exp[-(E_p + 20)/16.67]}{1 + exp[-(E_p + 20)/25]}. \tag{A.40}$$

[1] In the original paper [28], the gating variable is denoted s rather than k, however, in this study, s is reserved to indicate an SA node cell.

The second plateau potassium current is:

$$i_{x_2} = x_2\,(25 + 0.385E_p) \tag{A.41}$$

where the gating variable x_2 satisfies (A.2) and the rate constants are given by:

$$\alpha_{x_2} = \frac{0.000127}{1 + exp[-(E_p + 19)/5]}, \tag{A.42}$$

$$\beta_{x_2} = \frac{0.0003\,exp[-(E_p + 20)/16.67]}{1 + exp[-(E_p + 20)/25]}. \tag{A.43}$$

Transient chloride current:

$$i_{qr} = 2.5\,q\,r\,(E_p + 70) \tag{A.44}$$

where the gating variables q and r satisfy (A.2) and the rate constants are given by:

$$\alpha_q = \frac{0.008\,E_p}{1 - exp(-0.1E_p)}, \tag{A.45}$$

$$\beta_q = 0.08\,exp[-0.0888\,E_p], \tag{A.46}$$

$$\alpha_r = 0.00018\,exp[-0.04(E_p + 80)], \tag{A.47}$$

$$\beta_r = \frac{0.02}{exp[-0.087(E_p + 26)] + 1}. \tag{A.48}$$

Outward background current:

$$i_{K_1} = (\overline{i_{K_2}}/2.8) + \frac{0.2\,(E_p + 30)}{\{1 - exp[-0.04(E_p + 30)]\}}. \tag{A.49}$$

Inward background current carried by sodium ions:

$$i_{Na,b} = 0.105\,(E_p - 40). \tag{A.50}$$

Background current carried by chloride ions:

$$i_{Cl,b} = 0.01\,(E_p + 70). \tag{A.51}$$

A.4 The Ventricular Myocardial Cell

The model, due to Beeler and Reuter [1], for the ventricular muscle cell describes the ionic current by:

$$i_{ionic} = i_{Na} + i_{K_1} + i_{x_1} + i_{si}. \tag{A.52}$$

The individual current components are described by the following equations where E_v denotes the membrane potential of the ventricular muscle cell at a specific instance in time.

Sodium current:

$$i_{Na} = (4m^3hj + 0.003)(E_v - 50) \tag{A.53}$$

where the gating variables m, h, and j satisfy (A.2) and the rate constants are given by:

$$\alpha_m = \frac{-[E_v + 47]}{exp[-0.1(E_v + 47)] - 1}, \tag{A.54}$$

$$\beta_m = 40\,exp[-0.056(E_v + 72)], \tag{A.55}$$

$$\alpha_h = 0.126\,exp[-0.25(E_v + 77)], \tag{A.56}$$

$$\beta_h = \frac{1.7}{exp[-0.082(E_v + 22.5)] + 1}, \tag{A.57}$$

$$\alpha_j = \frac{0.055\,exp[-0.25(E_v + 78)]}{exp[-0.2(E_v + 78)] + 1}, \tag{A.58}$$

$$\beta_j = \frac{0.3}{exp[-0.1(E_v + 32)] + 1}. \tag{A.59}$$

Time-independent potassium current:

$$i_{K_1} = 0.35\left\{\frac{4\{exp[0.04(E_v+85)]-1\}}{exp[0.08(E_v+53)]+exp[0.04(E_v+53)]}+\frac{0.2(E_v+23)}{1-exp[-0.04(E_v+23)]}\right\}. \tag{A.60}$$

Outward current:

$$i_{x_1} = \frac{0.8\,x_1\,\{exp[0.04(E_v+77)]-1\}}{exp[0.04(E_v+35)]} \tag{A.61}$$

where the gating variable x_1 satisfies (A.2) and the rate constants are given by:

$$\alpha_{x_1} = \frac{0.0005\,exp[0.083(E_v+50)]}{exp[0.057(E_v+50)]+1}, \tag{A.62}$$

$$\beta_{x_1} = \frac{0.0013\,exp[-0.06(E_v+20)]}{exp[-0.04(E_v+20)]+1}. \tag{A.63}$$

Slow inward current:

$$i_{si} = 0.09\,d\,f\,(E_v - E_{si}) \tag{A.64}$$

where the gating variables d and f satisfy (A.2) and the rate constants are given by:

$$\alpha_d = \frac{0.095\,exp[-0.01(E_v-5)]}{exp[-0.072(E_v-5)]+1}, \tag{A.65}$$

$$\beta_d = \frac{0.07\,exp[-0.017(E_v+44)]}{exp[0.05(E_v+44)]+1}, \tag{A.66}$$

$$\alpha_f = \frac{0.012\,exp[-0.008(E_v+28)]}{exp[0.15(E_v+28)]+1}, \tag{A.67}$$

$$\beta_f = \frac{0.0065\,exp[-0.02(E_v+30)]}{exp[-0.2(E_v+30)]+1}, \tag{A.68}$$

$$E_{si} = -82.3 - 13.0287\ln[Ca]_i \tag{A.69}$$

$$d[Ca]_i/dt = -10^{-7}i_{si} + 0.07\{10^{-7} - [Ca]_i\}, \tag{A.70}$$

where this last equation models the movement of calcium which flows into the muscle cell and is subsequently removed by an uptake mechanism that reduces the intracellular calcium concentration to 10^{-7} M.